NASA CR-135086
IITRI D6073-III

WAVE PROPAGATION IN FIBER COMPOSITE LAMINATES

Final Report - Part II

by I. M. Daniel and T. Liber
IIT RESEARCH INSTITUTE

Prepared for

NATIONAL AERONAUTICS AND SPACE ADMINISTRATION

NASA - Lewis Research Center
Contract NAS3-16766

1 Report No	2 Government Accession No.	3. Recipient's Catalog No.
NASA CR-135086		

4 Title and Subtitle	5. Report Date
Wave Propagation in Fiber Composite Laminates	June 1976
	6. Performing Organization Code

7. Author(s)	8 Performing Organization Report No
I. M. Daniel and T. Liber	D6073-III
	10. Work Unit No

9. Performing Organization Name and Address	11 Contract or Grant No
IIT Research Institute 10 W. 35 Street Chicago, IL 60616	NAS3-16766
	13 Type of Report and Period Covered
12. Sponsoring Agency Name and Address National Aeronautics & Space Administration Washington, DC 20546	Final - Part II
	14 Sponsoring Agency Code

15 Supplementary Notes

Project Manager, C. C. Chamis
Materials & Structures Division
NASA Lewis Research Center
Cleveland, OH 44135

16. Abstract

An experimental investigation was conducted to determine the wave propagation characteristics, transient strains and residual properties in unidirectional and angle-ply boron/epoxy and graphite/epoxy laminates impacted with silicone rubber projectiles at velocities up to 250 ms^{-1} (820 ft/sec). The predominant wave is flexural, propagating at different velocities in different directions. In general, measured wave velocities were higher than theoretically predicted values. The amplitude of the in-plane wave is less than ten percent of that of the flexural wave. Peak strains and strain rates in the transverse to the (outer) fiber direction are much higher than those in the direction of the fibers. Strain rates up to 640 ε /sec were measured. The dynamics of impact were also studied with high speed photography. The projectile is completely flattened within 50-70 μs. The total contact time is of the order of 300 μs.

17. Key Words (Suggested by Author(s))	18. Distribution Statement
Wave propagation, transient strains, residual properties, high velocity impact, normal impact, oblique impact, fiber composites, boron/epoxy, graphite/epoxy	Unclassified, Unlimited

19. Security Classif (of this report)	20. Security Classif. (of this page)
Unclassified	Unclassified

* For sale by the National Technical Information Service, Springfield, Virginia 22161

FOREWORD

This is the Final Report on IIT Research Institute Project No. D6073-III, "Wave Propagation in Fiber Composite Laminates," prepared by IITRI for NASA-Lewis Research Center, under Contract No. NAS3-16766. The work described in this report was conducted in the period July 1, 1974 to February 29, 1976. The work performed in the preceding period August 1, 1972 to June 30, 1974 was reported in the First Interim Report, NASA CR-134826 dated March 1975. Dr. C.C. Chamis was the NASA-Lewis Project Manager. Dr. I.M. Daniel of IITRI was the principal investigator. Additional contributions to the work reported herein were made by Dr. T. Liber and Messrs. R. LaBedz, and M. Senninger.

Respectfully submitted,
IIT RESEARCH INSTITUTE

I.M. Daniel
Science Advisor
Mechanics of Materials Division

APPROVED:

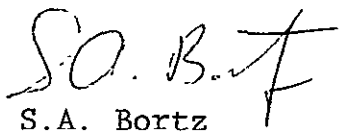

S.A. Bortz
Assistant Director
Mechanics of Materials Division

WAVE PROPAGATION IN FIBER COMPOSITE LAMINATES

ABSTRACT

An experimental investigation was conducted to determine the wave propagation characteristics, transient strains and residual properties for unidirectional and angle-ply boron/epoxy and graphite/epoxy laminates impacted with silicon rubber projectiles at velocities up to 250 ms^{-1} (820 ft/sec). The predominant wave is a flexural one propagating at different velocities in different directions. In general, measured wave velocities were higher than theoretically predicted values. The amplitude of the in-plane wave is less than ten percent of that of the flexural wave. Peak strains and strain rates in the transverse to the (outer) fiber direction are much higher than those in the direction of the fibers. Strain rates up to 640 ε/sec were measured. The dynamics of impact were also studied with high speed photography. The projectile is completely flattened within 50-70 μs. The total contact time is of the order of 300 μs.

TABLE OF CONTENTS

LIST OF TABLES

LIST OF TABLES (Cont'd)

LIST OF FIGURES

LIST OF FIGURES (Cont'd)

LIST OF FIGURES (Cont'd)

LIST OF FIGURES (Cont'd)

LIST OF FIGURES (Cont'd)

LIST OF FIGURES (Cont'd)

IITRI Research Project No. D6073-III

WAVE PROPAGATION IN FIBER COMPOSITE LAMINATES

1.0 INTRODUCTION

The application of fiber composites to jet engine blades exposes them to the hazards of foreign object damage, e.g., bird impact on rotating blades. Such impacts occur at velocities up to 305 ms^{-1} (1000 ft/sec) and can cause extensive damage to the composite blade. The high speed impact of these objects results in short duration impact times of the order of 100 μs. Damage in these cases is related to the wave propagation characteristics of the laminate, i.e., velocities, attenuation, reflection and amplitude of the induced stress waves and the response of the material to the high stress (strain) rates produced.

A survey of wave propagation and impact on composite materials was given by Moon.[1] Theoretical analyses of impact and wave propagation in anisotropic materials in general and composites in particular have been discussed by many investigators.[2-6] It was shown that the motion under dynamic impulse is composed of five waves, two waves related to in-plane motion and three related to flexural plate deformations. Some experimental studies have been reported on the subject but they do not deal specifically with the transverse impact problem.[7-11] The objective of the present task was to study the effects of lamination residual stresses on stress wave propagation in composite laminates under high velocity impact.

Two materials were investigated, boron/epoxy and graphite/high modulus epoxy. Sixteen-ply unidirectional $[0_{16}]$ and angle-ply $[0_2/\pm45]_{2s}$ laminates were impacted with silicon rubber projectiles at velocities up to 250 ms^{-1} (820 ft/sec). The impact characteristics, impact velocity and energy input, were determined by means of high-speed photography. The characteristics of the induced strain pulses

were studied by means of surface and embedded strain gages. Impact damage was assessed by measuring residual properties of the laminates after impact.

2.0 EXPERIMENTAL PROCEDURE

2.1 Specimen Preparation

The materials investigated were boron/epoxy (4 mil boron/AVCO 5505) and graphite/high modulus epoxy (HMS graphite/ ERLA 4617). The specimens were unidirectional $[0_{16}]$ and $[0_2/\pm45]_{2s}$ 25 cm x 22 cm (9.75 in. x 8.75 in.) 16-ply laminates. Some preliminary studies were conducted with a $[\pm45/\pm45]_s$ boron/ epoxy specimen.

All specimens were ultrasonically scanned before instrumentation and testing. During this scanning the specimen is immersed in a tank of water between two transducers, a transmitting and a receiving one. The transducers are fixed in space and the specimen is slowly translated between them. The specimen is moved so that the ultrasonic beam emitted from the transmitting transducer traverses the specimen along equidistant parallel lines. The transmitted and received pulses are amplified and displayed on a cathode ray tube. The signal from the receiving transducer is fed to an alarm circuit which measures the amplitude and initiates an audio and visual alarm should the signal fall below a predetermined level. Calibration is a matter of adjusting the alarm level such that the amplitude of the received signal passing through a calibration plate of known integrity is just sufficient to keep the alarm inactive. At this level any additional discontinuity will activate the alarm.

The test specimen is passed between the transducers by means of a horizontal slide mechanism which also drives a linear potentiometer. The potentiometer supplies a signal to one channel

of an X-Y plotter and gains are adjusted to drive the pen at the velocity of the plate. When a discontinuity is encountered, the alarm is activated opening a relay which causes the pen to be lifted from the chart paper. After passing through the defective area, the alarm is automatically reset closing the relay and causing the pen to return to the normal writing position. After completing one scan the test plate is moved vertically, the recording pen displaced an appropriate distance in the y-direction and another scan is initiated. By repeating this process the entire test plate can be mapped. The end product is an array of horizontal lines on the chart. Defects in the material are represented by discontinuous lines and areas without flaws by continuous lines.

A typical scan of an unflawed specimen, that for the $[0_{16}]$ boron/epoxy specimen before testing, is shown in Fig. 1. All other specimens made displayed similar continuous line patterns before testing.

The specimens above were instrumented with surface and embedded strain gages. The gage layout for the $[\pm 45/\pm 45]_s$ boron/epoxy specimen used for preliminary testing is shown in Fig. 2. The surface gage layout for the $[0_{16}]$ and $[0_2/\pm 45]_{2s}$ boron/epoxy and graphite/epoxy specimens is shown in Fig. 3. Two two-gage rosettes were applied on the horizontal and vertical axes (at 90- and 0-degrees with respect to the 0-degree fibers) and two three-gage rosettes were applied on the 45-degree axis. Specimens containing embedded gages had a different gage layout as shown in Fig. 4. The embedded gages were WK-00-125TM-350 (Micro-Measurements) encapsulated two-gage rosettes. These gages with attached ribbon leads (nickel-clad copper, 0.025 mm thick) were bonded between two 0.013 mm (0.0005 in.) thick polyimide films (Kapton) with ERLA 4617 resin. The assembly was cured in a vacuum

bag in the autoclave. Subsequently, the Kapton sheets were trimmed around the gages and the ribbon leads and the assembly embedded between the fourth and fifth plies of the laminate. Surface gages were bonded at the same locations on the top and bottom surfaces after curing.

2.2 Loading

Preliminary impact tests were conducted using an air rifle with a smooth bore of BB caliber. Pellets of 4.50 mm (0.177 in.) diameter were used. The pressure chamber is pressurized by means of a built-in hand pump. The recommended ten strokes of the pump build sufficient pressure to propel the 4.50 mm (0.177 in.) diameter steel pellets at 228 ms^{-1} (750 ft/sec). The velocity of the projectile was measured with the system shown in Fig. 5. For seven strokes of the hand pump the average measured velocity of the steel pellet was 182 ms^{-1} (598 ft/sec).

Preliminary tests with $[0/\pm45/0/9\bar{0}]_s$ boron/epoxy laminates impacted with this pellet, resulted in complete penetration. This was the case even at much lower velocities, when the number of strokes in the hand pump was reduced to three. An 18-ply boron/epoxy laminate of $[0/\pm45/0/9\bar{0}]_{2s}$ layup was almost completely penetrated at 183 ms^{-1} (600 ft/sec) projectile velocity. Reduction of this velocity (to four pump strokes) produced perforation on the front face, delamination on the back face but no complete penetration. Drastic reduction in air pressure (one pump stroke) produced only a small surface indentation, but the velocity was too low to be of interest in this task.

The steel pellets were replaced with silicon rubber pellets of the same size. These were produced by casting RTV 21 in molds. This RTV formulation has a specific gravity of 1.31 and a Shore A durometer hardness of 50. The average measured velocity of these

pellets (for seven pump strokes) was 200 ms^{-1} (657 ft/sec). At this velocity the RTV pellets did not produce any visible damage to the boron/epoxy laminates.

A new air gun with better velocity control allowing for larger pellets was designed and built (Fig. 6). It consists of a pressure chamber and a smooth-bore gun barrel with a 1.43 cm (9/16 in) inside diameter. The pressurized air in the chamber is suddenly released through the gun barrel by means of a solenoid-activated valve. The velocity of a 1.43 cm (9/16 in.) diameter RTV sphere was monitored for different chamber pressures. Results are plotted in Fig. 7. The RTV pellet penetrated easily a 9-ply $[0/\pm45/0/9\bar{0}]_s$ boron/epoxy panel at 201 ms^{-1} (661 ft/sec) and 219 ms^{-1} (718 ft/sec) and produced a small surface indentation at 130 ms^{-1} (427 ft/sec). At 232 ms^{-1} (760 ft/sec) the pellet produced some cracking and delamination on an 18-ply $[0/\pm45/0/9\bar{0}]_{2s}$ boron/epoxy laminate. At 189 ms^{-1} (619 ft/sec) the delamination was slight and at 166 ms^{-1} (543 ft/sec) no damage was visible.

The air gun system built allows for easy interchangeability of gun barrels. To maintain high velocities between 183 ms^{-1} (600 ft/sec) and 305 ms^{-1} (1000 ft/sec) without risking visible damage in the composite laminate, it was decided to use smaller diameter pellets. A new gun barrel of 7.9 mm (5/16 in.) inside diameter was used with silicon rubber pellets cast from Dow Silastic A. The velocity of a 7.9 mm (5/16 in.) diameter Silastic sphere was measured for different chamber pressures. Results are plotted in Fig. 8.

All unidirectional $[0_{16}]$ and angle-ply $[0_2/\pm45]_{2s}$ specimens were impacted with 7.9 mm (5/16 in.) Silastic spheres with the air gun described above. Impact velocities below the immediate damage threshold for the various specimens were selected. Tests under normal

and 45-degree oblique impact were conducted. The overall setup for impacting the composite plates and recording strain gage signals is shown in Figs. 9 and 10.

2.3 Data Recording

The strain gages were connected to potentiometric circuits and their signals recorded on four dual-beam oscilloscopes. The oscilloscopes were triggered when the Silastic projectile interrupted a light beam parallel to the specimen and at a short distance from it. A 0.5 mW He-Ne laser beam aimed at a photodiode was used.

To characterize the impact dynamics a moderately high speed camera (Fastax) was used to record the impact and rebound of the Silastic projectiles. Tests for various gun chamber pressures were conducted on all four types of specimens, boron/epoxy, graphite/epoxy, unidirectional and angle-ply. The projectile was photographed during its approach and rebound from the specimen with a Fastax 16 mm camera operating at rates between 7100 and 7460 frames per second.

A series of tests using a high-speed Beckman and Whitley Model 189 framing camera was conducted to characterize further the impact of the projectile on the composite plates and determine variation of contact area with time. The overall experimental setup for these tests is shown in Figs. 11 and 12. This camera is capable of recording twenty-five 35 mm images at rates up to 1,250,000 frames/second by means of a rotating mirror, 25 pairs of relay lenses and a stationary strip of film. Shuttering is accomplished by means of diamond stops, one located at the objective lens, and the other between each pair of refocusing lenses. With the normal apertures employed here, the exposure duration is one third the interframe time. Illumination was provided by an electronic light source prepared for the purpose. This source

employs a xenon flash lamp (GE Model FT 220). The system provides for variable duration of illumination. Kodak 2479 RAR film was used and developed in D-19 developer.

3.0 RESULTS AND DISCUSSION

3.1 Preliminary Testing

To establish pertinent timescales of interest and basic instrumentation parameters, preliminary tests were conducted by impacting a $[\pm 45/\pm 45]_s$ boron/epoxy laminate instrumented with surface strain gages. The strain gage layout used was shown in Fig. 2. The specimen was impacted normally at the center with 0.450 cm (0.177 in.) diameter RTV pellets and the strain gage output recorded on oscilloscopes. Results of one test are shown in Fig. 13. The dominant wave seen in these signals is the flexural wave propagating with a measured velocity of

$$v = 1{,}900 \text{ ms}^{-1} \text{ (75,000 in/sec)}$$

This value is identical to the values of shear wave velocity parallel and perpendicular to the fibers measured by Tauchert and Guzelsu.[19] This velocity is the same in both the x-direction and the 45-degree direction. The phenomenon of isotropic propagation of flexural waves is described by Moon.[5] The flexural or bending motion has three waves associated with it. The lowest flexural wave propagates with an isotropic velocity

$$v_3 = [C_{66} \kappa/\rho]^{1/2}$$

where

$\kappa = \frac{\pi^2}{12}$ is Mindlin's correction factor

C_{66} = transverse shear modulus

ρ = density

3.2 Impact on Unidirectional Boron/Epoxy Laminates

Preliminary tests were conducted on $[0_{16}]$ boron/epoxy specimens to determine a threshold impact velocity below which no visible damage could be seen in the plate. This velocity was established as 213 ms^{-1} (700 ft/sec). The first specimen (Specimen 9BU-1) was ultrasonically scanned as described before, instrumented with strain gages according to the gage layout of Fig. 3 and impacted with 7.9 mm (5/16 in.) diameter Silastic projectiles at 210 ms^{-1} (690 ft/sec).

Figure 14 shows strain gage signals along the y-axis (fiber direction) from two strain gage rosettes located at stations 5.08 cm (2 in.) apart. The predominant pulse observed corresponds to the transverse flexural wave in the direction of the fibers. The average wave propagation velocity measured from five tests is

$$c_{11LF} = 2159 \text{ ms}^{-1} \text{ (85,000 in/sec) (Flexural velocity)}$$

This flexural wave is related to the transverse shear modulus G_{13} (where 1- and 3- denote directions along the fibers and normal to the plate) and the density by the relation

$$c_{11LF} = \sqrt{\frac{G_{13}}{\rho}}$$

Using the value of

$$G_{13} \cong G_{12} = 0.8 \times 10^6 \text{ psi}$$

we obtain

$$c_{11LF} = 65{,}000 \text{ in/sec} = 1{,}650 \text{ ms}^{-1}$$

The discrepancy between the measured and calculated values is due to the fact that the G_{13} modulus is actually higher than G_{12} due to the pressure applied in the 3-direction during curing.

Figure 14a also shows evidence of a very low amplitude high-velocity precursor pulse which may be related to a longitudinal wave along the boron fibers. No accurate measure of this velocity could be made from these records.

Figure 15 shows strain gage signals along the x-axis (transverse to the fibers) from two strain gage rosettes located at stations 5.08 cm (2 in.) apart. Here, the precursor pulse corresponding to in-plane wave propagation is very pronounced. Measured velocities of propagation for the in-plane and flexural waves are

$$c_{22LI} = 3{,}790 \text{ ms}^{-1} \text{ (149,300 in/sec) (In-plane velocity)}$$

$$c_{22LF} = 1{,}790 \text{ ms}^{-1} \text{ (70,330 in/sec) (Flexural velocity)}$$

The calculated velocities for these two waves are:

$$c_{22LI} = \sqrt{\frac{E_{22}}{\rho(1-\nu_{12}\nu_{21})}} = 3{,}280 \text{ ms}^{-1} \text{ (129,000 in/sec)}$$

$$c_{22LF} = \sqrt{\frac{G_{23}}{\rho}} \cong \sqrt{\frac{E_{33}}{2\rho(1+\nu_{23})}} \cong \sqrt{\frac{E_{22}}{2\rho(1+\nu_{23})}} \cong$$

$$\cong \sqrt{\frac{3.15 \times 10^6 \times 386}{2 \times 0.073 \times (1+0.5)}} = 74{,}500 \text{ in/sec} = 1890 \text{ ms}^{-1}$$

The differences between measured and calculated values are likely due to the uncertainty about the exact values of the elastic constants involved.

Figure 16 shows strain gage signals along the 45-degree axis from two three-gage rosettes located at stations 7.62 cm (3 in.) apart. A small in-plane precursor wave followed by a much more pronounced flexural wave is seen. Measured velocities of these two waves are:

$$c_{45LI} = 3,380 \text{ ms}^{-1} \text{ (133,200 in/sec)}$$

$$c_{45LF} = 1,940 \text{ ms}^{-1} \text{ (76,300 in/sec)}$$

The calculated values for these velocities are:

$$c_{45LI} = \sqrt{\frac{E_{45}}{\rho(1-\nu_{45}\nu_{-45})}} = \sqrt{\frac{2.51 \times 10^6 \times 386}{0.073\ (1-0.5 \times 0.5)}} =$$

$$= 133,000 \text{ in/sec} = 3,380 \text{ ms}^{-1}$$

$$c_{45LF} = \sqrt{\frac{G_{45/3}}{\rho}} \cong \sqrt{\frac{E_{33}}{2\rho(1+\nu_{45/3})}} \cong \sqrt{\frac{E_{22}}{2\rho(1+\nu_{23})}} =$$

$$= 1890 \text{ ms}^{-1} \text{ (74,500 in/sec)}$$

The agreement here between theoretical predictions and experimental values is very good.

The maximum strain rates measured at the first station 2.54 cm (1 in.) from the point of impact along the y-axis (parallel to the fibers) averaged for three tests are:

$$\frac{d\varepsilon_{11}}{dt} = 340 \ \varepsilon/\text{sec}$$

$$\frac{d\varepsilon_{22}}{dt} = 240 \ \varepsilon/\text{sec}$$

The maximum strain rate in the x-direction measured along the x-axis is

$$\frac{d\varepsilon_{22}}{dt} = 640 \ \varepsilon/\text{sec}$$

which is much higher than the maximum strain rate along the y-axis. This is due to the fact that the rise times to peak strain are approximately the same in both directions, since the flexural wave velocities are approximately equal, and the fact that ε_{22} has the highest peak value.

The plate showed visible damage after a few impacts. The extent of the damage is plainly manifested in the ultrasonic scan taken after the impact tests. (Fig. 17).

A second 16-ply unidirectional boron/epoxy specimen was prepared with surface and embedded gages according to the gage layout of Fig. 4.

The instrumented specimen was impacted with 7.9 mm (5/16 in.) diameter Silastic spheres at 192 ms^{-1} (630 ft/sec). Strain gage signals on the top (front), bottom (back) and middle surfaces were recorded on oscilloscopes. Figures 18 and 19 show signals obtained along the y-axis (fiber direction). One pair of traces in each figure shows surface strains and the other pair shows strains in the middle of the laminate. The surface strains are predominantly flexural strains whereas the mid-surface strains represent the in-plane component of the pulse. Based on such records from gages 1 through 6 the following in-plane and flexural wave propagation velocities were obtained, respectively:

$$c_{11LI} \cong 12{,}700 \text{ ms}^{-1} \text{ (500,000 in/sec)}$$

$$c_{11LF} = 2{,}090 \text{ ms}^{-1} \text{ (82,270 in/sec)}$$

Figures 20, 21 and 22 show strain gage signals along the x-axis. Flexural wave velocities were obtained from records such as that of Figure 21a. The in-plane wave velocity was obtained from embedded-gage strains such as those of Figs. 20b, 21b and 22. The average measured velocities from gages 7 through 12 are:

$$c_{22LI} = 3{,}490 \text{ ms}^{-1} \text{ (137,400 in/sec)}$$

$$c_{22LF} = 1{,}710 \text{ ms}^{-1} \text{ (67,250 in/sec)}$$

The near symmetry of the two traces in Fig. 20a shows that the pulse is predominantly flexural. The bottom trace of Fig. 21a shows clearly the precursor in-plane pulse in front of the slower flexural pulse. The similarity of the top and bottom traces in Figs. 22a and 22b shows that the in-plane component of the pulse can be obtained by summing the two opposite-surface strains, and that the neutral plane coincides with the mid-surface of the laminate.

The measured velocities above for the two specimens tested are tabulated in Table 1 and compared with calculated values obtained using the known properties of the material. The discrepancy between the measured and computed values for c_{11L} is probably due partly to the fact that the measured time interval in the records was too short to be measured with accuracy and partly due to pulse propagation along the fibers themselves at a higher velocity than the one based on a homogeneous material. The reason for the higher experimental value for c_{22L} is probably that the static value for E_{22} used in the computation of c_{22L} is lower than the dynamic value under impact conditions. The measured flexural wave velocity in the fiber direction is higher than that in the transverse to the fiber direction. The calculated values show the opposite relationship, but it must be due to the approximations used for the pertinent shear moduli G_{13} and G_{23}. In the 45-degree direction the agreement between measured and calculated values is very good.

The specimen with surface and embedded gages was subsequently impacted obliquely by rotating it by 45-degrees, first about the x-axis and recording gages on the y-axis and then rotating it about the y-axis and recording gages on the x-axis. Typical strain gage records are shown in Fig. 23.

Table 1

WAVE PROPAGATION VELOCITIES IN TRANSVERSELY IMPACTED $[0_{16}]$ BORON/EPOXY SPECIMEN

Velocity Direction and Type of Wave	Velocity, ms^{-1} (in/sec)	
	Measured	Calculated
c_{11LI}	12,700 (500,000)	10,110 (398,100)
c_{22LI}	3,640 (143,300)	3,280 (129,000)
c_{45LI}	3,380 (133,200)	3,380 (133,000)
c_{11LF}	2,120 (83,630)	1,650 (65,000)
c_{22LF}	1,750 (68,790)	1,890 (74,500)
c_{45LF}	1,940 (76,300)	1,890 (74,500)

Peak strains were measured at various stations both on the outer surfaces and in the middle surface. These strains are tabulated in Table 2 for normal impact and in Table 3 for oblique impact. The in-plane components of strain are in general less than 10 percent of the flexural ones. The peak flexural strains under oblique impact range between 38 and 56 percent of those under normal impact. This reduction is accounted for by the reduction of the normal force component and the reduction in the amount of absorbed kinetic energy due to the obliqueness of the impact.

An attempt was made to evaluate the material attenuation of the pulse by fitting an expression of the form

$$\varepsilon_{max} = \frac{ae^{-kr}}{\sqrt{r}}$$

to the peak strain distribution. Here r is the distance from the point of impact and k is the coefficient of attenuation. The factor $1/\sqrt{r}$ accounts for the geometric attenuation. The two types of attenuation can be separated by plotting $\varepsilon_{max}\sqrt{r}$ versus r on a semilog scale (Fig. 24). Points were plotted for the peak flexural strains ε_{xx} and ε_{yy} along the x-axis and y-axis, respectively and for the peak in-plane strain ε_{xx} along the x-axis. The plot was normalized by dividing the function $\varepsilon_{max}\sqrt{r}$ by its value at r = 2.54 cm. A straight line drawn roughly through all points yields a coefficient of attenuation

$$k = 0.105 \text{ cm}^{-1}$$

Table 2

PEAK DYNAMIC STRAINS IN NORMALLY IMPACTED $[0_{16}]$ BORON/EPOXY SPECIMEN

Strain ($\mu\varepsilon$)	Gage Location x(cm)	y(cm)	Surface
ε_{xx} = 2620	2.54	0	Top (Front)
-1380	-5.08	0	Top (Front)
900	7.62	0	Top (Front)
ε_{yy} = 130	2.54	0	Top (Front)
-50	-5.08	0	Top (Front)
15	7.62	0	Top (Front)
ε_{xx} = -220	2.54	0	Middle
-120	-5.08	0	Middle
-85	7.62	0	Middle
ε_{yy} = 14	2.54	0	Middle
11	-5.08	0	Middle
7	7.62	0	Middle
ε_{xx} = -900	0	2.54	Top (Front)
380	0	-5.08	Top (Front)
250	0	7.62	Top (Front)
ε_{yy} = 1400	0	2.54	Top (Front)
860	0	-5.08	Top (Front)
-450	0	7.62	Top (Front)
ε_{xx} = 120	0	2.54	Middle
65	0	-5.08	Middle
25	0	7.62	Middle
ε_{yy} = 100	0	2.54	Middle
40	0	-5.08	Middle
25	0	7.62	Middle

Table 3

PEAK DYNAMIC STRAINS IN OBLIQUELY IMPACTED $[0_{16}]$ BORON/EPOXY SPECIMEN

Strain ($\mu\varepsilon$)	Gage Location x(cm)	y(cm)	Surface
ε_{xx} = 1150	2.54	0	Top (Front)
-800	-5.08	0	Top (Front)
190	7.62	0	Top (Front)
ε_{yy} = 50	2.54	0	Top (Front)
-50	-5.08	0	Top (Front)
15	7.62	0	Top (Front)
ε_{xx} = -90	2.54	0	Middle
-85	-5.08	0	Middle
-35	7.62	0	Middle
ε_{yy} = 12	2.54	0	Middle
7	-5.08	0	Middle
5	7.62	0	Middle
ε_{xx} = -500	0	2.54	Top (Front)
140	0	-5.08	Top (Front)
200	0	7.62	Top (Front)
ε_{yy} = 640	0	2.54	Top (Front)
540	0	-5.08	Top (Front)
-200	0	7.62	Top (Front)
ε_{xx} = 90	0	2.54	Middle
30	0	-5.08	Middle
20	0	7.62	Middle
ε_{yy} = -15	0	-5.08	Middle
20	0	7.62	Middle

3.3 Impact on Unidirectional Graphite/Epoxy Laminates

Preliminary tests were conducted on $[0_{16}]$ graph epoxy specimens to establish a safe impact velocity that would not produce visible damage on first impact. Specimens split at impact velocities as low as 141 ms^{-1} (464 ft/sec). An impact velocity of 91 ms^{-1} (300 ft/sec) was selected for all subsequent testing. The specimen (No. 9GU-1) was instrumented with surface strain gages according to the gage layout of Fig. 3 and impacted with 7.9 mm (5/16 in.) diameter Silastic projectiles.

Figure 25 shows strain gage signals along the y-axis from two strain gage rosettes located at stations 5.08 cm (2 in.) apart. The pulse observed is that of the dominant flexural (transverse) wave in the direction of the fibers. The average wave propagation velocity measured from fifteen sets of gage readings in nine tests is

$$c_{11LF} = 1{,}930\ ms^{-1}\ (76{,}100\ in/sec)$$

which compares well with the calculated value of

$$c_{11LF} = \sqrt{\frac{G_{13}}{\rho}} \cong \sqrt{\frac{G_{12}}{\rho}} \cong 1995\ ms^{-1}\ (78{,}600\ in/sec)$$

Figure 26 shows strain gage signals in the x-direction for two pairs of gages located at stations 5.1 cm (2 in.) apart. The average flexural wave propagation velocity computed from strains in the x- and y-directions is

$$c_{22LF} = 1{,}290\ ms^{-1}\ (50{,}900\ in/sec)$$

The theoretical value is obtained as

$$c_{22LF} = \sqrt{\frac{G_{23}}{\rho}} \cong \sqrt{\frac{E_{33}}{2\rho(1+\nu_{23})}} \cong \sqrt{\frac{1.02 \times 10^6 \times 386}{2 \times 0.06 \times (1+0.5)}} \cong$$

$$= 46{,}800\ in/sec = 1{,}190\ ms^{-1}$$

The lower theoretical value is probably due to the fact that E_{33} was approximated by the lower value of E_{22}.

Figure 26b also shows the precursor in-plane pulse along the x-axis. The measured wave propagation velocity is

$$c_{22LI} = 2{,}380 \text{ ms}^{-1} \text{ (93,600 in/sec)}$$

which is appreciably higher than the calculated value of

$$c_{22LI} = \sqrt{\frac{E_{22}}{\rho(1-\nu_{12}\nu_{21})}} = 2{,}060 \text{ ms}^{-1} \text{ (81,300 in/sec)}$$

Figure 27 shows strain gage signals along the 45-degree axis. The measured velocity of the flexural wave is

$$c_{45LF} = 1{,}430 \text{ ms}^{-1} \text{ (56,200 in/sec)}$$

The measured velocity of the in-plane precursor visible in Fig. 27c is

$$c_{45LI} = 2{,}090 \text{ ms}^{-1} \text{ (82,100 in/sec)}$$

which is much lower than the calculated value of

$$c_{45LI} = \sqrt{\frac{E_{45}}{\rho(1-\nu_{45}\nu_{-45})}} \cong 2{,}860 \text{ ms}^{-1} \text{ (112,600 in/sec)}$$

Measured and calculated values of wave propagation velocities are tabulated in Table 4. The measured value of c_{22LI} is higher than the calculated one, as in the case of the boron/epoxy specimen before, because the static value for E_{22} used in the computation is lower than the dynamic value under impact conditions. The measured propagation velocities of the flexural wave in the fiber and transverse to the fiber directions are in good agreement with calculated values. Furthermore, the flexural wave velocities in the two directions are appreciably different because the transverse shear moduli G_{13} and G_{23} are different in a realistic composite.

Table 4

WAVE PROPAGATION VELOCITIES IN TRANSVERSELY IMPACTED $[0_{16}]$ GRAPHITE/EPOXY SPECIMEN

Velocity Direction and Type of Wave	Velocity, ms^{-1} (in/sec)	
	Measured	Calculated
c_{11LI}	-	11,560 (455,000)
c_{22LI}	2,380 (93,600)	2,060 (81,300)
c_{45LI}	2,090 (82,100)	2,860 (112,600)
c_{11LF}	1,930 (76,100)	1,995 (78,600)
c_{22LF}	1,290 (50,900)	1,275 (50,200)
c_{45LF}	1,430 (56,200)	1,300 (51,200)

Peak strains measured from the various strain signals from the gages nearest the point of impact are tabulated in Table 5 below:

Table 5

PEAK DYNAMIC STRAINS IN TRANSVERSELY IMPACTED $[0_{16}]$ GRAPHITE/EPOXY SPECIMEN ($\mu\varepsilon$)

Signals	Gage Location		
	x-axis	y-axis	45-deg. axis
ε_{11}	135	1280	110
ε_{22}	3900	-900	3580
ε_{45}	-	-	2120

The transverse to the fibers strain on the x-axis (normal to the fibers) is the highest, reaching a value of 3900 $\mu\varepsilon$. This is an appreciable fraction of the transverse ultimate strain of the unidirectional material 5100 $\mu\varepsilon$. This result also indicates that the transverse ultimate strain was probably exceeded at points closer to the point of impact, resulting in immediate damage.

Maximum strain rates measured from the various strain signals from the gages nearest the point of impact are tabulated in Table 6 below:

Table 6

MAXIMUM STRAIN RATES IN TRANSVERSELY IMPACTED $[0_{16}]$ GRAPHITE/EPOXY SPECIMEN (ε/sec)

Strain Rate	Gage Location		
	x-axis	y-axis	45-deg. axis
$\dot{\varepsilon}_{11}$	16	260	50
$\dot{\varepsilon}_{22}$	520	180	85
$\dot{\varepsilon}_{45}$	-	-	230

3.4 Impact on Angle-Ply Boron/Epoxy Laminates

An angle-ply $[0_2/\pm 45]_{2s}$ boron/epoxy plate of dimensions 24.8 cm x 22.2 cm (9.75 in. x 8.75 in.) was prepared and tested (Spec. No. 9BA-1). The specimen was instrumented with surface strain gages according to the gage layout of Fig. 3. It was impacted with 7.9 mm (5/16 in.) diameter Silastic spheres at 210 ms^{-1} (690 ft/sec).

Figure 28 shows signals of gages on the y-axis (0-deg. fiber direction). The gages in the y-direction respond primarily to the flexural wave and those in the x-direction to the in-plane wave. Measured propagation velocities of these waves are:

$$c_{yyLI} = 6{,}950 \text{ ms}^{-1} \text{ (273,700 in/sec)}$$

$$c_{yyLF} = 1{,}890 \text{ ms}^{-1} \text{ (74,600 in/sec)}$$

Theoretical values for these velocities are:

$$c_{yyLI} = \sqrt{\frac{E_{yy}}{\rho(1-\nu_{xy}\nu_{yx})}} = 7{,}750 \text{ ms}^{-1} \text{ (305,000 in/sec)}$$

$$c_{yyLF} \cong \sqrt{\frac{G_{yz}}{\rho}} \cong \sqrt{\frac{G_{12}}{\rho}} = 1{,}650 \text{ ms}^{-1} \text{ (65,000 in/sec)}$$

The reason for the lower theoretical value in the flexural velocity is that the transverse shear modulus G_{yz} is higher than the in-plane shear modulus.

Figure 29 shows strain gage signals on the x-axis. The gages in the y-direction respond primarily to the in-plane wave along the x-axis, those in the x-direction respond primarily to the flexural wave along the x-axis. Measured propagation velocities of these waves are:

$$c_{xxLI} = 3{,}510 \text{ ms}^{-1} \text{ (138,100 in/sec)}$$

$$c_{xxLF} = 1{,}890 \text{ ms}^{-1} \text{ (74,300 in/sec)}$$

Theoretical values for these velocities are:

$$c_{xxLI} = \sqrt{\frac{E_{xx}}{\rho(1-\nu_{xy}\nu_{yx})}} \cong 3{,}310 \text{ ms}^{-1} \text{ (130,200 in/sec)}$$

$$c_{xxLF} = \sqrt{\frac{G_{xz}}{\rho}} \cong \sqrt{\frac{G_{12}}{\rho}} = 1{,}650 \text{ ms}^{-1} \text{ (65,000 in/sec)}$$

The discrepancies are most likely due to the uncertainty about the exact values of the elastic constants involved.

Figure 30 shows strain gage signals on the 45-deg. axis. All gages show a small in-plane precursor wave followed by a much more pronounced flexural wave. The in-plane strains are positive in the x-direction and 45-deg. direction and negative in the y-direction. Measured velocities of these two waves are:

$$c_{45LI} = 6{,}230 \text{ ms}^{-1} \text{ (245,200 in/sec)}$$

$$c_{45LF} = 1{,}770 \text{ ms}^{-1} \text{ (69,600 in/sec)}$$

Theoretical values for these velocities are:

$$c_{45LI} = \sqrt{\frac{E_{45}}{\rho(1-\nu_{45}\nu_{-45})}} \cong 5{,}850 \text{ ms}^{-1} \text{ (230,000 in/sec)}$$

$$c_{45LF} = \sqrt{\frac{G_{45/z}}{\rho}} \cong \sqrt{\frac{G_{12}}{\rho}} = 1{,}650 \text{ ms}^{-1} \text{ (65,000 in/sec)}$$

The discrepancies are most likely due to the uncertainty about the exact values of the elastic constants involved.

Maximum strain rates were measured from the various strain gage signals. Average values of these strain rates are tabulated below:

Table 7

MAXIMUM STRAIN RATES IN $[0_2/\pm45]_{2s}$ BORON/EPOXY SPECIMEN UNDER NORMAL IMPACT, (ε/sec)

Strain Rate	Gage Location		
	x-axis	y-axis	45-deg axis
$\dot{\varepsilon}_{xx}$	340	67	310
$\dot{\varepsilon}_{yy}$	14	170	120
$\dot{\varepsilon}_{45}$	-	-	380

Peak strains measured from the various strain gage signals are tabulated below:

Table 8

PEAK STRAINS IN $[0_2/\pm45]_{2s}$ BORON/EPOXY SPECIMEN UNDER NORMAL IMPACT, ($\mu\varepsilon$)

Strain	Gage Location		
	x-axis	y-axis	45-deg axis
ε_{xx}	3,700	-2,050	2,500
ε_{yy}	-600	2,000	-660
ε_{45}	-	-	2,500

A second 16-ply $[0_2/\pm45]_{2s}$ boron/epoxy specimen (No. 9BA-2) was prepared with surface and embedded gages according to the gage layout of Fig. 4. The instrumented specimen was impacted as the other specimen before. Strain gage signals on the top (impacted), back and middle surfaces of the laminates were recorded and analyzed.

The wave propagation velocities were close to those measured with the surface instrumented specimen No. 9BA-1. The measured values of these velocities averaged for all tests on the two specimens tested are tabulated in Table 9 and compared with calculated values. The discrepancies between measured and calculated values in the in-plane wave velocities are probably due to the fact that the measured time intervals in the records are too short to be measured with accuracy. The measured flexural wave velocities are different in different directions and higher than the calculated value which is based on an approximate value for the transverse shear moduli equal to G_{12}. The wave velocity c_{yyT} along the direction of half of the fibers is higher than c_{xxT} in the transverse to the surface fiber direction.

Peak strains, measured at various stations both on the outer surfaces and in the middle surface, are tabulated in Table 3-10. The in-plane components of strain are in general less than 10 percent of the flexural ones.

As can be seen from Tables 7, 8 and 10, the strain rates and peak strains in the x-direction on the x-axis are higher than those in the y-direction on the y-axis. This difference was much more pronounced in the case of the unidirectional specimens, as discussed before. This difference could be explained roughly by assuming nearly isotropic propagation of energy through the flexural wave and that this energy is roughly proportional to $\int E_{xx}\, \varepsilon_{xx}^2\, dt$ in the x-direction and $\int E_{yy}\, \varepsilon_{yy}^2\, dt$ in the y-direction. Assuming further the same time variation of the pulse in both directions one would obtain

$$\frac{\varepsilon_{xx}}{\varepsilon_{yy}} \cong \sqrt{\frac{E_{yy}}{E_{xx}}} \cong 2.35$$

Table 9

WAVE PROPAGATION VELOCITIES IN NORMALLY IMPACTED $[0_2/\pm 45]_{2s}$ BORON/EPOXY SPECIMEN

Velocity Direction and Type of Wave	Velocity, ms^{-1} (in/sec)	
	Measured	Calculated
c_{xxLI}	3,520 (138,400)	3,310 (130,200)
c_{yyLI}	6,970 (274,400)	7,750 (305,000)
c_{45LI}	6,230 (245,200)	5,850 (230,000)
$c_{xx\,LF}$	1,810 (71,400)	1,650 (65,000)
$c_{yy\,LF}$	1,900 (74,800)	1,650 (65,000)
$c_{45\,LF}$	1,770 (69,600)	1,650 (65,000)

Table 10

PEAK DYNAMIC STRAINS IN NORMALLY IMPACTED $[0_2/\pm45]_{2s}$ BORON/EPOXY SPECIMEN

Strain (με)	Gage Location, (cm)		
	x	y	Surface
ε_{xx} = 3900	2.54	0	Front
-1560	-5.08	0	Front
600	7.62	0	Front
-3850	2.54	0	Back
1560	-5.08	0	Back
-730	7.62	0	Back
-62	-5.08	0	Middle
-18	7.62	0	Middle
ε_{yy} = -750	2.54	0	Front
-75	-5.08	0	Front
-38	7.62	0	Front
820	2.54	0	Back
-47	7.62	0	Back
ε_{xx} = 2360	0	2.54	Front
-360	0	-5.08	Front
-170	0	7.62	Front
-2580	0	2.54	Back
-240	0	7.62	Back
-280	0	-5.08	Middle
-180	0	7.62	Middle
ε_{yy} = 2100	0	2.54	Front
1380	0	-5.08	Front
-620	0	7.62	Front
-2000	0	2.54	Back
890	0	7.62	Back
150	0	-5.08	Middle
78	0	7.62	Middle

This is only a rough approximation since it does not account for the different stress biaxiality in the two directions and the non-uniform distribution of kinetic energy. The latter would tend to reduce the predicted ratio of peak strains above and bring it closer to the actually measured ratio of peak strains.

The attenuation characteristics of the various pulses along the various directions appear to be different. The flexural ε_{yy} strain shows the lowest attenuation along the y-axis (direction of outer fibers). This attenuation is appreciably lower than that of the ε_{xx} flexural strain along the x-axis.

3.5 Impact on Angle-Ply Graphite/Epoxy Laminate

An angle-ply $[0_2/\pm 45]_{2s}$ graphite/epoxy plate of dimensions 24.8 cm x 22.2 cm (9.75 in. x 8.75 in.) was prepared and tested as before (Spec. No. 9GA-1). The specimen was first instrumented with surface strain gages as in the case of the unidirectional specimen. It was impacted with 7.9 mm (5/16 in.) diameter Silastic spheres at velocities of 91 ms^{-1} (300 ft/sec) and 122 ms^{-1} (400 ft/sec).

Figure 31 shows signals of gages on the y-axis. The gages in the y-direction respond primarily to the flexural wave and those in the x-direction to the in-plane wave. Measured propagation velocities of these waves are:

$$c_{yyLI} = 7{,}110 \text{ ms}^{-1} \text{ (280,000 in/sec)}$$

$$c_{yyLF} = 1{,}740 \text{ ms}^{-1} \text{ (68,400 in/sec)}$$

Calculated values for these velocities are:

$$c_{yyLI} = \sqrt{\frac{E_{yy}}{\rho(1-\nu_{xy}\nu_{yx})}} = 8{,}520 \text{ ms}^{-1} \text{ (335,000 in/sec)}$$

$$c_{yyLF} = \sqrt{\frac{G_{yz}}{\rho}} \cong \sqrt{\frac{G_{12}}{\rho}} = 1{,}990 \text{ ms}^{-1} \text{ (78,300 in/sec)}$$

The observed discrepancies may be due to the uncertainty about the exact values of the elastic constants.

Figure 32 shows strain gage signals on the x-axis. The gages in the y-direction respond primarily to the in-plane wave along the x-axis, those in the x-direction respond primarily to the flexural wave along the x-axis. Measured propagation velocities of these waves are:

$$c_{xxLI} = 3{,}150 \text{ ms}^{-1} \text{ (124,000 in/sec)}$$

$$c_{xxLF} = 1{,}335 \text{ ms}^{-1} \text{ (52,600 in/sec)}$$

Theoretical values for these velocities, based in part on computed or approximated values of the elastic constants are:

$$c_{xxLI} = \sqrt{\frac{E_{xx}}{\rho(1-\nu_{xy}\nu_{yx})}} \cong 2{,}540 \text{ ms}^{-1} \text{ (100,000 in/sec)}$$

$$c_{xxLF} = \sqrt{\frac{G_{xz}}{\rho}} \cong \sqrt{\frac{G_{12}}{\rho}} = 1{,}990 \text{ ms}^{-1} \text{ (78,300 in/sec)}$$

The discrepancies observed are probably due to the uncertainty about the exact values of the elastic constants.

Figure 33 shows strain gage signals on the 45-degree axis. The gages in the y-direction show the influence of the in-plane wave. Measured wave propagation velocities are:

$$c_{45LI} = 5{,}880 \text{ ms}^{-1} \text{ (230,000 in/sec)}$$

$$c_{45LF} = 1{,}370 \text{ ms}^{-1} \text{ (53,900 in/sec)}$$

Theoretical values for these velocities are:

$c_{45LI} \cong 6{,}240\ ms^{-1}$ (246,000 in/sec)

$c_{45LF} \cong 1{,}990\ ms^{-1}$ (78,300 in/sec)

The same specimen above was subsequently instrumented with additional surface gages on the other side located exactly opposite the original set of gages. A series of tests was conducted with the gages on opposite faces of the plate recorded individually in pairs as shown in Figs. 34 and 35. These signals confirm the fact that the primary pulse propagating in the plate is a pure flexural pulse. The only evidence of an in-plane precursor wave appears in Fig. 34d (gages in x-direction on the y-axis) and in Fig. 35b (gages in y-direction on the x-axis). To isolate the pure flexural component of the pulse the algebraic differences of the gage signals were recorded directly as shown in Figs. 36 and 37. To obtain the pure in-plane components of the pulse the gages at each station on opposite faces of the specimen were connected in series for recording. Figures 38 and 39 show the records obtained. The measured in-plane wave velocities are:

$c_{xxLI} = 3{,}630\ ms^{-1}$ (143,000 in/sec)

$c_{yyLI} = 8{,}380\ ms^{-1}$ (330,000 in/sec)

The same specimen was subsequently loaded obliquely by rotating it by 45-deg. first about the x-axis and recording the gages on the y-axis and then rotating it about the y-axis and recording the gages on the x-axis. The signals of Figs. 40 and 41 show that the in-plane contribution of the oblique impact is very small, as in the case of normal impact. The primary pulse is again the flexural one.

The measured wave propagation velocities in the various tests above are tabulated in Table 11 and compared with calculated

Table 11

WAVE PROPAGATION VELOCITIES IN TRANSVERSELY IMPACTED $[0_2/\pm45]_{2s}$ GRAPHITE/EPOXY SPECIMEN

Velocity Direction and Type of Wave	Velocity ms^{-1} (in/sec)	
	Measured	Calculated
c_{xxLI}	3,390 (133,500)	2,540 (100,000)
c_{yyLI}	7,750 (305,000)	8,520 (335,000)
c_{45LI}	5,880 (230,000)	6,240 (246,000)
c_{xxLF}	1,335 (52,600)	1,990 (78,300)
c_{yyLF}	1,740 (68,400)	1,990 (78,300)
c_{45LF}	1,370 (53,900)	1,990 (78,300)

values. The discrepancies between measured and calculated values in the in-plane wave velocities are partly due to the fact that the measured time intervals in the records are too short to be measured with accuracy and partly due to some uncertainty about the exact elastic constants used in the computations. The measured flexural wave velocities are different in different directions and lower than the calculated value which is based on an approximate value for the transverse shear moduli equal to G_{12}. The wave velocity c_{yyLF} along the direction of the surface fibers is appreciably higher than c_{xxLF} in the transverse direction.

Maximum strain rates were measured from the various strain gage signals at stations 2.54 cm (1 in.) from the point of impact. Average values of these strain rates are tabulated below:

Table 12

MAXIMUM STRAIN RATES IN $[0_2/\pm45]_{2s}$ GRAPHITE/EPOXY SPECIMEN UNDER NORMAL IMPACT (ε/sec)

Strain Rate	Gage Location		
	x-axis	y-axis	45-deg. axis
$\dot{\varepsilon}_{xx}$	-610	-73	350
$\dot{\varepsilon}_{yy}$	-10	400	-17
$\dot{\varepsilon}_{45}$	-	-	230

The peak strains recorded on one side of the plate at the same stations 2.54 cm (1 in.) from the point of impact are tabulated as follows:

Table 13

PEAK STRAINS IN $[0_2/\pm45]_{2s}$ GRAPHITE/EPOXY SPECIMEN UNDER NORMAL IMPACT ($\mu\varepsilon$)

Strain	Gage Location		
	x-axis	y-axis	45-deg. axis
ε_{xx}	2600	-1600	2200
ε_{yy}	-330	980	-400
ε_{45}	-	-	1260

As in the case of the boron/epoxy specimen before, the peak strains (and strain rates) in the x-direction on the x-axis are higher than those in the y-direction on the y-axis.

Pure flexural strains were determined from the algebraic differences of the gage signals of Figs. 36 and 37. In-plane strains were determined from the algebraic sums of the gage signals of Figs. 38 and 39. Peak flexural and in-plane strains measured at stations 2.54 cm (1 in.) from the point of impact are compared in Table 14 below:

Table 14

PEAK FLEXURAL AND IN-PLANE STRAINS IN $[0_2/\pm45]_{2s}$ GRAPHITE/EPOXY SPECIMEN UNDER NORMAL IMPACT ($\mu\varepsilon$)

Gage Location	Strain	Flexural	In-Plane
x-axis	ε_{xx}	2600	80
	ε_{yy}	330	-30
y-axis	ε_{xx}	1500	-56
	ε_{yy}	960	46

The in-plane components range in magnitude from 3 to 9 percent of the flexural components. The radial components of the in-plane pulse (ε_{xx} on x-axis and ε_{yy} on y-axis) are tensile which indicates that the specimen is drawn slightly towards the center due to the high flexural deformation produced at the point of impact.

Peak strains under oblique impact were measured from the records of Figs. 40 and 41. These are compared below with those under normal impact:

Table 15

PEAK STRAINS UNDER NORMAL AND OBLIQUE IMPACT IN $[0_2/\pm45]_{2s}$ GRAPHITE/EPOXY SPECIMEN ($\mu\varepsilon$)

Gage Location	Strain	Normal Impact	Oblique Impact
x-axis	ε_{xx}	2600	1090
y-axis	ε_{yy}	980	435

These strains are 42 to 45 percent of the corresponding strains under normal impact. If the total impact force were the same under oblique and normal impact, then the obliquity would produce a normal force component equal to sin 45° = 0.707 of the force under normal impact. This corresponds to change in linear momentum. Change in kinetic energy would yield an apparent force component equal to $(\sin 45°)^2 = 0.5$. The measured strains appear to correlate better with the change in kinetic energy.

3.6 Residual Properties of Impacted Boron/Epoxy Laminates

Unidirectional $[0_{16}]$ and angle-ply $[0_2/\pm45]_{2s}$ boron/epoxy plates were subjected to a single impact at one point with a 7.9 mm (5/16 in.) diameter Silastic sphere at a velocity of 210 ms^{-1} (690 ft/sec). Ultrasonic C-scans taken of the specimens

before and after impact did not reveal any differences, although the unidirectional specimen showed clear evidence of transverse failure at the point of impact.

Coupons were machined from the impacted specimens around the points of impact. One specimen was taken around each point of impact for each of the two principal material directions of the laminate. These coupons were tabbed, instrumented with strain gages, and tested statically to failure. A similar set of specimens was prepared from similar undamaged laminates and tested statically to failure. Stress-strain curves for each pair of specimens are shown in Figs. 42 to 45. Results are tabulated in Table 16.

The only significant effect of the single impact was on the transverse strength of the unidirectional laminate. The strength was reduced from the initial value of 61 MPa (8.8 ksi) to 8.6 MPa (1.25 ksi) after impact. This was accompanied by a slight reduction in modulus. The unidirectional laminate in the fiber direction showed also a slight reduction in modulus, which may not be significant, however. The $[0_2/\pm 45]_{2s}$ laminate showed a small, approximately 6 percent, reduction in strength at 90-degrees to the 0-deg. fibers possibly due to some transverse to the fibers damage. The modulus and Poisson's ratio remained unchanged.

3.7 Residual Properties of Impacted Graphite/Epoxy Laminates

The material used in these tests was a new batch of graphite/epoxy which is said to have properties similar to Modmor I/ERLA 4617 which was no longer available. This material is HM-S graphite/Code 69 resin supplied by Fothergill and Harvey Ltd. Unidirectional $[0_{16}]$ and angle-ply $[0_2/\pm 45]_{2s}$ plates of this material were subjected to a single impact at one point with a 7.9 mm (5/16 in.) diameter Silastic sphere at a velocity of 192 ms^{-1} (630 ft/sec). Ultrasonic C-scans taken of the specimens before

Table 16

COMPARISON OF INITIAL AND RESIDUAL PROPERTIES OF BORON/EPOXY LAMINATES IMPACTED WITH 7.9 mm (5/16 in) SILASTIC SPHERES AT 210 ms^{-1} (690 ft/sec)

Laminate	Initial Properties			Residual Properties		
	Strength, S MPa (ksi)	Modulus, E GPa (10^6 psi)	Poisson's Ratio ν	Strength S MPa (ksi)	Modulus E GPa (10^6 psi)	Poisson's Ratio ν
$[0_{16}]$	1403 (203)	218 (31.7)	0.18	1459 (211)	214 (31.0)	0.17
$[90_{16}]$	61 (8.8)	22.2(3.22)	0.013	8.6 (1.25)	21.3 (3.08)	0.012
$[0_2/\pm45]_{2s}$	753 (109)	124 (17.9)	0.61	773 (112)	124 (17.9)	0.60
$[90_2/\pm45]_{2s}$	101 (14.6)	39 (5.7)	0.18	95 (13.7)	39 (5.7)	0.18

and after impact did not reveal any differences, although the unidirectional specimen showed some evidence of transverse failure at the point of impact.

Coupons were machined from the impacted specimens around the points of impact. One specimen was taken around each point of impact along each of the two principal material directions of the laminate. These coupons were tabbed, instrumented with strain gages and tested statically to failure. A similar set of specimens prepared from similar non-impacted (undamaged) laminates was tested for comparison purposes. Stress-strain curves for each pair of specimens are shown in Figs. 46 to 49. Results are tabulated in Table 17.

The most significant effect of the single impact tests is on the transverse strength of the unidirectional laminate. The strength was reduced from the initial value of 26 MPa (3.7 ksi) to one-tenth that value after impact. The unidirectional laminate in the fiber direction showed also some reduction in strength and modulus. The angle-ply laminate did not show any significant changes in strength and modulus after impact.

3.8 Impact Dynamics

A series of tests using a moderately high speed camera (Fastax) was conducted to characterize the impact energetics. Impact tests for various gun chamber pressures were conducted on all four types of specimens, boron/epoxy and graphite/epoxy, unidirectional and angle-ply. The Silastic projectile was photographed during its approach and rebound from the specimen with a Fastax 16 mm camera operating at rates between 7100 and 7460 frames per second. Two sequences of frames for incident velocities of 250 ms^{-1} (820 ft/sec) and 192 ms^{-1} (630 ft/sec) are shown in Figs. 50 and 51. The relative magnitudes of incident and rebound velocities are clearly

Table 17

COMPARISON OF INITIAL AND RESIDUAL PROPERTIES OF GRAPHITE/EPOXY LAMINATES IMPACTED WITH 7.9 mm (5/16 in.) SILASTIC SPHERES AT 192 ms^{-1} (630 ft/sec)

Laminate	Initial Properties			Residual Properties		
	Strength, S MPa (ksi)	Modulus, E GPa (10^6 psi)	Poisson's Ratio ν	Strength, S MPa (ksi)	Modulus, E GPa (10^6 psi)	Poisson's Ratio ν
$[0_{16}]$	1308 (190)	203 (29.5)	0.31	1178 (171)	197 (28.6)	0.21
$[90_{16}]$	26 (3.7)	8.3 (1.2)	0.015	2.6(0.38)	8.3 (1.2)	-
$[0_2/\pm45]_{2s}$	696 (101)	110 (16.0)	0.68	667 (97)	108 (15.7)	0.69
$[90_2/\pm45]_{2s}$	172 (25)	30 (4.4)	0.22	184 (27)	28 (4.1)	0.21

visible in these records. Graphic plots of projectile distance from the specimen versus frame number (or time) were obtained from the photographic records (Figs. 52 to 59). Incident and rebound velocities were computed from these graphs. Chamber pressure was plotted versus incident and rebound velocity (Fig. 60). This relationship between chamber pressure and incident velocity is more accurate than the one described before, because of the purely optical method used in this case. The rebound velocity seems to be relatively independent of the type of specimen used probably because the flexural stiffnesses of the various plates are not too far apart. The energy imparted on the specimen was computed as the change in the kinetic energy of the projectile.

$$E = \frac{1}{2} m (v_i^2 - v_r^2)$$

where

E = energy
m = projectile mass
v_i, v_r = incident and rebound velocities, respectively

The imparted energy, like the rebound velocity, was independent of the type of specimen used. The variation of this energy with incident velocity is plotted in Fig. 61.

The photographic records described above obtained with the Fastax camera did not have sufficient detail to yield information on the projectile contact area and contact time. A new series of tests using a high-speed Beckman and Whitley Model 189 framing camera was conducted to characterize further the impact of the projectile on the composite plates. This camera is capable of recording twenty-five 35 mm images at rates up to 1,250,000 frames/second by means of a rotating mirror, 25 pairs of relay lenses and a stationary strip of film. Shuttering is accomplished by means

of diamond stops, one located at the objective lens, and the other between each pair of refocusing lenses. With the normal apertures employed here, the exposure duration is one third the interframe time. Illumination was provided by an electronic light source prepared for the purpose. This source employs a xenon flash lamp (GE Model FT 220). The system provides for variable duration of illumination. Kodak 2479 RAR film was used and developed in D-19 developer.

A sequence of frames taken at a rate of 85,700 frames per second and showing the impact and rebound phenomenon is shown in Fig. 62. The projectile in this figure is impacting a $[0_2/\pm 45]_{2s}$ boron/epoxy plate at a velocity of 180 ms^{-1} (590 ft/sec). The impacting projectile gives the appearance of a splashing drop of water with a rapid increase in contact area. The contact area as a function of time is plotted in Fig. 63. The projectile is completely flattened within approximately 70 μs after impact reaching a maximum contact area of 3.25 cm^2 (0.5 in^2). The maximum contact radius at this point is 20.3 mm (0.80 in.) which is more than two and one-half times the diameter of the undeformed projectile. The total contact time is longer than 300 μs. The force and pressure distributions associated with this impact cannot be determined from the photographic records alone. It can be said, however, that the peak contact pressure occurs between 0 and 70 μs after initial contact.

A similar photographic record was obtained for a higher incident velocity, 242 ms^{-1} (794 ft/sec) (Fig. 64). The variation of contact area with time is shown in Fig. 65. The time to peak contact area is shorter than before (approximately 50 μs), however, there is a longer dwell time during which the area is near the maximum and the projectile is nearly flat.

4.0 SUMMARY, CONCLUSIONS AND RECOMMENDATIONS FOR FUTURE WORK

Stress wave propagation in composite laminates under projectile impact was studied experimentally. Two materials were investigated, boron/epoxy and graphite/high modulus epoxy. Sixteen-ply unidirectional $[0_{16}]$ and angle-ply $[0_2/\pm45]_{2s}$ laminates were used. The specimens were ultrasonically scanned before instrumentation and testing. They were instrumented with surface and embedded gages. An air gun system was designed and built for propelling projectiles on the specimens. It consists of a pressure chamber and a smooth-bore gun barrel of 7.9 mm (5/16 in.) inside diameter. The specimens were impacted with silicon rubber (Silastic) spheres at velocities up to 250 ms^{-1} (820 ft/sec). Impact velocities were kept below the immediate damage threshold for the various specimens. Tests under normal and 45-degree oblique impact were conducted. Wave propagation characteristics were studied by recording the strain gage signals at various stations. These records were analyzed to determine the types of wave, propagation velocities, peak strains, strain rates and attenuation characteristics.

Unidirectional boron/epoxy specimens were impacted with Silastic projectiles at velocities of 192 ms^{-1} (630 ft/sec) and 210 ms^{-1} (690 ft/sec). The predominant wave induced was a flexural wave propagating at somewhat different velocities along the different directions contrary to the theoretical prediction of isotropic propagation.[5,6] This is because of the inhomogeneous nature of the plate which makes the various transverse shear moduli different in different directions. Experimental results indicate that the flexural wave propagation velocity is direction-dependent and it decreases from the maximum value of 2,120 ms^{-1} (86,360 in/sec) in the fiber direction to 1,750 ms^{-1} (68,790 in/sec) in the transverse to the fiber direction. The theoretical value in the fiber direction is much lower, 1650 ms^{-1} (65,000 in/sec) because it approximates the transverse shear modulus G_{13} with the lower

in-plane shear modulus G_{12}. A low amplitude in-plane precursor wave was evident in some of the signals. It was most pronounced in the transverse to the fiber direction. The measured velocities of the in-plane wave were higher than the calculated values. The high measured value of c_{11L} is due partly to the fact that the measured time interval was too short to be measured with accuracy and partly due to pulse propagation along the high-modulus fibers themselves at a much higher velocity than the one based on a homogeneous material. The reason for the higher measured value for c_{22L} is that the static value of E_{22} used in the computation of the theoretical value is lower than the dynamic value of E_{22} under impact conditions. The agreement between measured and calculated values of wave propagation was best in the 45-degree direction.

Peak strains were measured at the various stations. The maximum strains measured at a station 2.54 cm (1 in.) from the point of impact were $\varepsilon_{11} = 1400$ με and $\varepsilon_{22} = 2620$ με in the fiber and transverse to the fiber directions, respectively. The difference in these two peak strains can be explained in part assuming nearly isotropic propagation of energy. A similar relationship exists between the two corresponding peak strain rates, $\dot{\varepsilon}_{11} = 340$ ε/sec and $\dot{\varepsilon}_{22} = 640$ ε/sec because the flexural velocites and rise times to peak strain are roughly the same in both directions. Strain gage signals from the top, bottom and middle surfaces of the laminate indicate that the neutral plane coincides with the mid-plane of the plate. The in-plane components of strain were in general lower than 10 percent of the flexural ones. The flexural wave is still the predominant one under oblique 45-degree impact. The peak flexural strains under oblqiue impact range between 36 and 56 percent of those under normal impact. This reduction is accounted for by the reduction of the normal force component and the reduction in the amount of absorbed kinetic energy due to the obliqueness of the impact. An exponential fit for the measured peak strains indicated

that there is appreciable material attenuation of the pulse.

Unidirectional graphite/epoxy specimens were impacted with Silastic projectiles at a velocity of 91 ms^{-1} (300 ft/sec). The flexural wave propagation velocities measured were 1,930 ms^{-1} (76,100 in/sec) and 1,290 ms^{-1} (50,900 in/sec) in the fiber and transverse to the fiber directions, respectively. These values were in good agreement with calculated values based on realistic values for G_{13} and G_{23}. The measured in-plane wave velocity c_{22L}, 2,380 ms^{-1} (93,600 in/sec) is higher than the calculated one probably because the static value of E_{22} used in the computation is lower than the dynamic value under impact conditions.

Peak strains measured at a station 2.54 cm (1 in.) from the point of impact were ε_{11} = 1280 με and ε_{22} = 3900 με. The difference between these two strains is higher than in the case of the boron/epoxy specimen because the modulus ratio E_{11}/E_{22} is higher for the graphite/epoxy. The value of 3900 με is an appreciable fraction of the transverse ultimate strain of the unidirectional material ε_{22T} = 5100 με. It is quite probable that this ultimate strain was exceeded at points closer to the point of impact, resulting in immediate localized damage. This damage, however, was not easily detectable by ultrasonic scanning. Maximum strain rates corresponding to the peak strains above were $\dot{\varepsilon}_{11}$ = 260 ε/sec and $\dot{\varepsilon}_{22}$ = 520 ε/sec.

Angle-ply $[0_2/\pm45]_{2s}$ boron/epoxy specimens were impacted with Silastic projectiles at a velocity of 210 ms^{-1} (690 ft/sec). Along the y-axis (0-deg. fiber direction) gages in the y-direction respond primarily to the flexural wave and those in the x-direction to the in-plane wave. Along the x-axis, gages in the x-direction respond primarily to the flexural wave and those in the y-direction to the in-plane wave. Along the 45-degree axis all strain gage signals show a small in-plane precursor wave followed by a much more pronounced flexural wave. The measured in-plane wave velocities

c_{xxLI}= 3,520 ms^{-1} (138,400 in/sec) and c_{yyLI}= 6,970 ms^{-1} (274, 400 in/sec) are close to the calculated values. The flexural wave velocity in the direction of the outer fibers, c_{yyLF}= 1,900 ms^{-1} (74,800 in/sec), is a little higher than that in the transverse direction, c_{xxLF}= 1,810 ms^{-1} (71,400 in/sec). Both of these measured values are higher than the calculated value of 1,650 ms^{-1} (65,000 in/sec) based on an approximation of transverse shear moduli with G_{12}.

Peak strains measured at a station 2.54 cm (1 in.) from the point of impact were ε_{xx} = 3900 με and ε_{yy} = 2100 με. Assuming isotropic energy propagation, a rough estimate of the ratio of these two strains equal to $\frac{\varepsilon_{xx}}{\varepsilon_{yy}} \cong \sqrt{\frac{E_{yy}}{E_{xx}}} \cong 2.35$ was predicted. This estimate does not take into account the different stress biaxiality in the two directions and the nonuniform distribution of kinetic energy. The latter would tend to reduce the predicted ratio above and bring it closer to the actually measured ratio of peak strains. The attenuation characteristics are different in different directions. The flexural ε_{yy} strain shows the lowest attenuation along the y-axis, much lower than that of the ε_{xx} flexural strain along the x-axis.

Angle-ply $[0_2/\pm45]_{2s}$ graphite/epoxy specimens were impacted with Silastic projectiles at velocities of 91 ms^{-1} (300 ft/sec) and 122 ms^{-1} (400 ft/sec). As in the case of the boron/epoxy specimen above, along the two principal material axes the radial gages respond primarily to the flexural wave and circumferential gages respond primarily to the in-plane wave along the respective radial direction. Measured in-plane wave velocities were c_{xxLI}= 3,390 ms^{-1} (133,500 in/sec) and c_{yyLI}= 7,750 ms^{-1} (305,000 in/sec) which are somewhat different from predicted values because of some uncertainty in the elastic constants and some inaccuracies in the measured short time intervals. The measured flexural wave velocities are c_{xxLF}= 1,335 ms^{-1} (52,600 in/sec) and c_{yyLF}= 1,740 ms^{-1}

(68,400 in/sec), which are lower than the calculated value of 1,990 ms^{-1} (78,300 in/sec). The latter was based on approximation of the transverse shear moduli with G_{12}.

Peak strains measured at a station 2.54 cm (1 in.) from the point of impact were ε_{xx} = 2600 με and ε_{yy} = 980 με. The predicted grossly approximate ratio of these strains is $\varepsilon_{xx}/\varepsilon_{yy}$ = 3.35. Measured peak strain rates were $\dot{\varepsilon}_{xx}$ = 610 ε/sec and $\dot{\varepsilon}_{yy}$ = 400 ε/sec. The measured in-plane components of strain range in magnitude between 3 and 9 percent of the flexural components. The radial components of the in-plane strains are tensile, which indicates that the specimen is drawn slightly towards the center due to the high flexural deformation at the point of impact. Peak strains under 45-degree oblique impact are 42 to 45 percent of the corresponding strains under normal impact. This reduction is due to the reduction of the normal component of force and of the portion of absorbed kinetic energy due to the obliqueness of the impact.

Residual elastic properties and strength were measured around the point of impact after a single impact and compared with initial values from unloaded specimens. In the boron/epoxy plates the most significant effect of the single impact was a reduction in the transverse strength of the unidirectional laminate from 61 MPa (8.8 ksi) to 8.6 MPa (1.25 ksi). The $[0_2/\pm45]_{2s}$ laminate showed a small reduction, approximately 6 percent, in strength in the 90-deg. direction. Results were similar for the graphite/epoxy plates. The transverse strength of the unidirectional laminate was reduced from 26 MPa (3.7 ksi) to one-tenth that value after a single impact. The unidirectional laminate also showed some modulus and strength degradation in the fiber direction.

Photographic records of the impacting projectile were taken to characterize the dynamics of impact to some extent.

A series of records taken with a Fastax camera at rates of up to 7460 frames per second was used to determine the incident and rebound velocities of the projectile, hence the energy imparted on the specimen. The rebound velocity, hence the imparted energy, appeared to be relatively independent of the type of laminate used, probably because the flexural stiffnesses of the various plates are close to each other. A second set of high-speed closeup photographic records was obtained with a Beckman and Whitley camera at a speed of 85,700 frames per second. The Silastic projectile gives the appearance of a splashing drop of water and is completely flattened within 50-70 μs. The variation of contact area with time was determined. The maximum contact diameter is more than two and one-half times the diameter of the undeformed projectile. The total contact time is of the order of 300 μs. Increasing the velocity of impact reduces the time of maximum area contact, reduces slightly the total contact time but it increases the dwell time during which the contact area is near maximum.

The scope of the work reported here should be extended to take full advantage of the expertise developed in the course of this investigation. It is proposed to conduct a systematic investigation to study the dynamic deformation, wave propagation, induced damage, and residual elastic and strength properties in composite plates subjected to impact loading as a function of a number of material and loading parameters. It is recommended that materials such as boron/epoxy, graphite/epoxy, S-glass/epoxy, Kevlar 49/epoxy and hybrids thereof be investigated in unidirectional and angle-ply configurations. The materials and hybrids could be graded from the point of view of impact resistance with a view to approaching an optimum hybrid. The effects of parameters such as impact velocity, projectile mass and elasticity and material prestress should also be investigated.

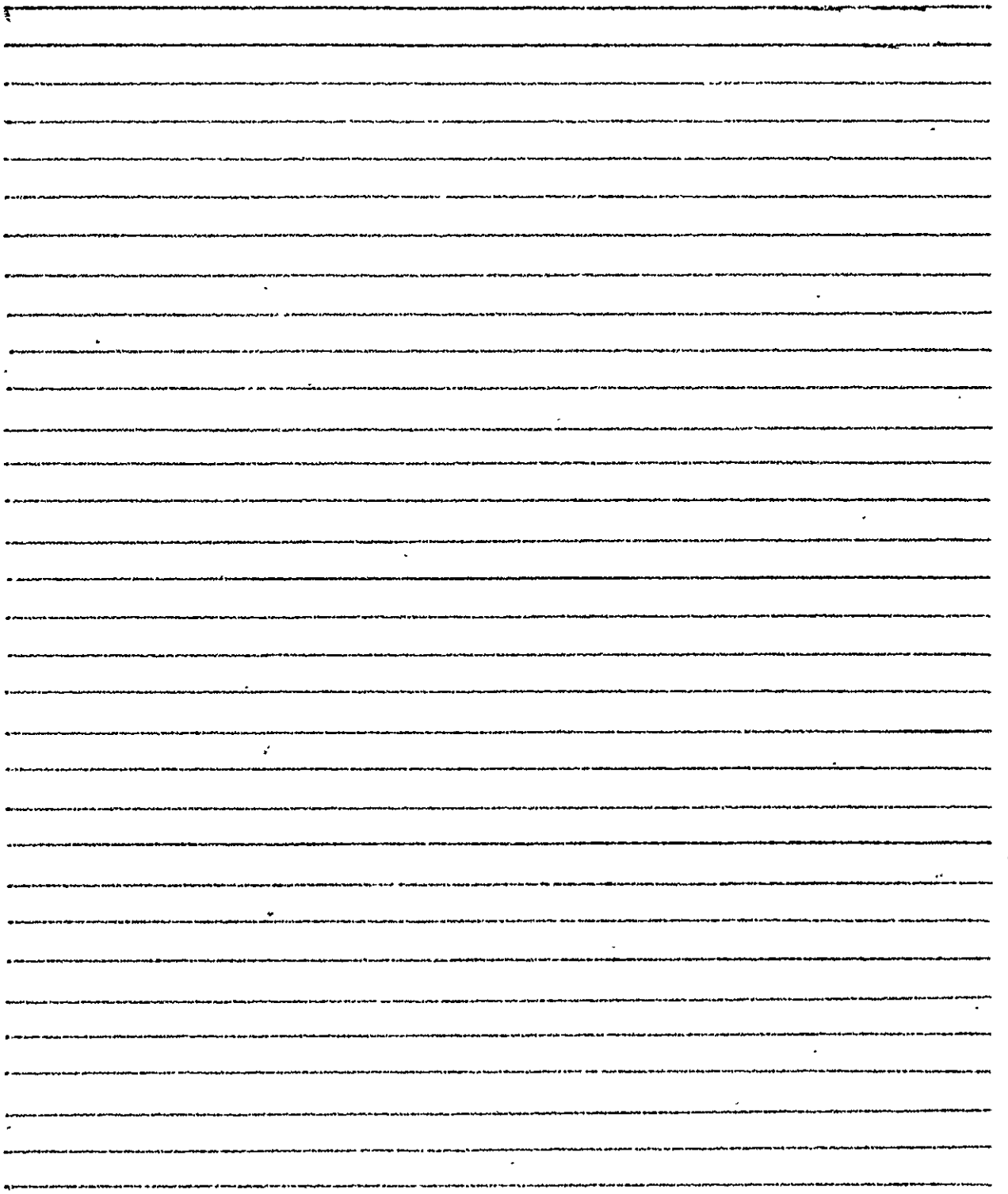

Fig. 1 ULTRASONIC SCAN OF $[0_{16}]$ BORON/EPOXY SPECIMEN BEFORE IMPACT.

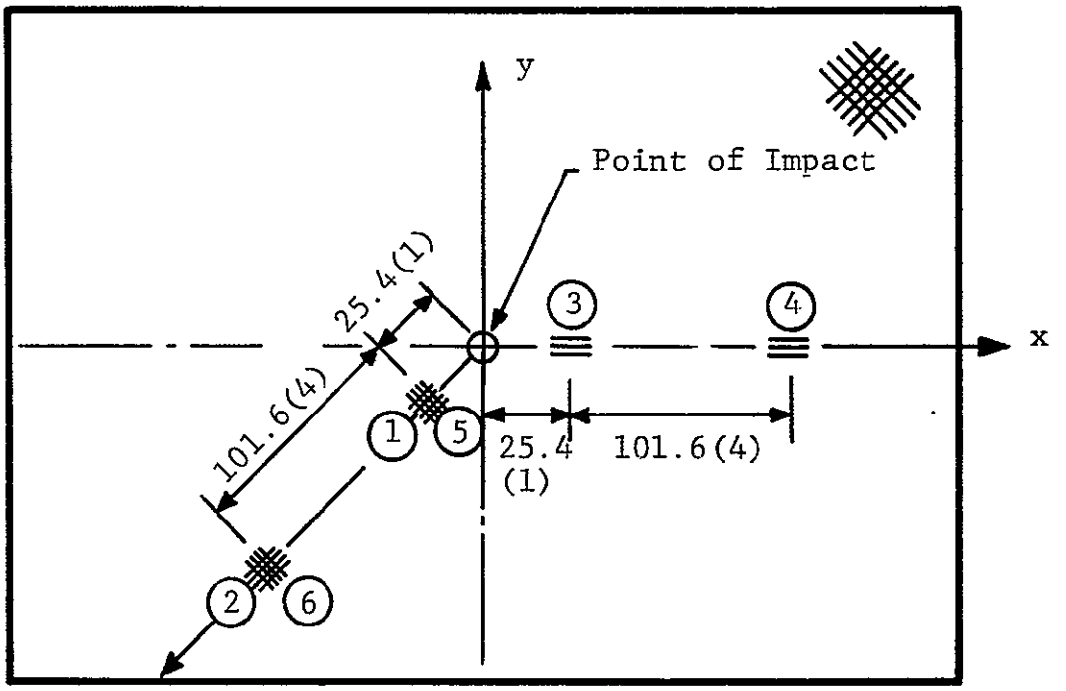

Fig. 2 STRAIN GAGE LAYOUT FOR $[\pm 45/\pm 45]_s$ BORON/ EPOXY SPECIMEN USED FOR PRELIMINARY TESTING (Dimensions are in mm and inches)

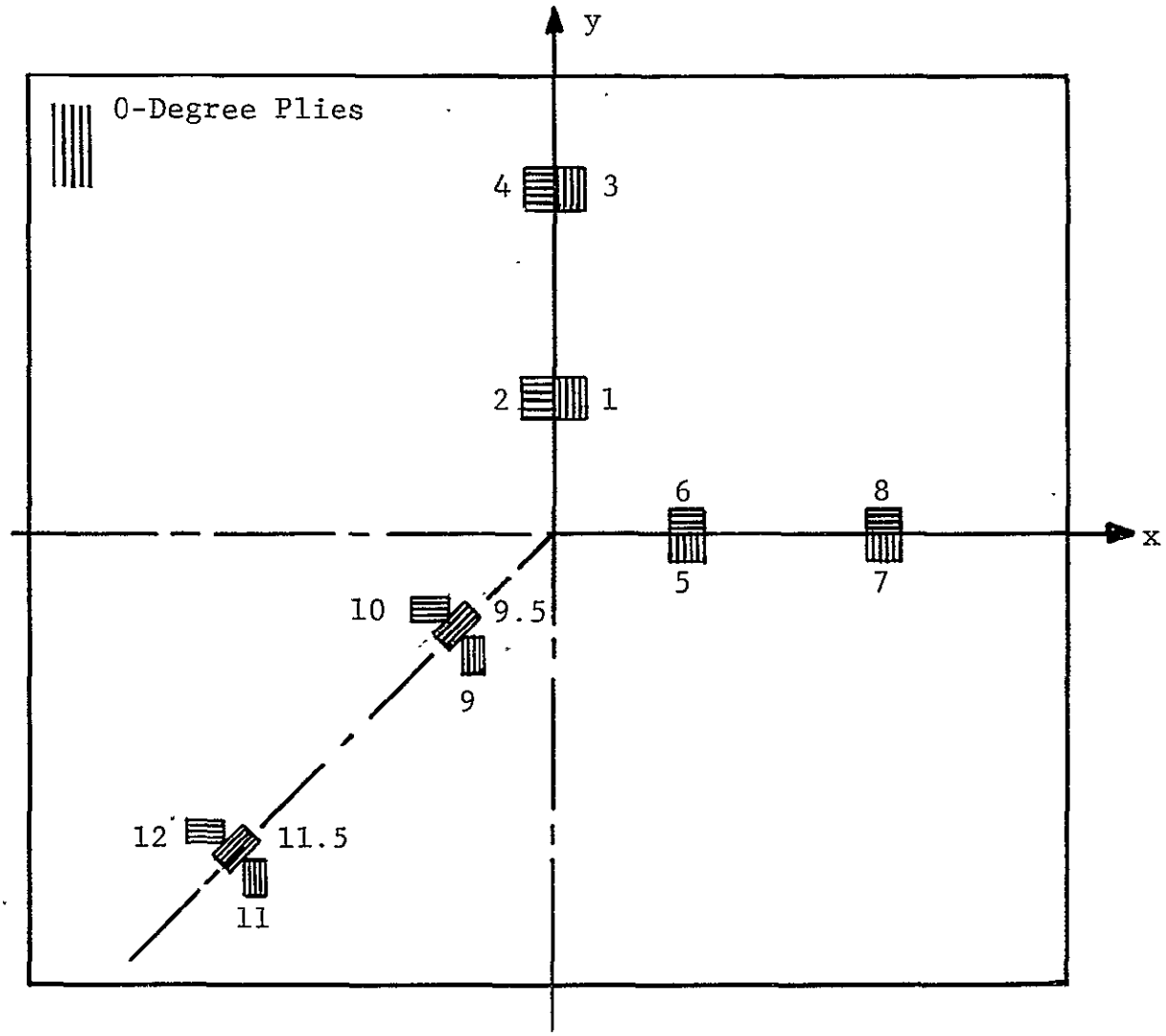

Gage No.	x mm (in)	y mm (in)
1,2	0	25.4(1.00)
3,4	0	76.2(3.00)
5,6	25.4(1.00)	0
7,8	76.2(3.00)	0
9,9.5,10	-18.0(-0.71)	-18.0(-0.71)
11,11.5,12	-71.8(-2.83)	-71.8(-2.83)

Fig. 3 GAGE LAYOUT FOR $[0_{16}]$ AND $[0_2/\pm 45]_{2s}$ BORON/EPOXY AND GRAPHITE EPOXY PLATES

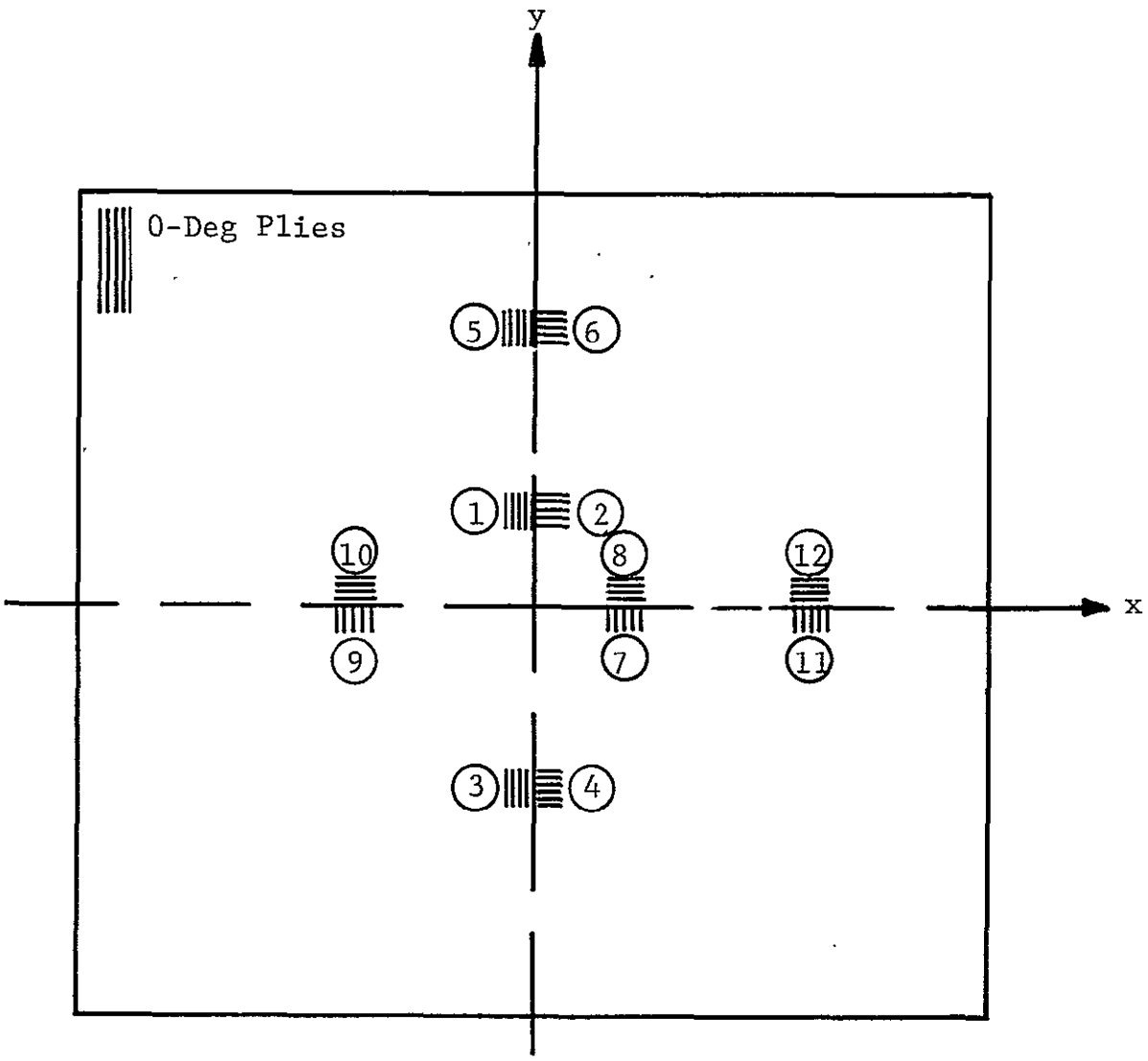

Gage No.	x mm (in)	y mm (in)	Through the Thickness Locations
1,2	0	25.4 (1.00)	Top, Middle and Bottom
3,4	0	-50.8 (2.00)	Top, Middle and Bottom
5,6	0	76.2 (3.00)	Top, Middle and Bottom
7,8	25.4 (1.00)	0	Top, Middle and Bottom
9,10	-50.8 (2.00)	0	Top, Middle and Bottom
11,12	76.2 (3.00)	0	Top, Middle and Bottom

Fig. 4 STRAIN GAGE LAYOUT FOR SPECIMEN WITH SURFACE AND EMBEDDED GAGES

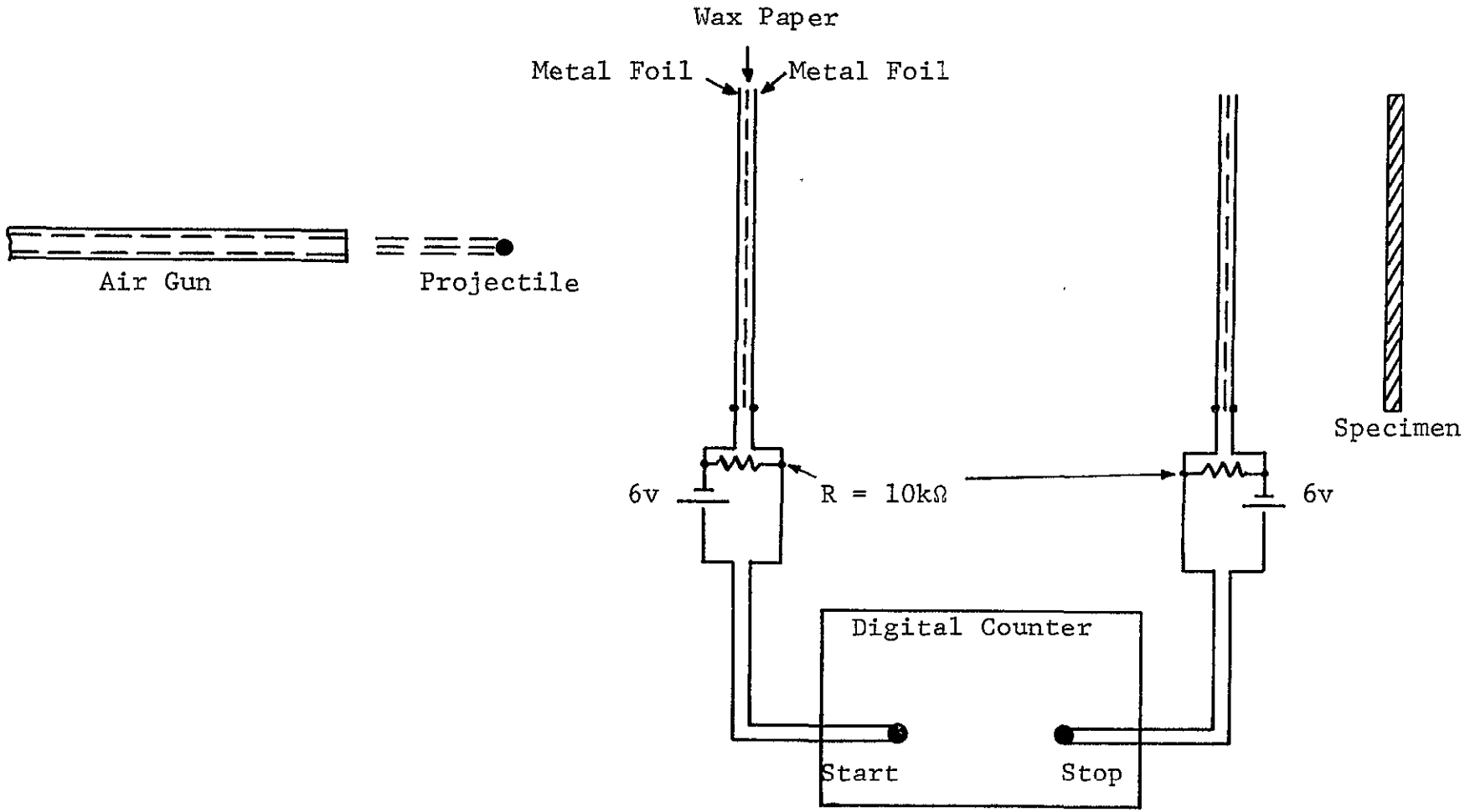

Fig. 5 SCHEMATIC DIAGRAM OF SETUP FOR MEASUREMENT OF PROJECTILE VELOCITY

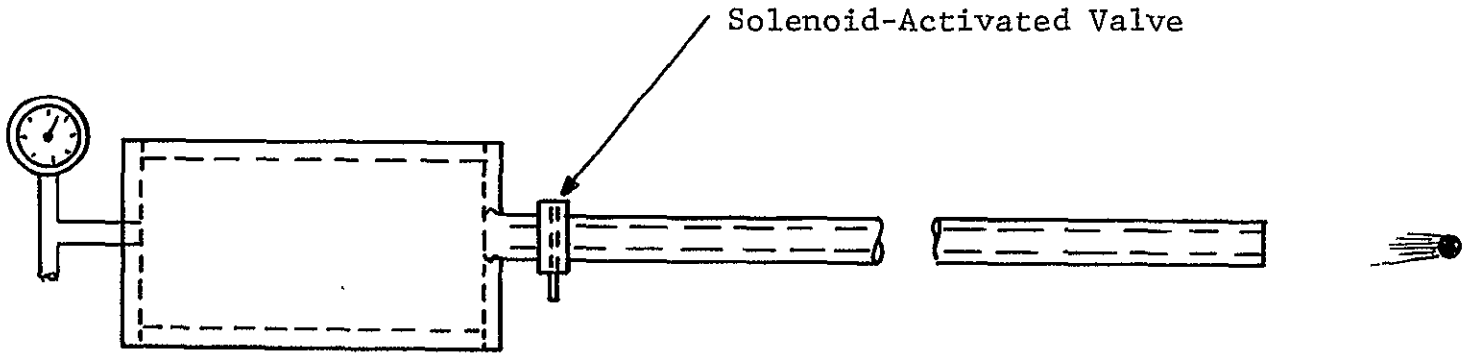

Pressure Chamber	Gun Barrel	RTV Sphere
Diam. = 11.4 cm (4.5 in.)	I.D. = 1.43 cm (9/16 in.)	1.43 cm (9/16 in.) Diam.
Length = 20.3 cm (8 in.)	Length = 180 cm (71 in)	

Fig. 6 AIR GUN FOR PROPELLING 1.43 cm (9/16 in.) DIAMETER RTV SPHERES

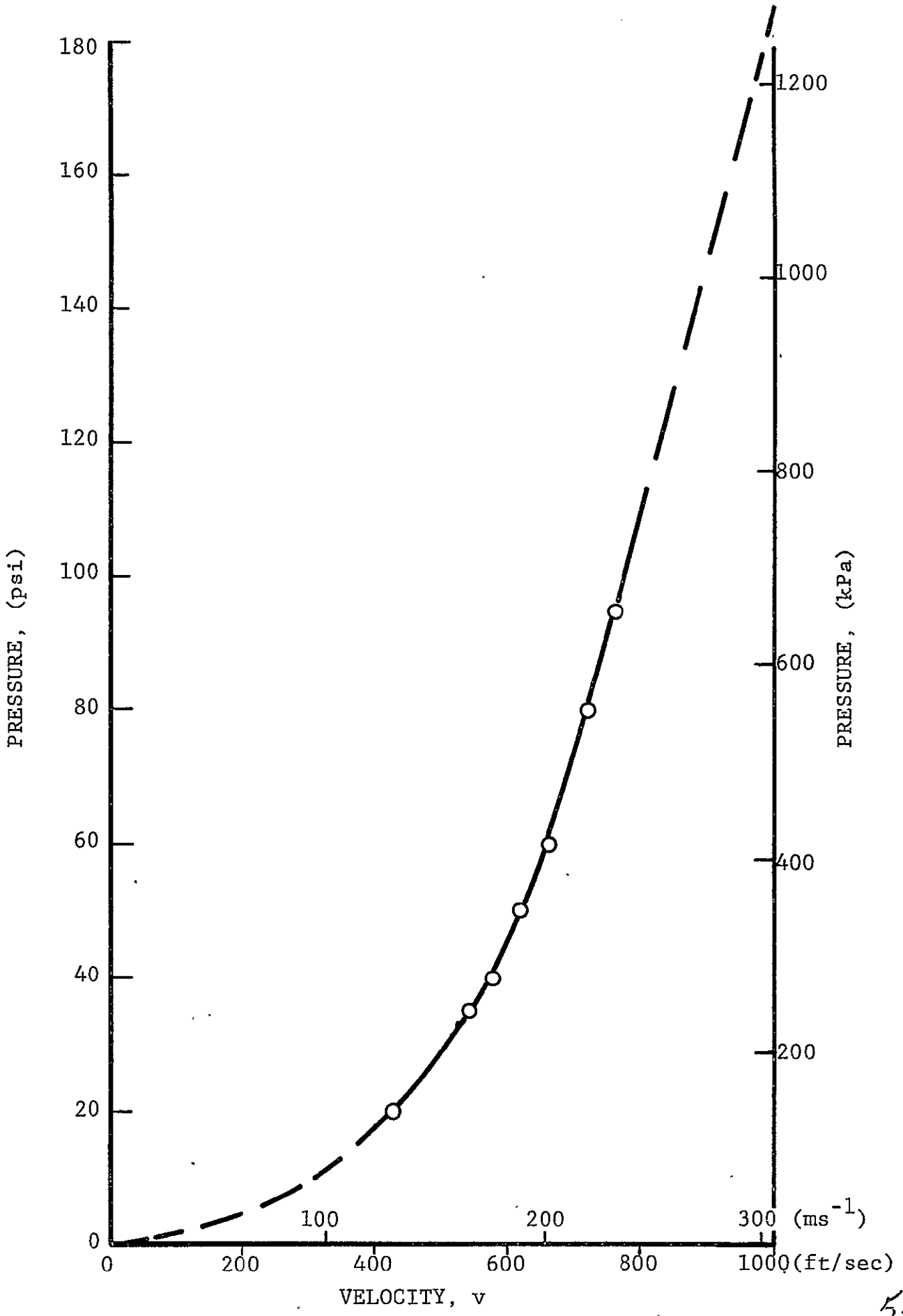

Fig. 7 VELOCITY OF 1.43 cm (9/16 in.) DIAMETER RTV PROJECTILE AS A FUNCTION OF CHAMBER PRESSURE

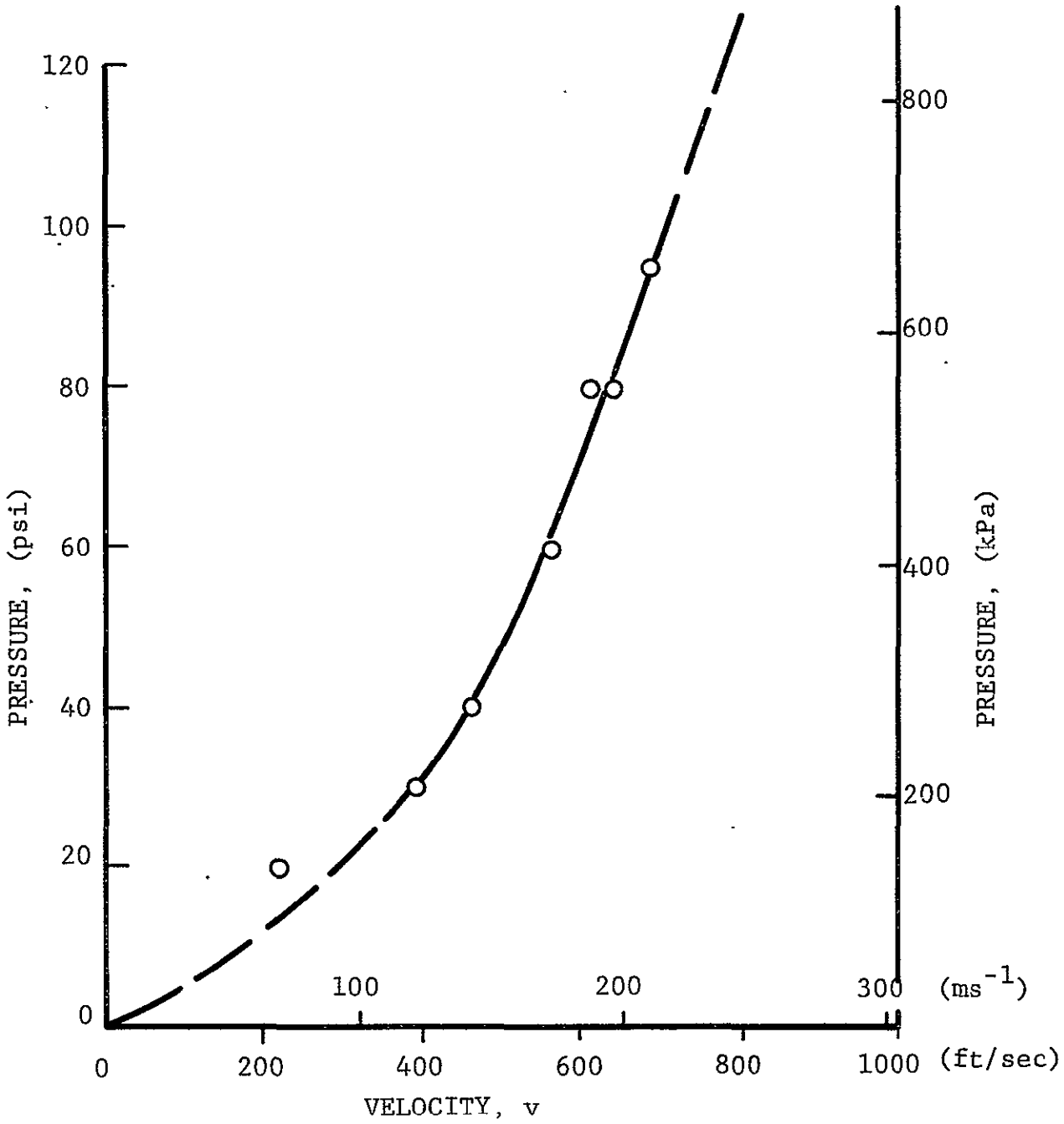

Fig. 8 VELOCITY OF 7.9 mm (5/16 in.) DIAMETER SILASTIC PROJECTILE AS A FUNCTION OF CHAMBER PRESSURE

Fig. 9 EXPERIMENTAL SETUP FOR IMPACTING COMPOSITE PLATES AND RECORDING INSTRUMENTATION

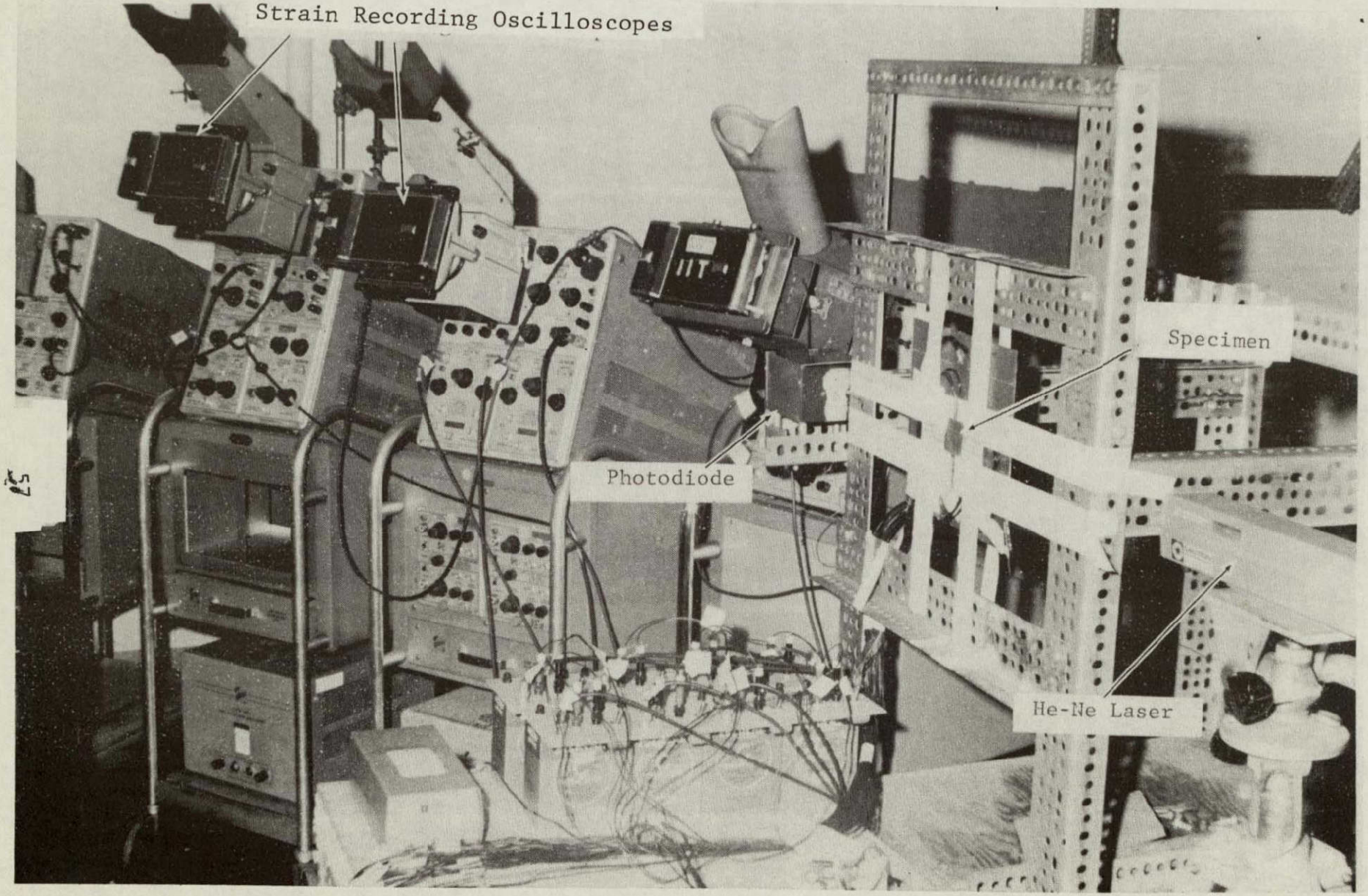

Fig. 10 EXPERIMENTAL SETUP FOR IMPACTING COMPOSITE PLATES AND RECORDING INSTRUMENTATION

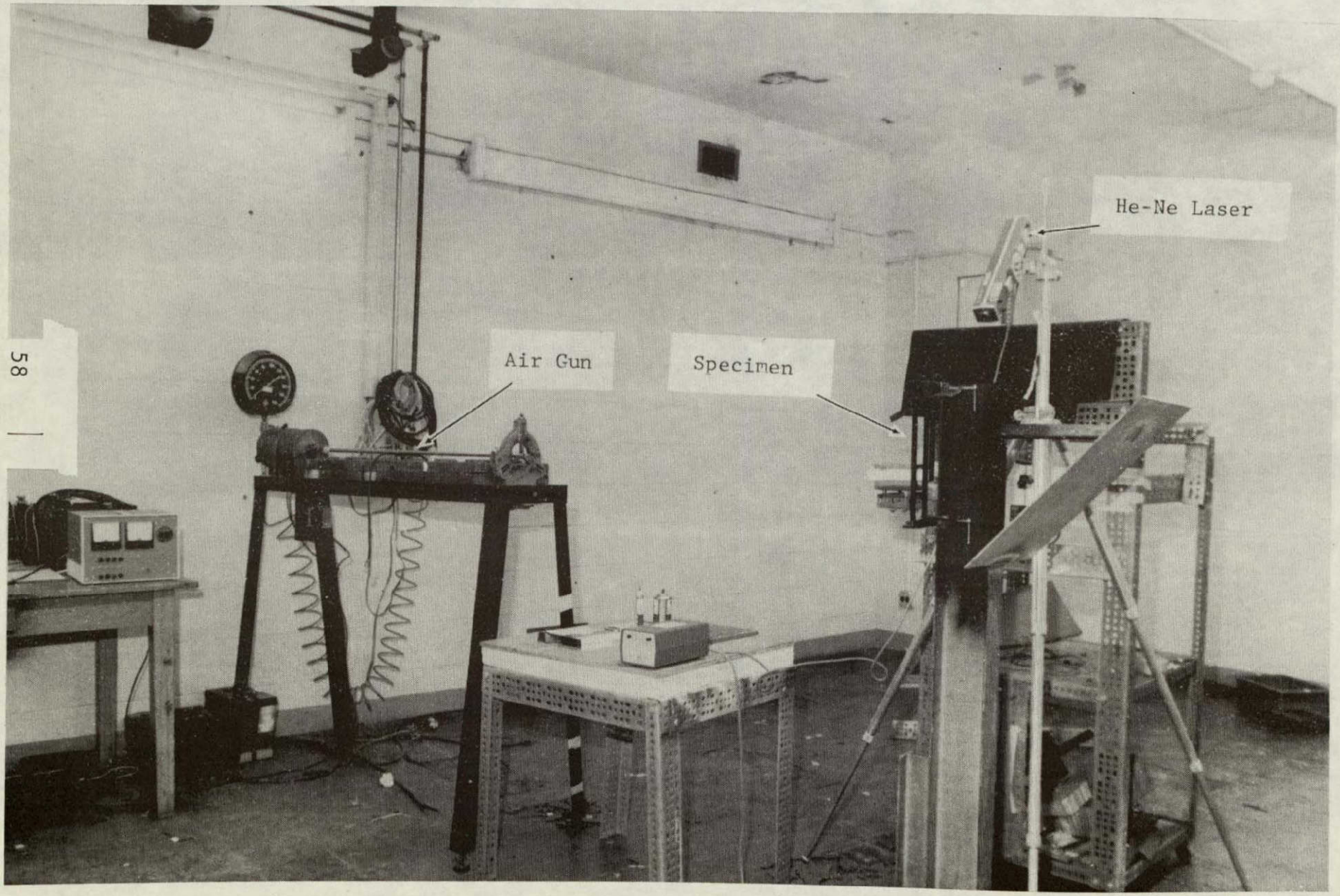

Fig. 11 EXPERIMENTAL SETUP FOR PHOTOGRAPHIC RECORDING OF PROJECTILE IMPACT ON COMPOSITE PLATES

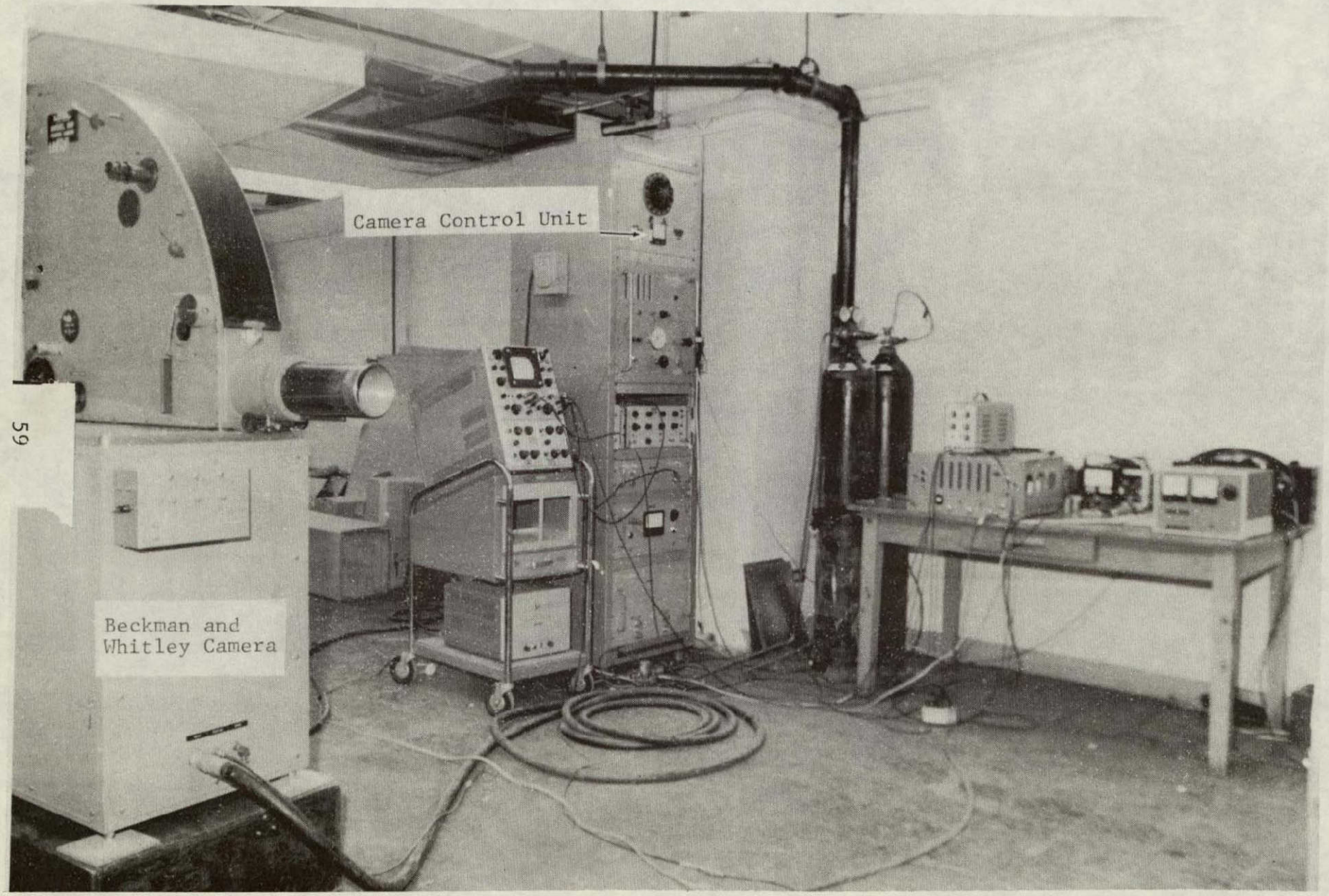

Fig. 12 EXPERIMENTAL SETUP FOR PHOTOGRAPHIC RECORDING OF PROJECTILE IMPACT ON COMPOSITE PLATES

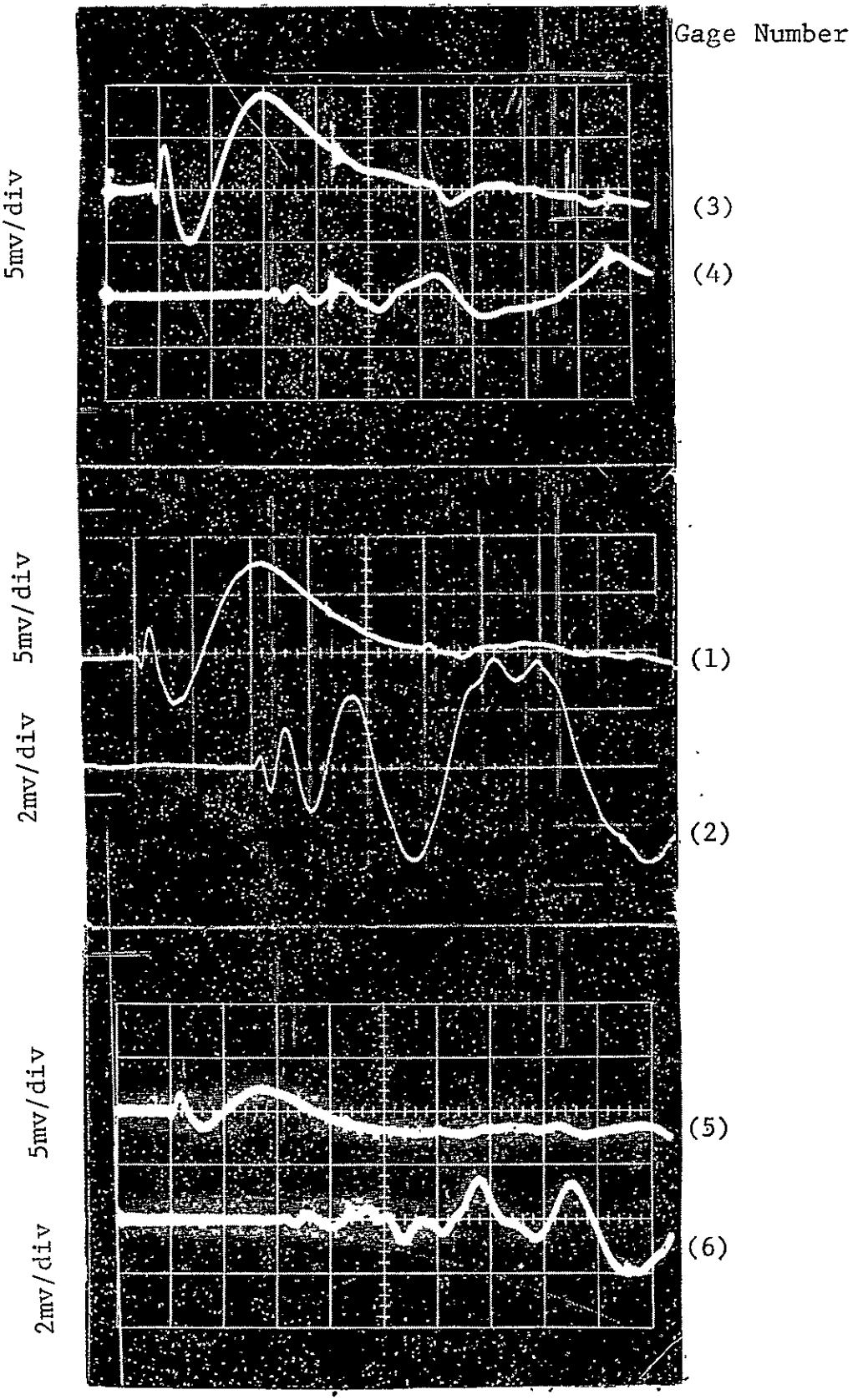

Fig. 13 STRAIN GAGE SIGNALS IN TRANSVERSELY IMPACTED $[\pm 45]_{2s}$ BORON/EPOXY LAMINATE (SWEEP: 20 μsec/div; Refer to Fig. 3-2 for Gage Layout).

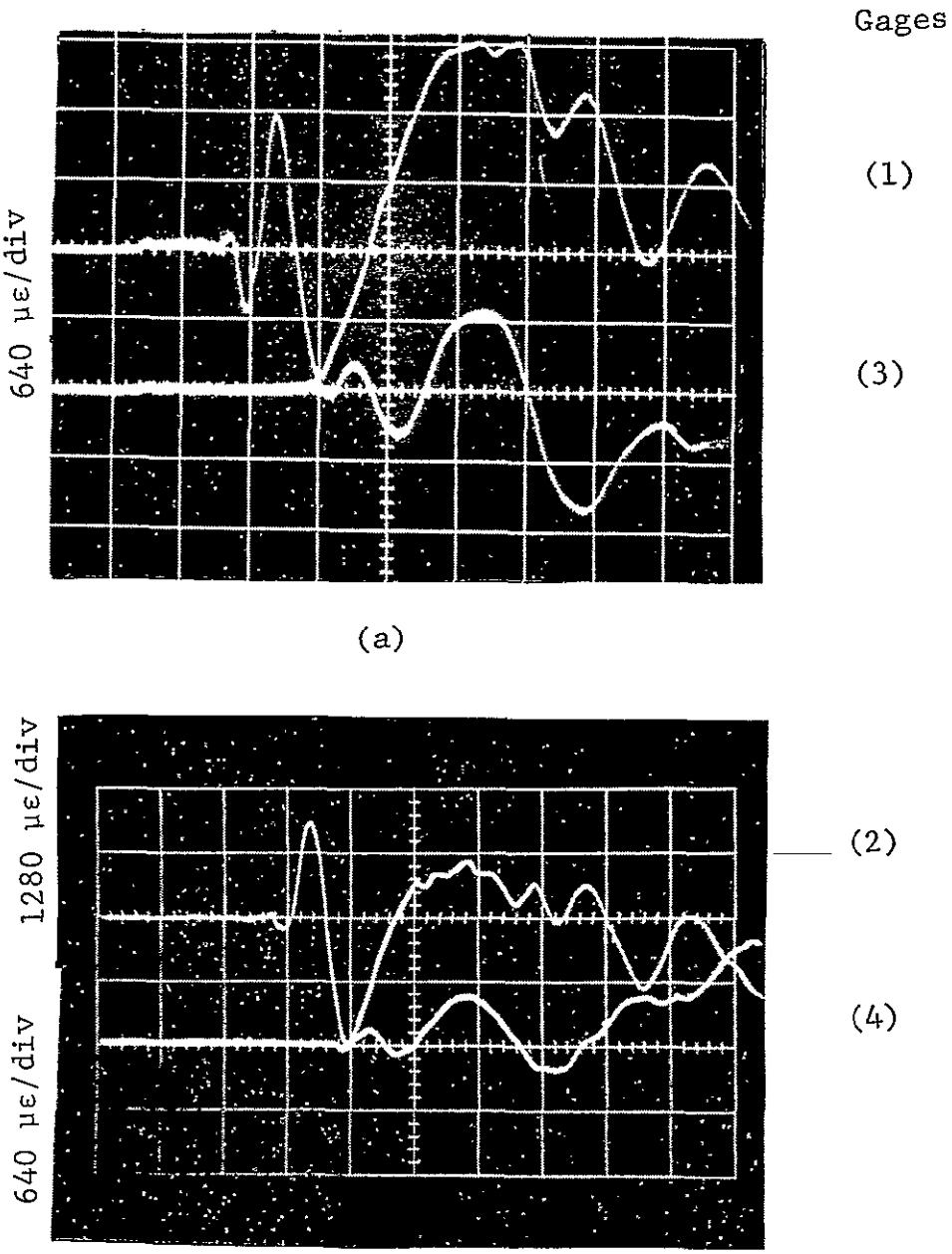

Fig. 14 STRAIN GAGE SIGNALS ALONG y-AXIS OF TRANSVERSELY IMPACTED $[0_{16}]$ BORON/EPOXY SPECIMEN (Sweep: 20 μs/div)
(a) Gages in y-direction 5.08 cm (2 in.) apart
(b) Gages in x-direction 5.08 cm (2 in.) apart

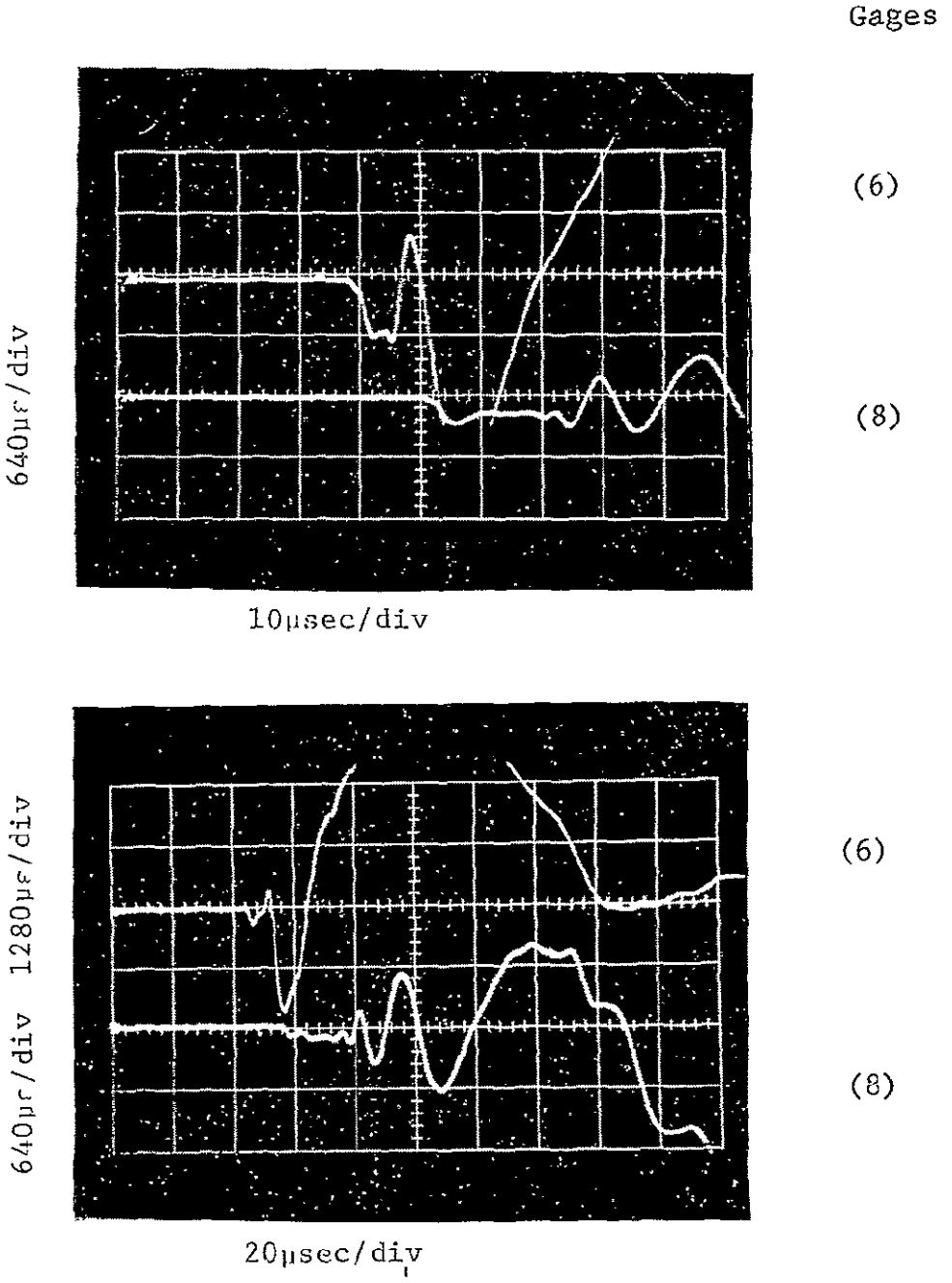

Fig. 15 STRAIN GAGE SIGNALS ALONG x-AXIS OF TRANSVERSELY IMPACTED $[0_{16}]$ BORON/EPOXY SPECIMEN (Gages in x-direction 5.08 cm (2 in.) apart).

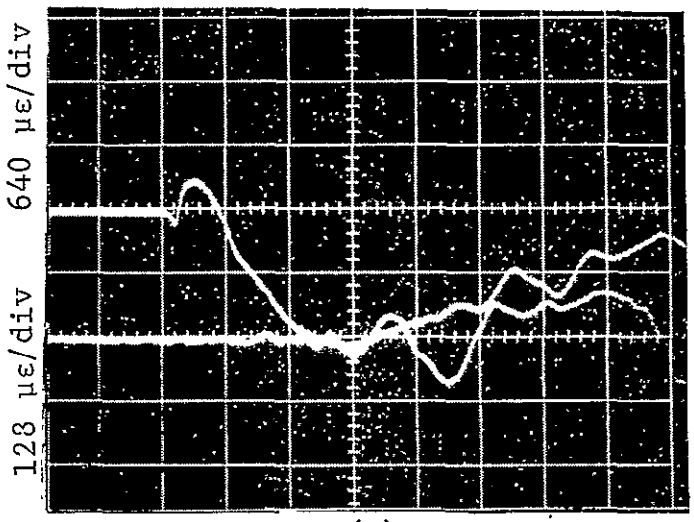

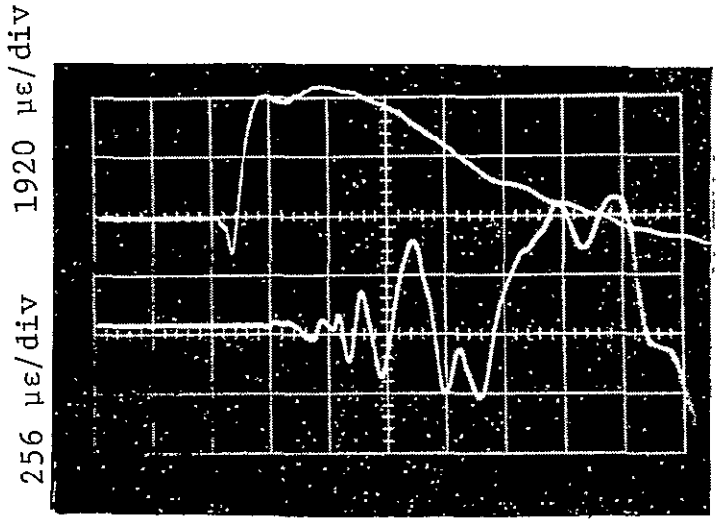

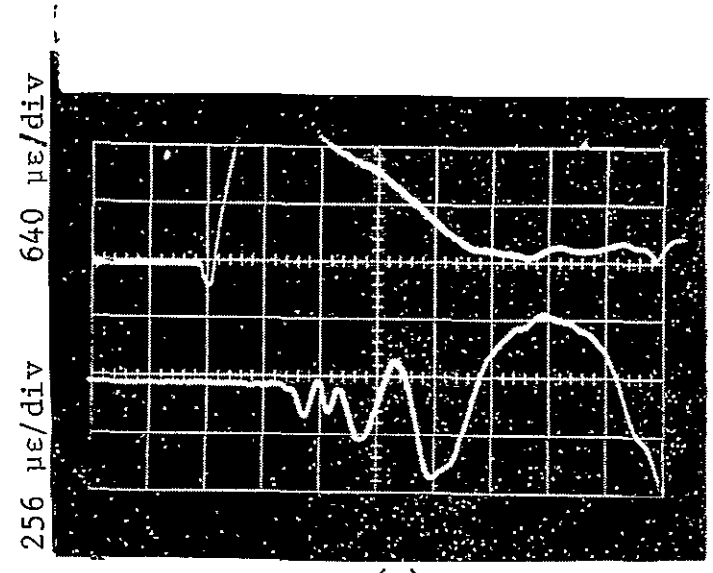

Fig. 16 STRAIN GAGE SIGNALS ALONG 45-DEGREE AXIS OF TRANSVERSELY IMPACTED [0_{16}] BORON/EPOXY SPECIMEN (Sweep: 20 μs/div)
(a) Gages in y-direction 7.62 cm (3 in.) apart
(b) Gages in x-direction 7.62 cm (3 in.) apart
(c) Gages in 45-degree direction 7.62 cm (3 in.) apart

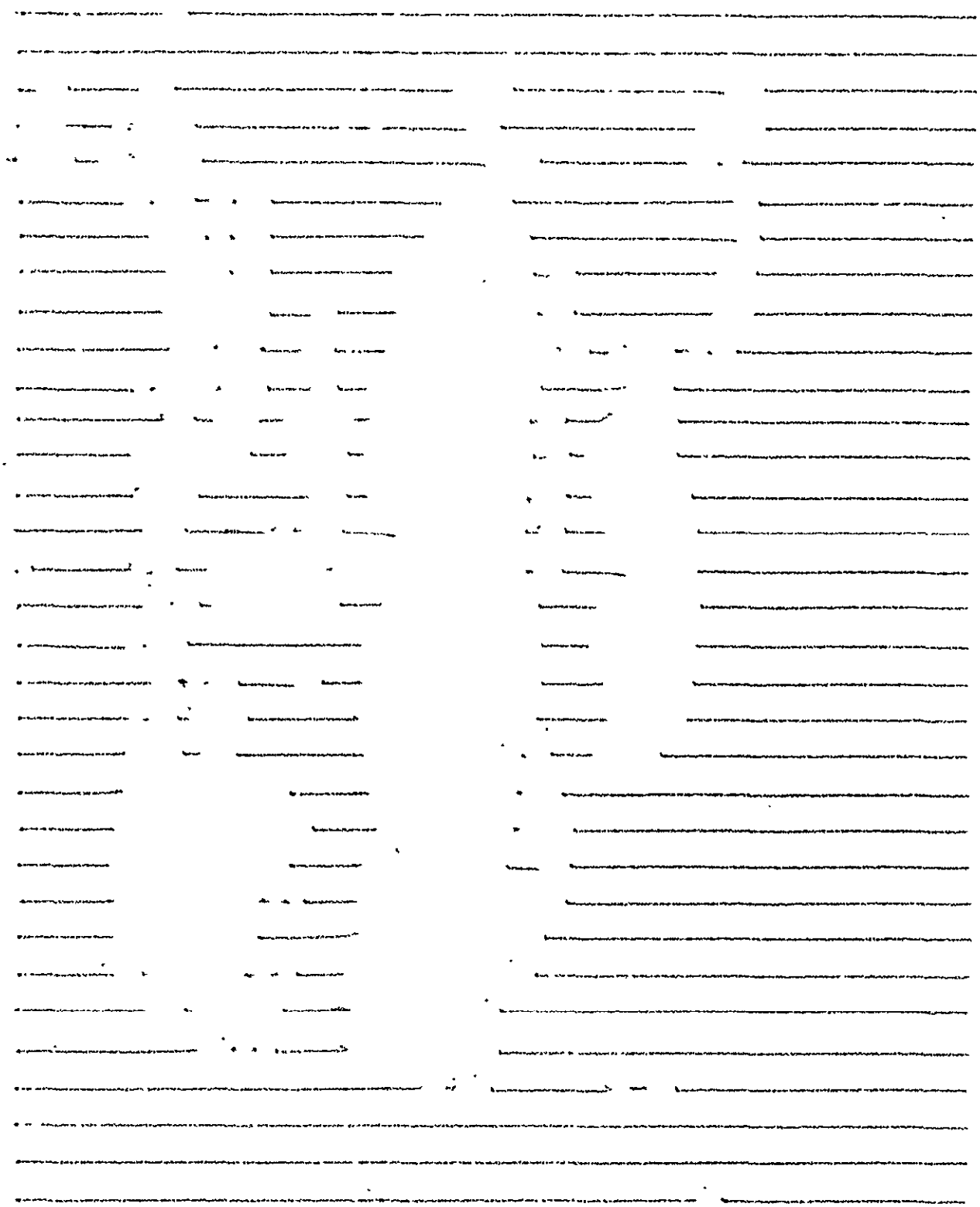

Fig. 17 ULTRASONIC SCAN OF $[0_{16}]$ BORON/EPOXY SPECIMEN AFTER IMPACT TESTING (Specimen 9BU-1)

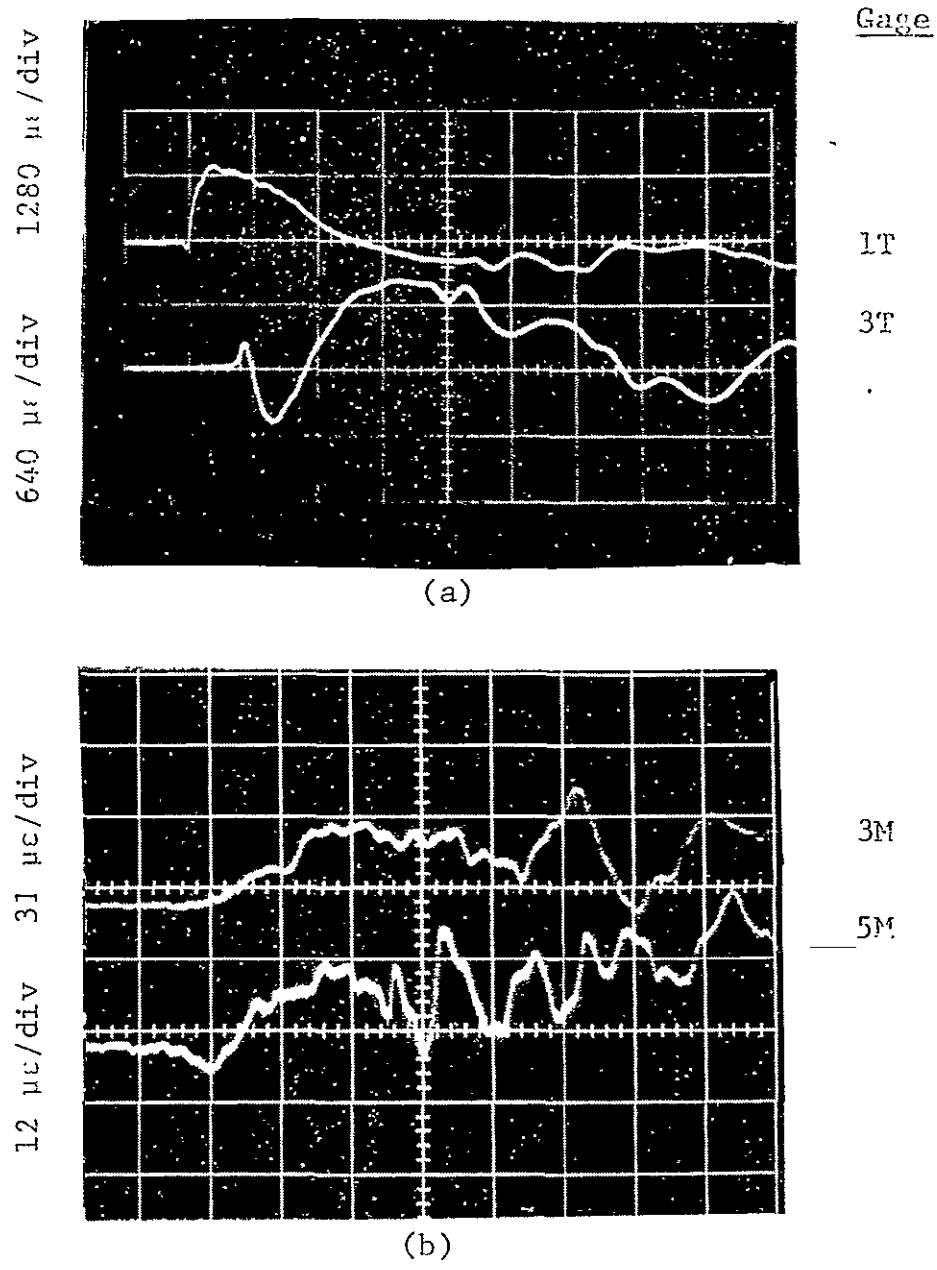

Fig. 18 STRAIN GAGE SIGNALS (LONGITUDINAL) ALONG y-AXIS OF TRANSVERSELY IMPACTED $[0_{16}]$ BORON/EPOXY SPECIMEN (Sweep: 20 μs/div)

(a) Gages in y-direction 2.54 cm and 5.08 cm from Center on Top Surface

(b) Gages in y-direction 5.08 cm and 7.62 cm from Center in Middle Surface

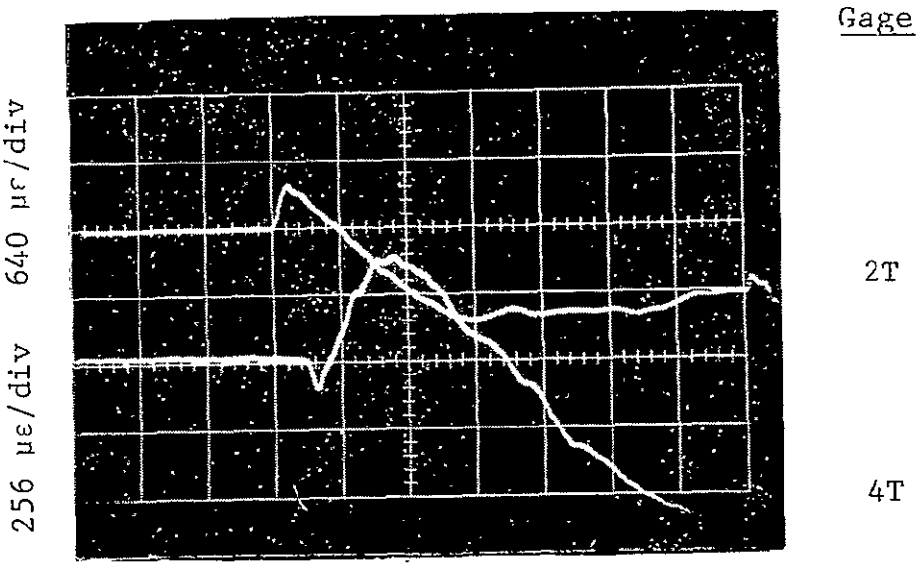

(a)

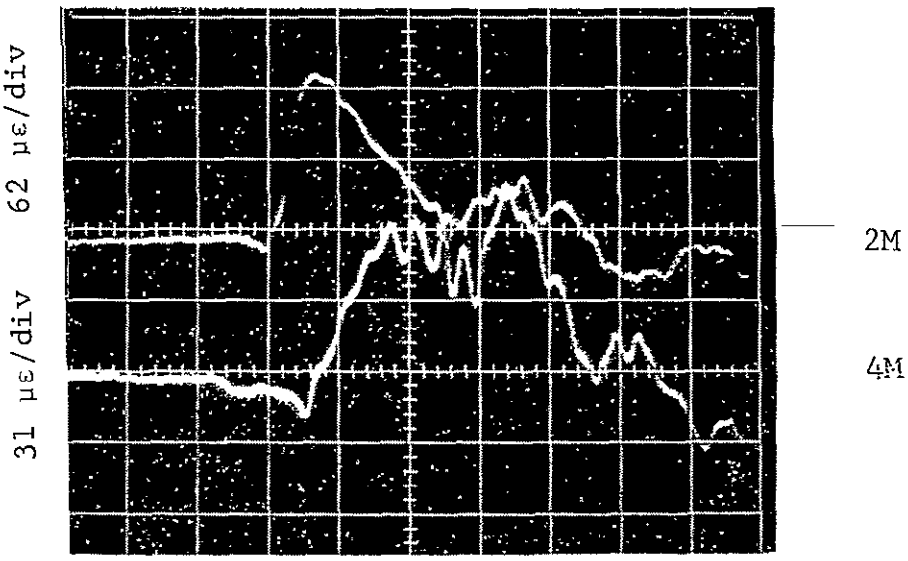

(b)

Fig. 19 STRAIN GAGE SIGNALS(TRANSVERSE)ALONG y-AXIS OF TRANSVERSELY IMPACTED $[0_{16}]$ BORON/EPOXY SPECIMEN (Sweep: 20 μs/div)

(a) Gages in x-direction 2.54 cm and 5.08 cm from Center on Top Surface

(b) Gages in x-direction 2.54 cm and 5.08 cm from Center in Middle Surface

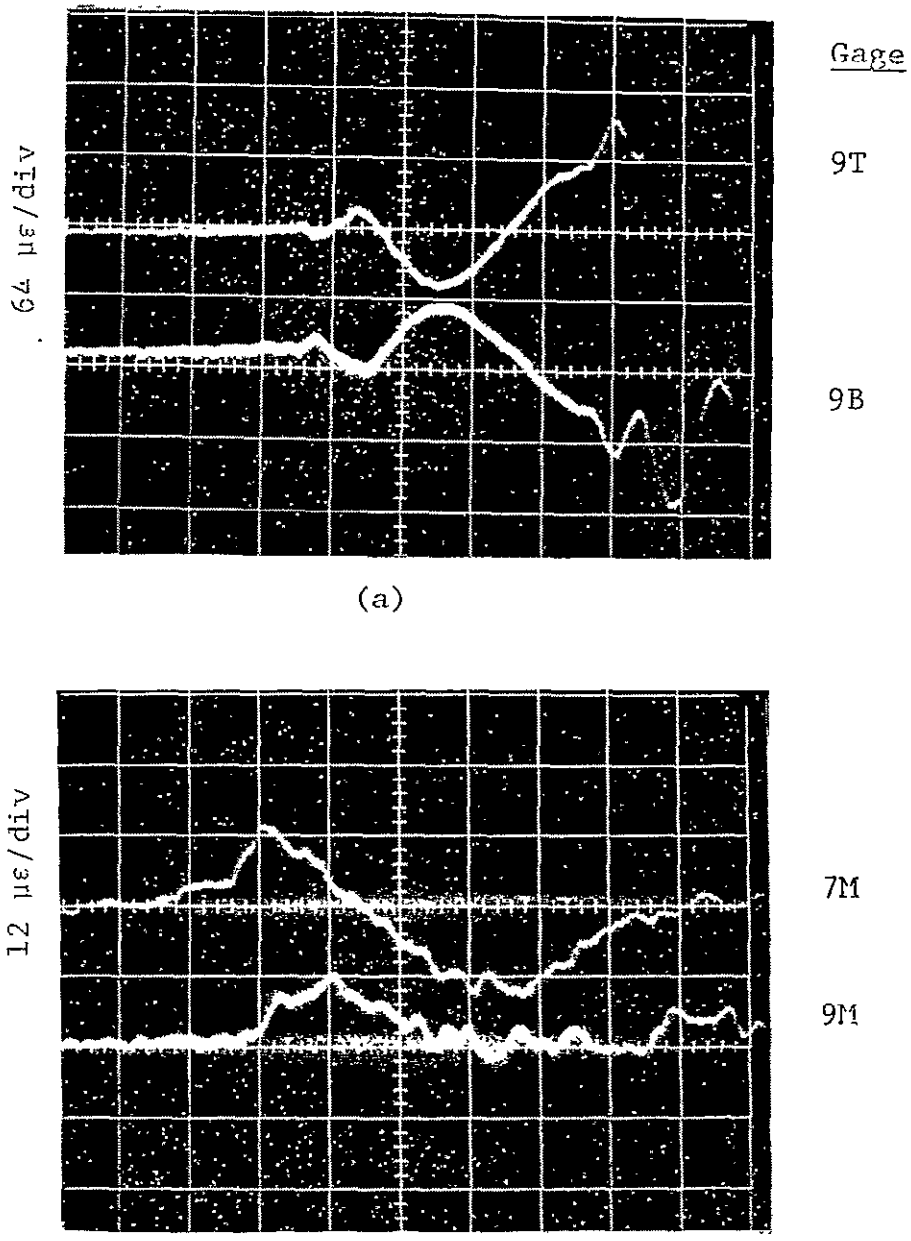

Fig. 20 STRAIN GAGE SIGNALS ALONG x-AXIS OF TRANSVERSELY IMPACTED $[0_{16}]$ BORON/EPOXY SPECIMEN (Sweep: 20 μs/div)

(a) Gages in y-direction 5.08 cm from Center on Top and Bottom Surfaces

(b) Gages in y-direction 2.54 cm and 5.08 cm from Center in Middle Surface

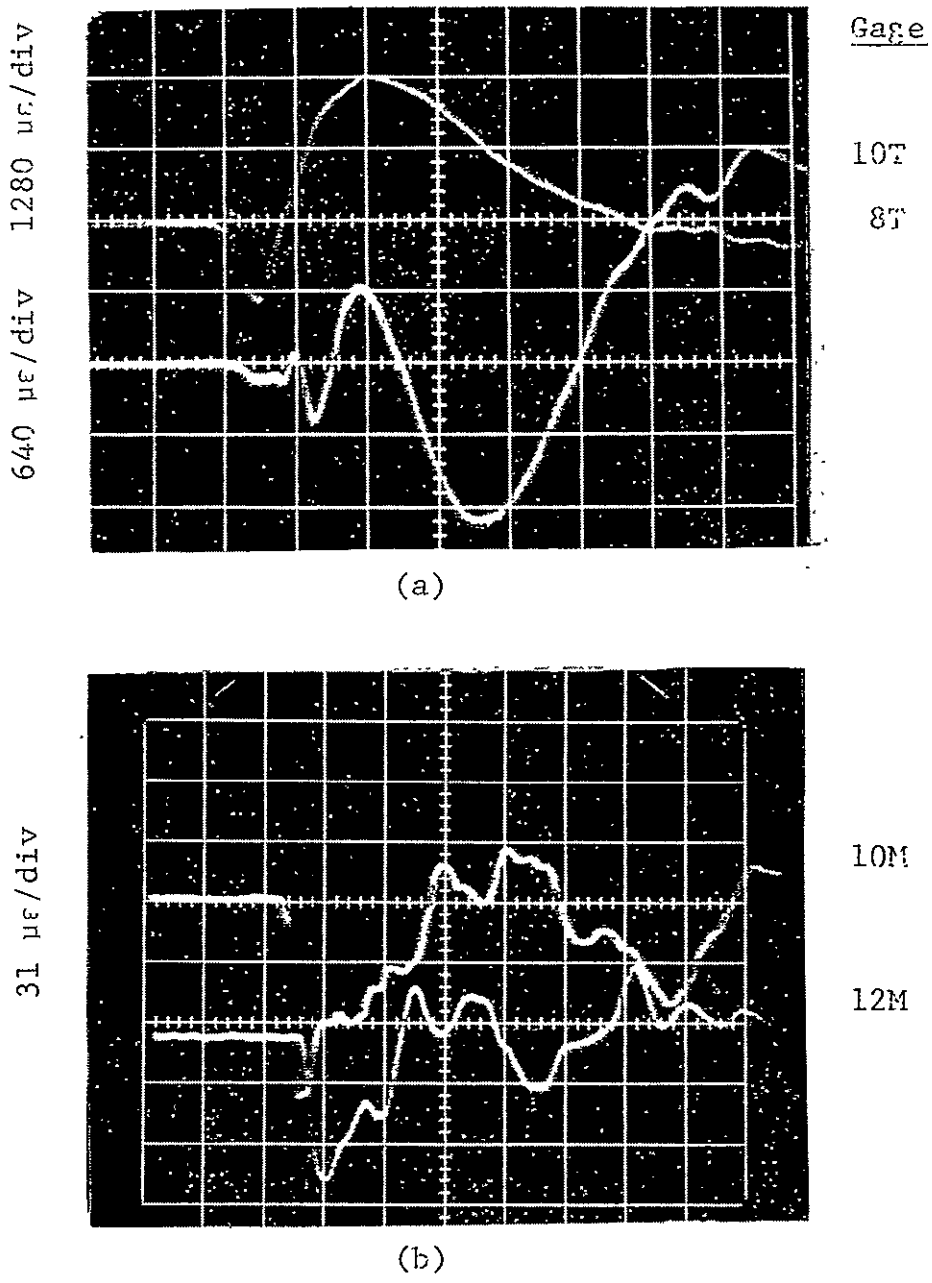

Fig. 21 STRAIN GAGE SIGNALS ALONG x-AXIS OF TRANSVERSELY IMPACTED $[0_{16}]$ BORON/EPOXY SPECIMEN (Sweep: 20 μs/div)

(a) Gages in x-direction 2.54 cm and 5.08 cm from Center on Top Surface

(b) Gages in x-direction 5.08 cm and 7.62 cm from Center in Middle Surface

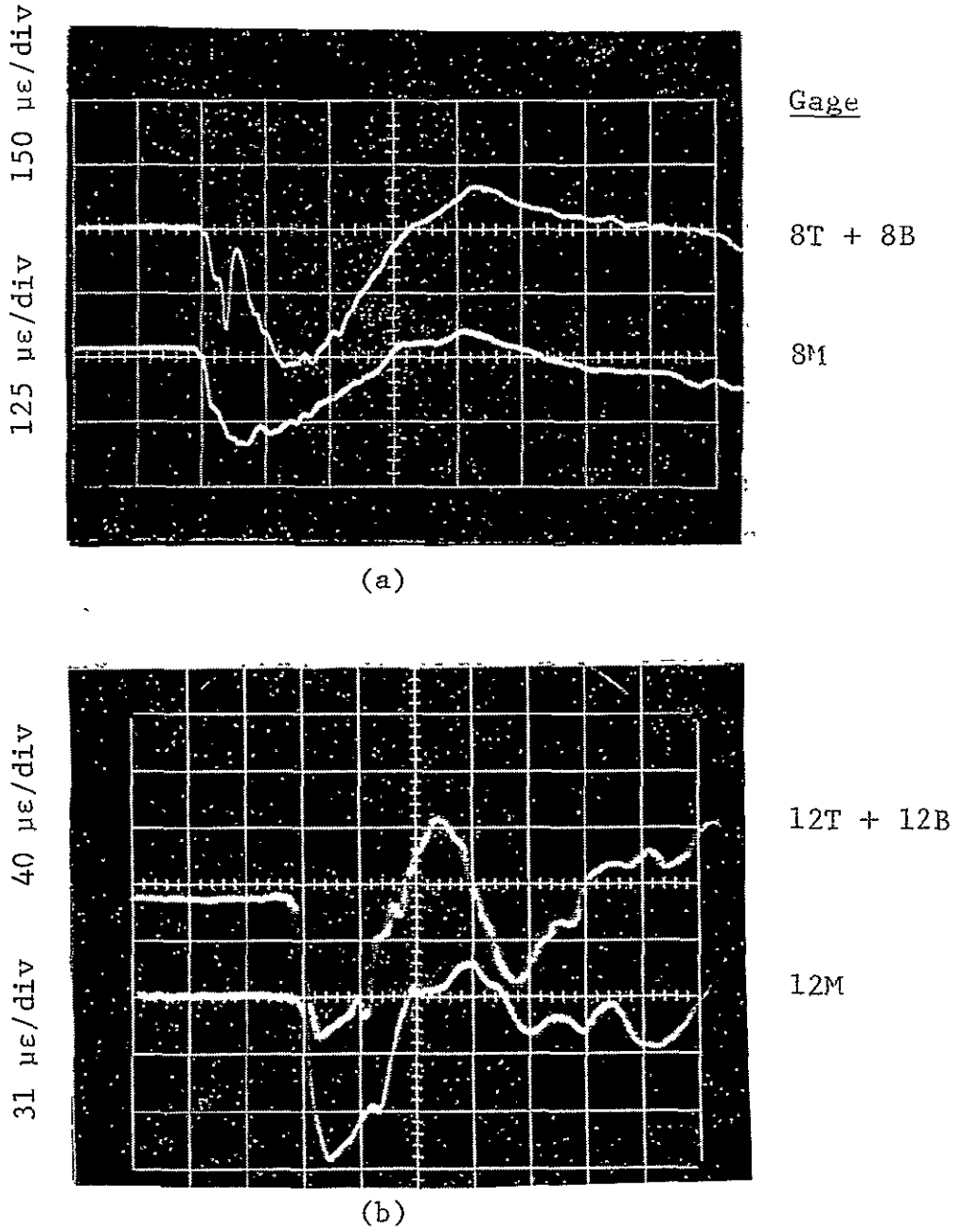

Fig. 22 STRAIN GAGE SIGNALS ALONG x-AXIS OF TRANSVERSELY IMPACTED $[0_{16}]$ BORON/EPOXY SPECIMEN (Sweep: 20 μs/div)

(a) Gages in x-direction 2.54 cm from Center. Top Trace: Sum of Top and Bottom Surface Strains; Bottom Trace: Strain in Middle Surface

(b) Gages in x-direction 7.62 cm from Center. Top Trace: Sum of Top and Bottom Surface Strains; Bottom Trace: Strain in Middle Surface.

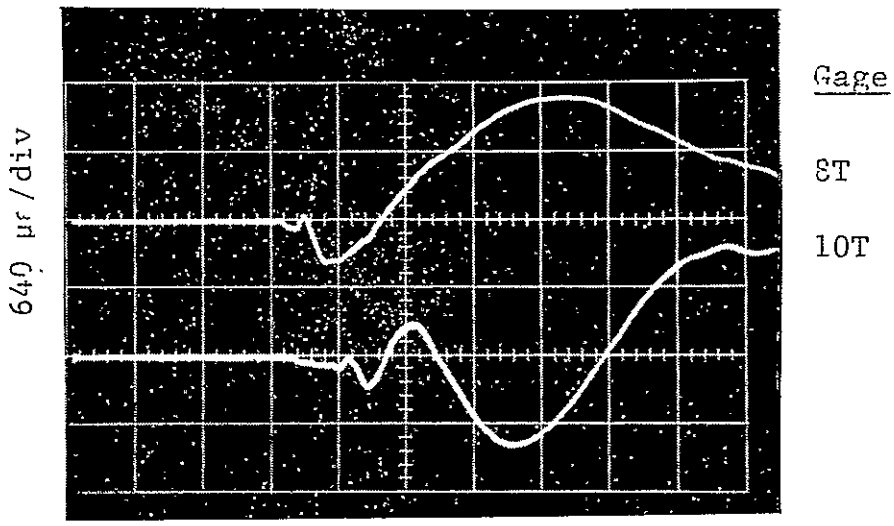

(a)

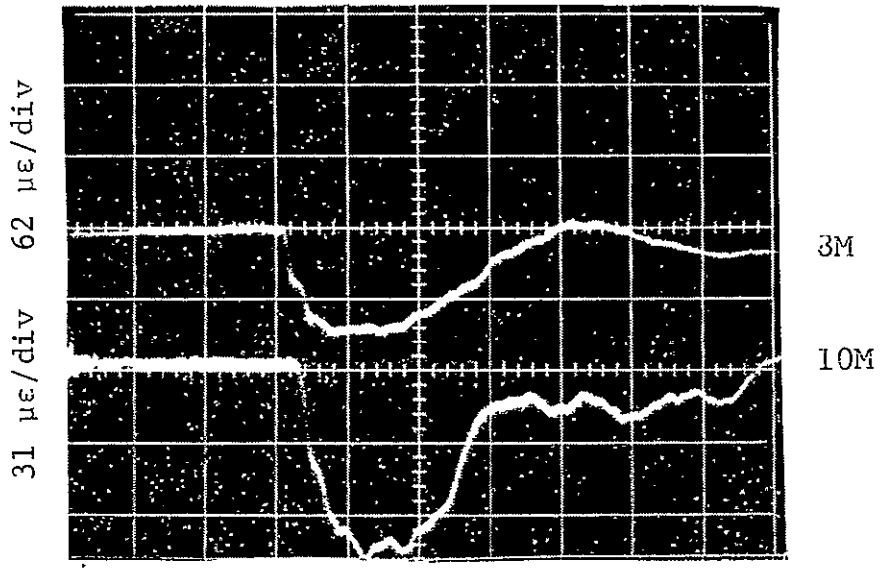

(b)

Fig. 23 OBLIQUE IMPACT. STRAIN GAGE SIGNALS IN TRANSVERSELY IMPACTED $[0_{16}]$ BORON/EPOXY SPECIMEN ALONG x-AXIS. (Sweep: 20 μs/div)

(a) Gages in x-direction 2.54 cm and 5.08 cm from Center on Top Surface

(b) Gages in x-direction 2.54 cm and 5.08 cm from Center on Middle Surface.

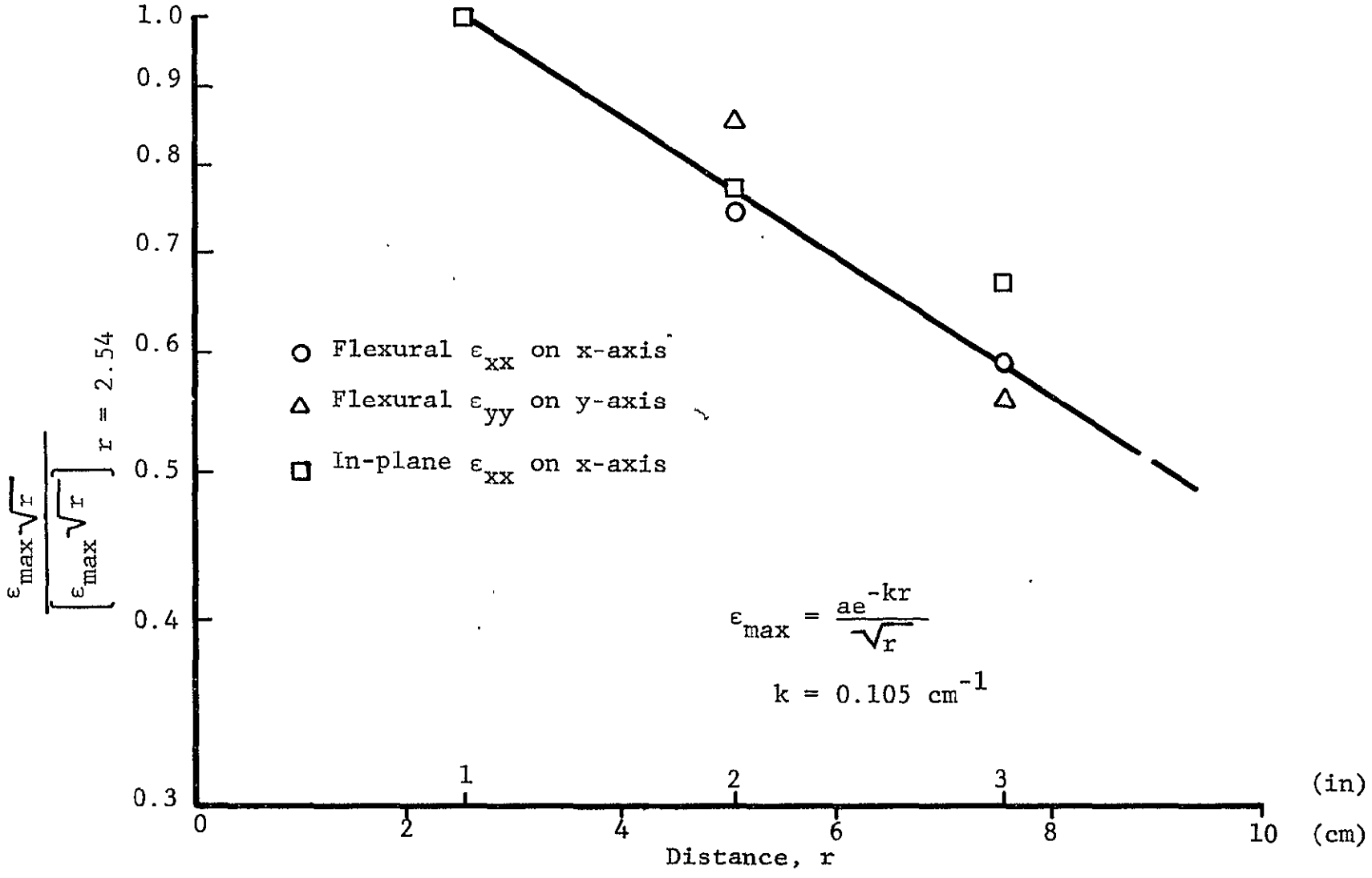

Fig. 24 SEMILOGARITHMIC PLOT FOR SEPARATING MATERIAL AND GEOMETRIC ATTENUATION IN $[0_{16}]$ BORON/EPOXY SPECIMEN IMPACTED NORMALLY WITH A SILASTIC SPHERE

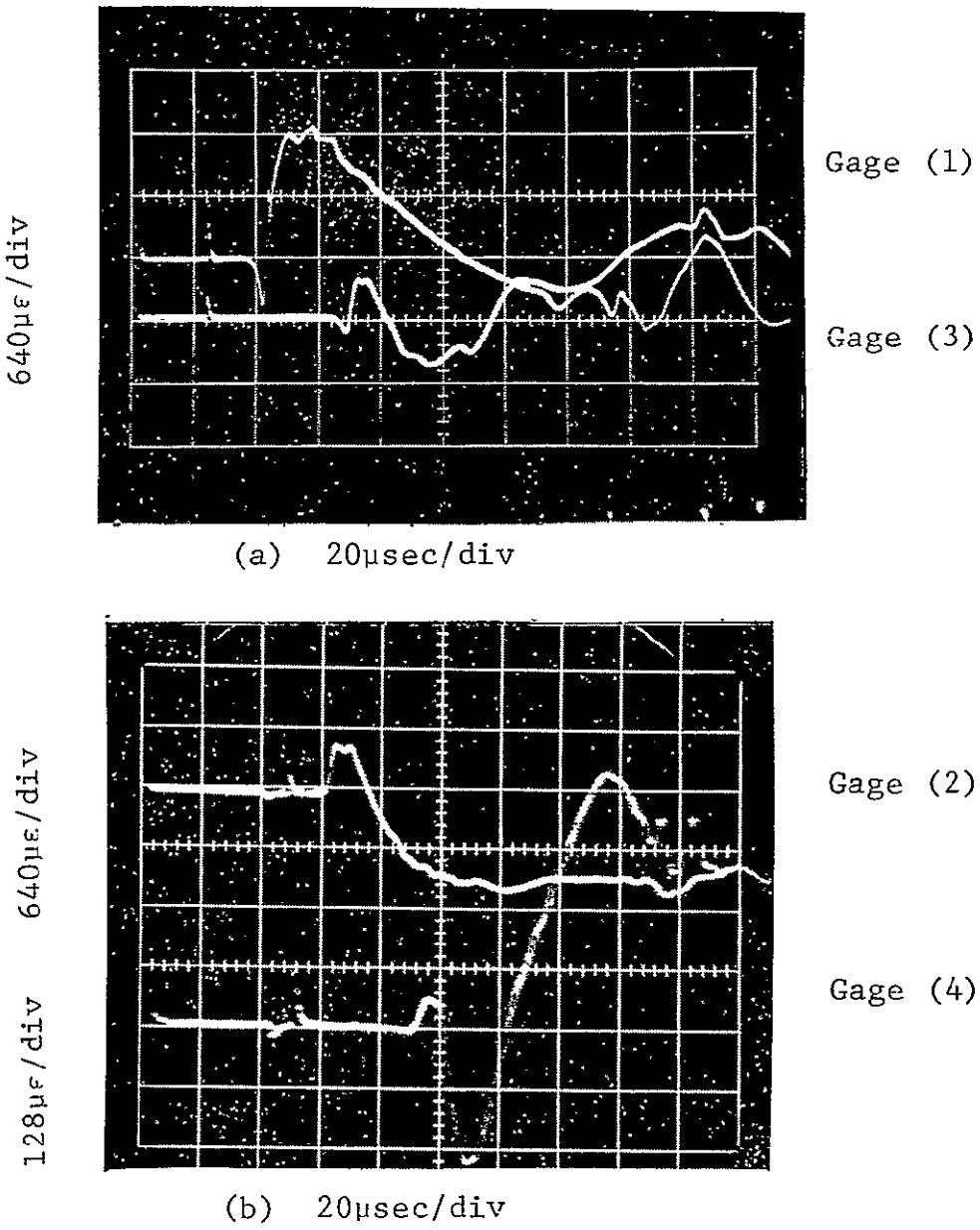

Fig. 25 STRAIN GAGE SIGNALS ALONG y-AXIS IN TRANSVERSELY IMPACTED $[0_{16}]$ GRAPHITE/EPOXY SPECIMEN

(a) Gages in y-direction 5.08 cm (2 in.) apart

(b) Gages in x-direction 5.08 cm (2 in.) apart

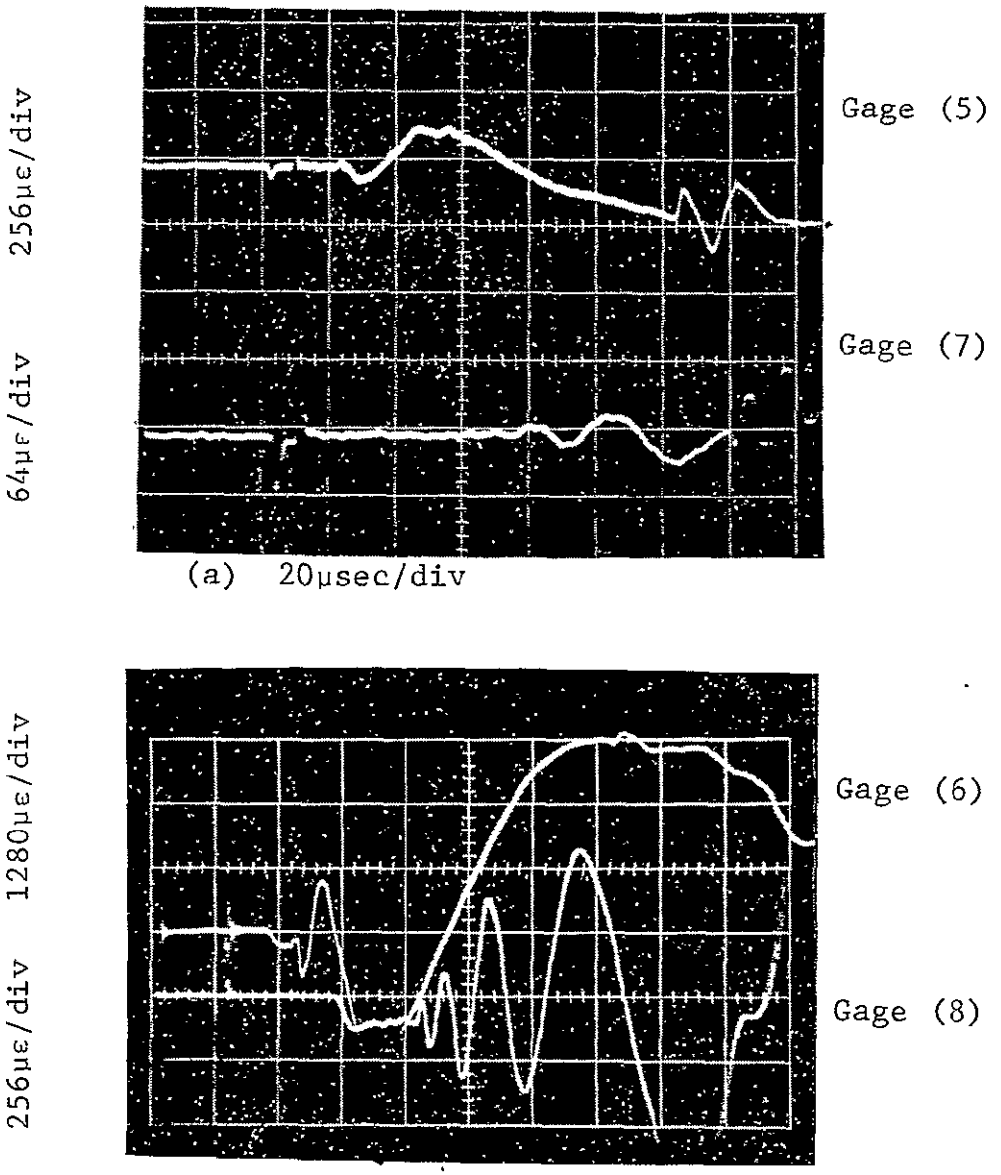

Fig. 26 STRAIN GAGE SIGNALS ALONG x-AXIS IN TRANSVERSELY IMPACTED $[0_{16}]$ GRAPHITE/EPOXY SPECIMEN

(a) Gages in y-direction 5.08 cm (2 in.) apart

(b) Gages in x-direction 5.08 cm (2 in.) apart

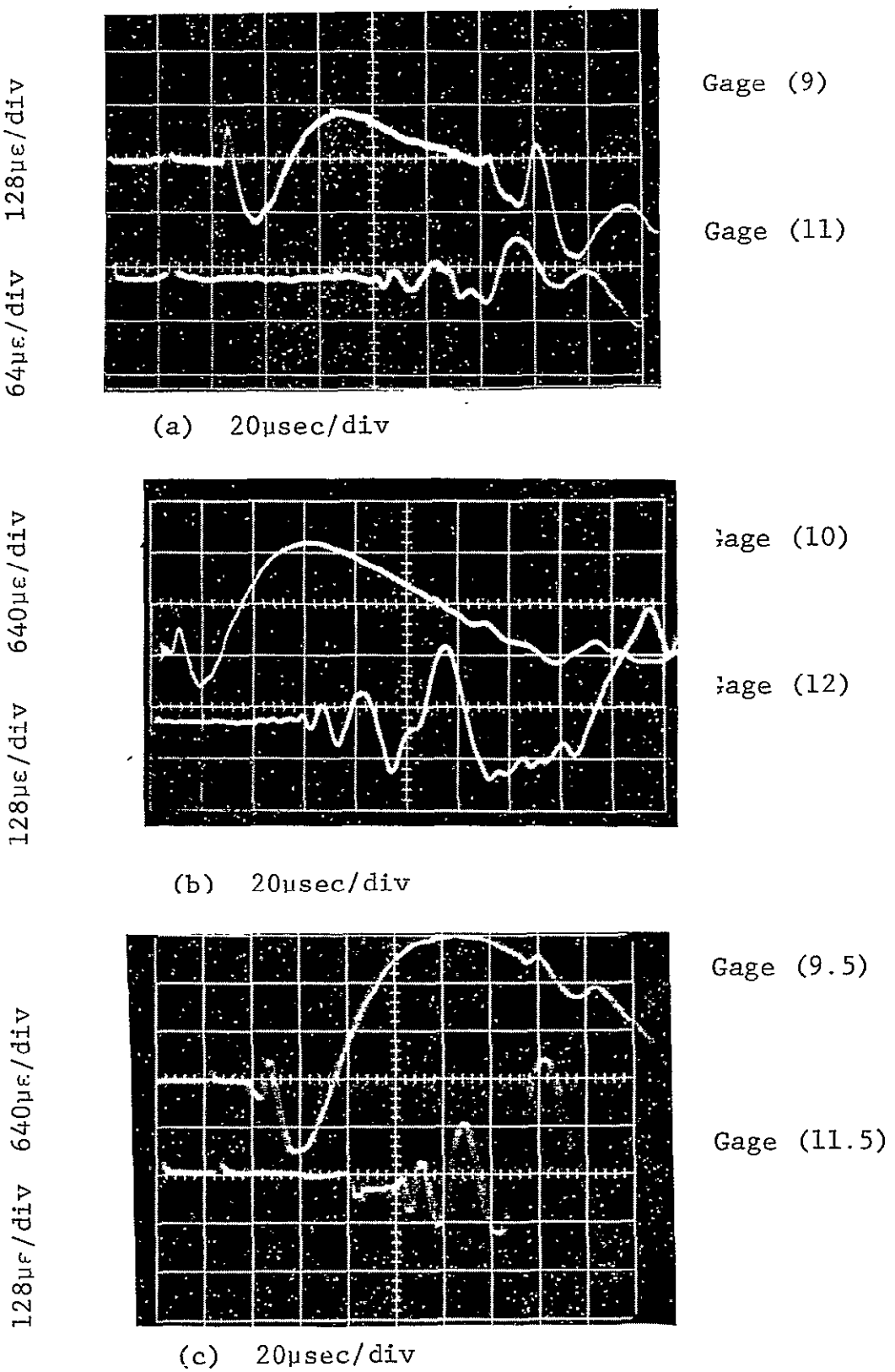

Fig. 27 STRAIN GAGE SIGNALS ALONG 45-DEGREE AXIS IN TRANSVERSELY IMPACTED $[0_{16}]$ GRAPHITE/EPOXY SPECIMEN

(a) Gages in y-direction 7.62 cm (3 in.) apart

(b) Gages in x-direction 7.62 cm (3 in.) apart

(c) Gages in 45-degree direction 7.62 cm (3 in.) apart

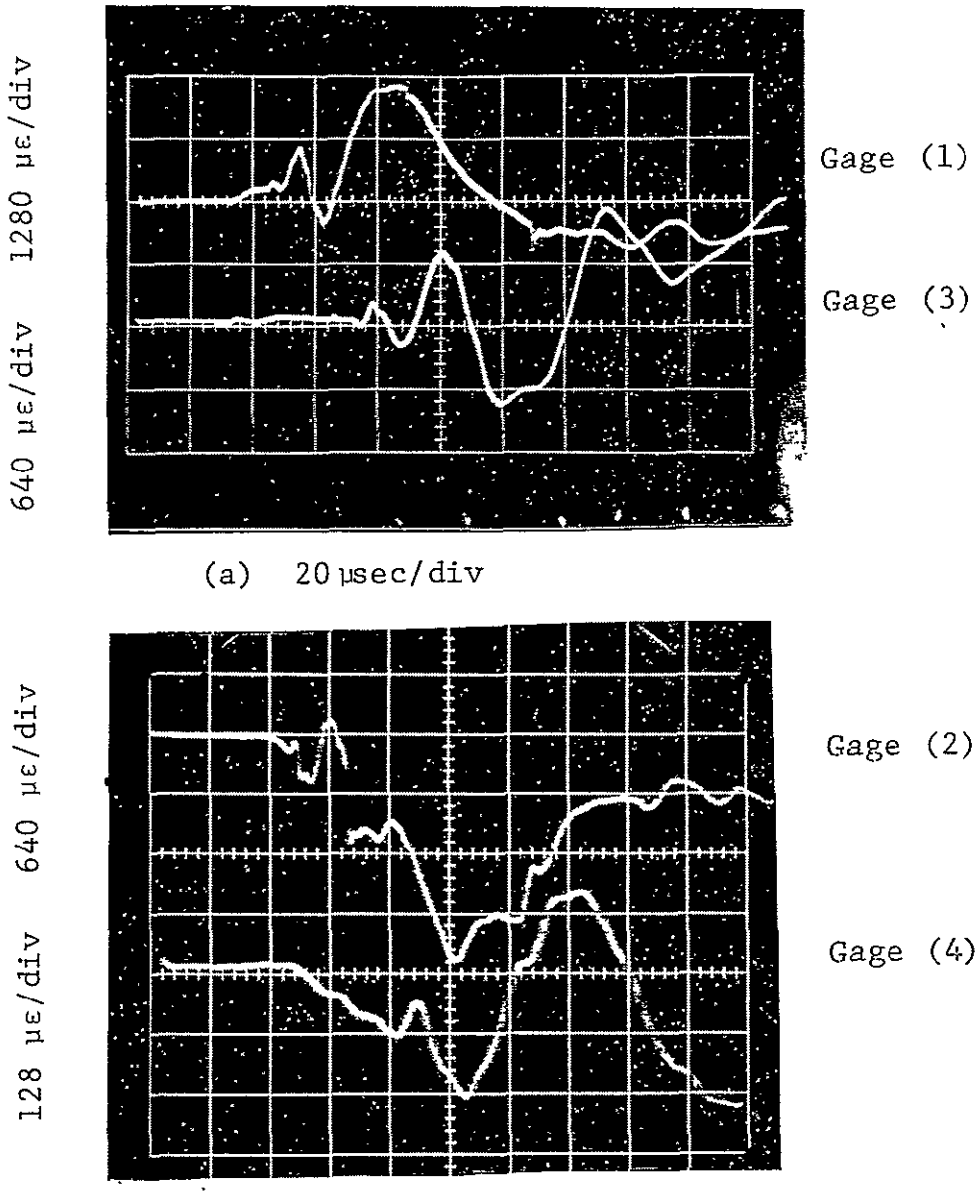

Fig. 28 STRAIN GAGE SIGNALS IN TRANSVERSELY IMPACTED $[0_2/\pm 45]_{2s}$ BORON/EPOXY SPECIMEN 9BA-1 ALONG VERTICAL AXIS.

a) Gages in y-Direction
b) Gages in x-Direction

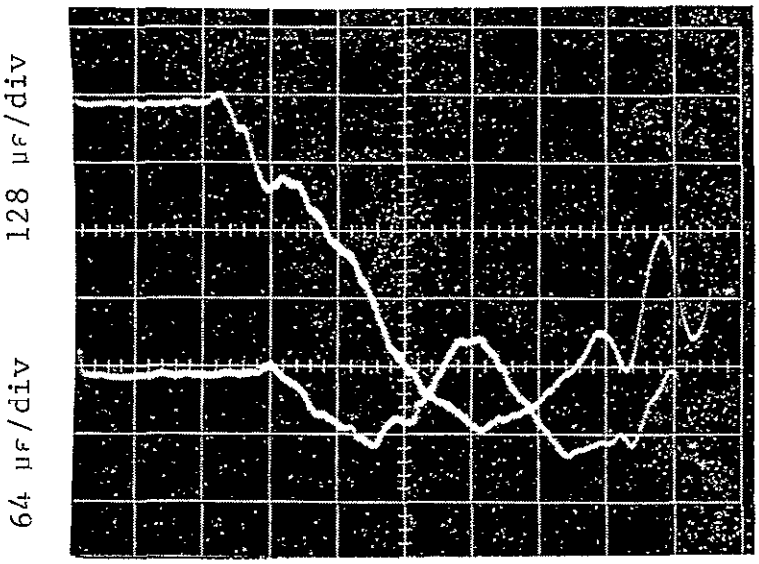

(a) 20μsec/div

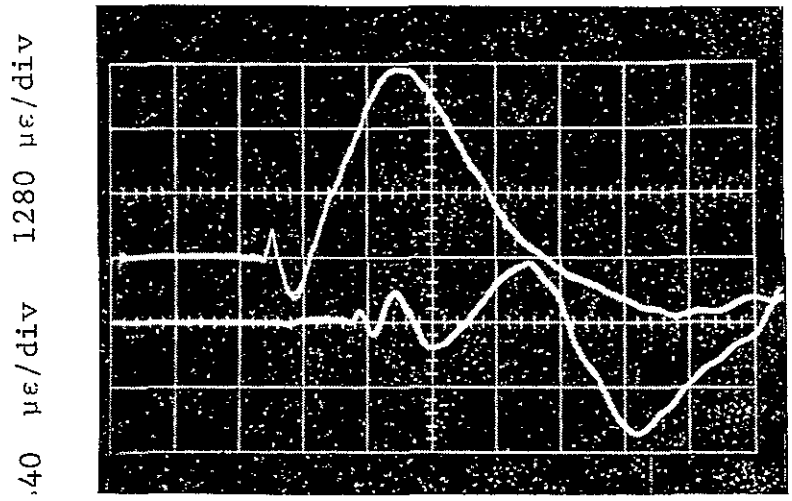

(b) 20μsec/div

Fig. 29 STRAIN GAGE SIGNALS IN TRANSVERSELY IMPACTED $[0_2/\pm 45]_{2s}$ BORON/EPOXY SPECIMEN 9BA-1 ALONG HORIZONTAL AXIS.

a) Gages in y-Direction
b) Gages in x-Direction

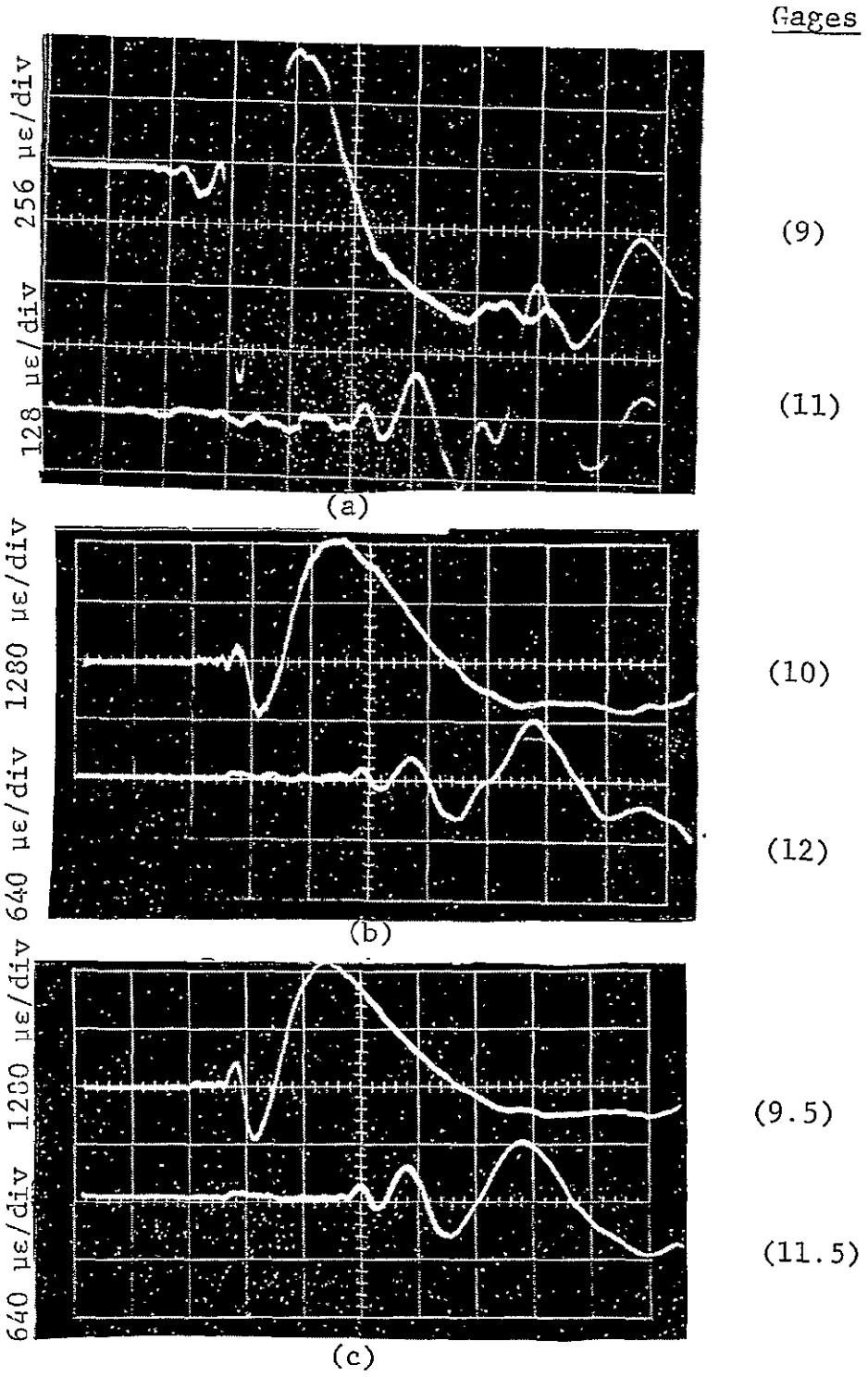

Fig. 30 STRAIN GAGE SIGNALS IN TRANSVERSELY IMPACTED $[0_2/\pm45]_{2s}$ BORON/EPOXY SPECIMEN 9BA-1 ON 45-DEGREE AXIS (Sweep: 20 μsec/div)

(a) Gages in y-Direction
(b) Gages in x-Direction
(c) Gages in 45-degree Direction

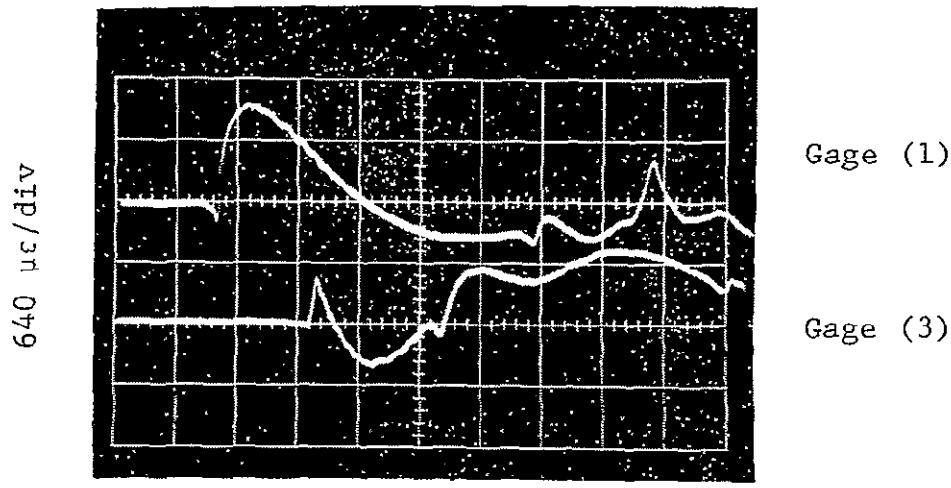

(a) 20 μsec/div

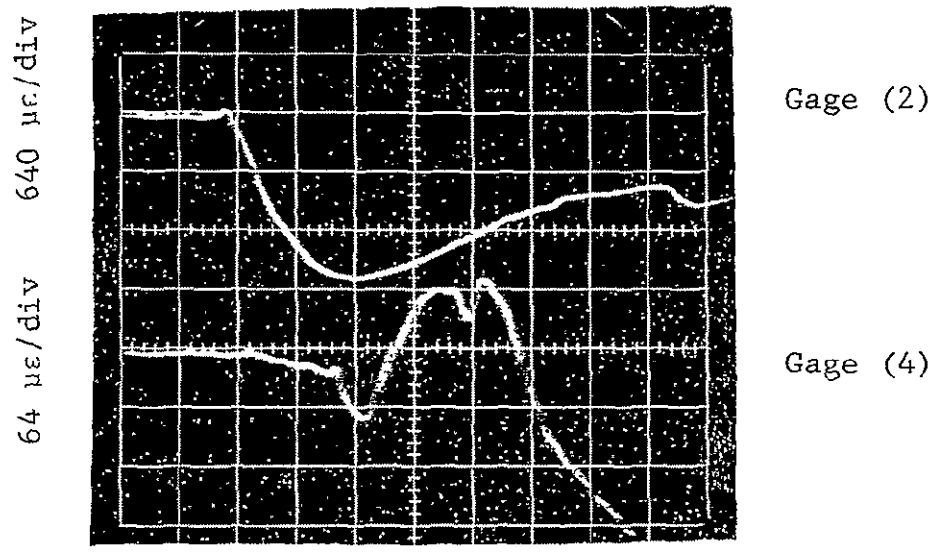

(b) 20 μsec/div

Fig. 31 STRAIN GAGE SIGNALS IN TRANSVERSELY IMPACTED $[0_2/\pm 45]_{2s}$ GRAPHITE/EPOXY SPECIMEN 9GA-1 ALONG VERTICAL AXIS

a) Gages in y-Direction
b) Gages in x-Direction

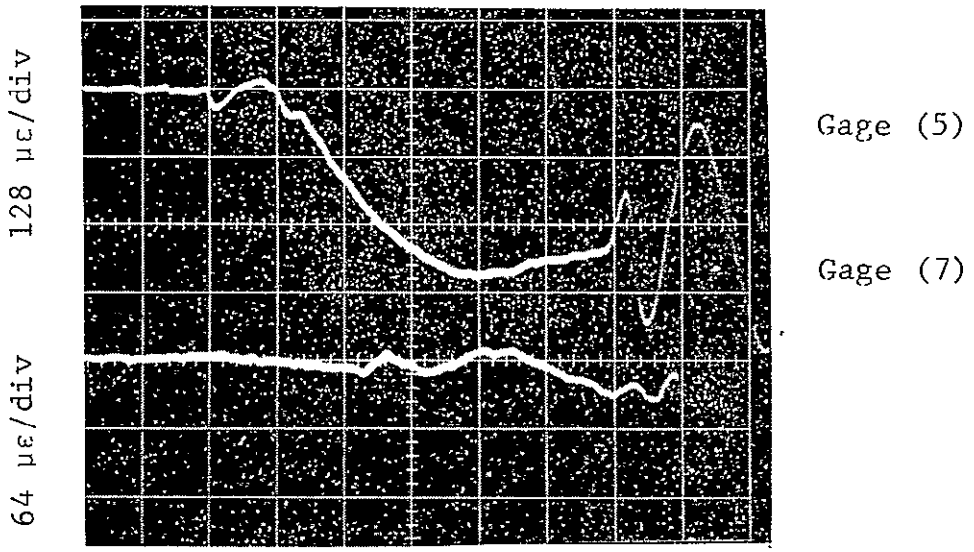

(a) 20 μsec/div

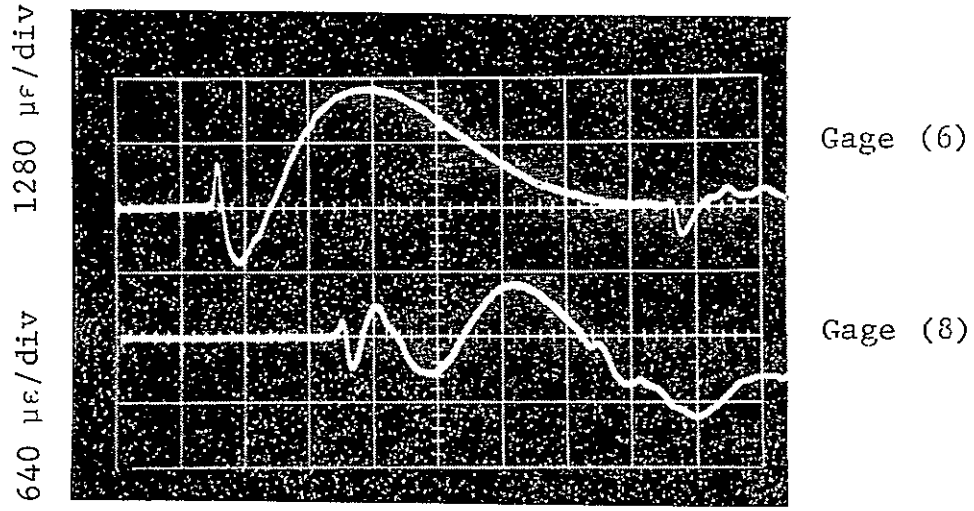

(b) 20 μsec/div

Fig. 32 STRAIN GAGE SIGNALS IN TRANSVERSELY IMPACTED $[0_2/\pm 45]_{2s}$ GRAPHITE/EPOXY SPECIMEN 9GA-1 ALONG HORIZONTAL AXIS

(a) Gages in y-Direction
(b) Gages in x-Direction

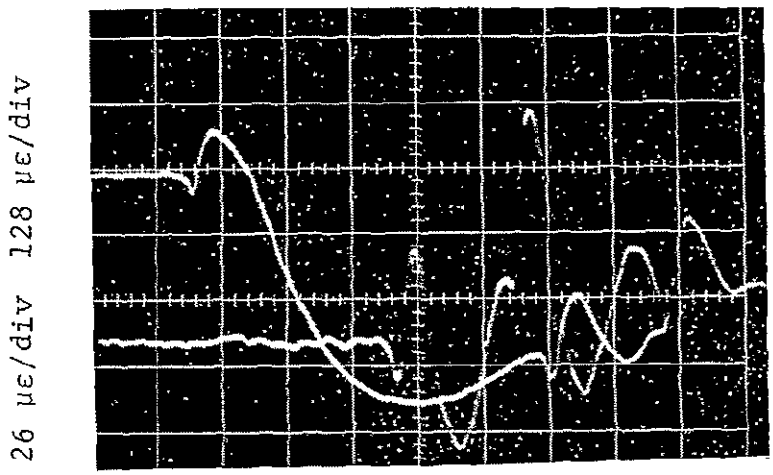

(a) 20 μsec/div

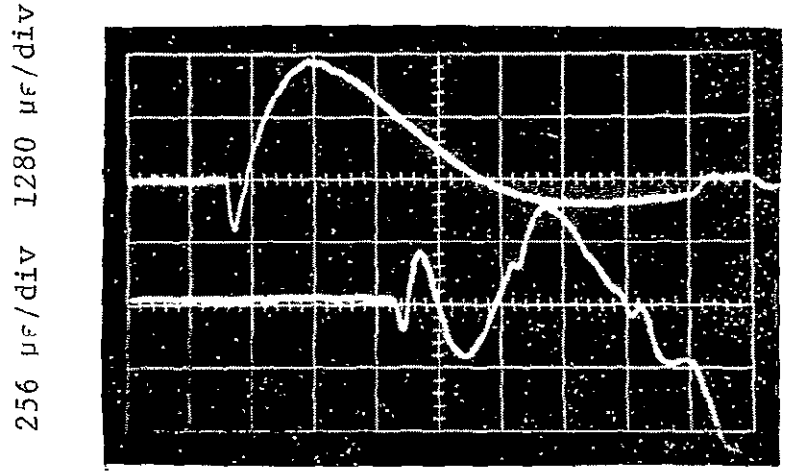

(b) 20 μsec/div

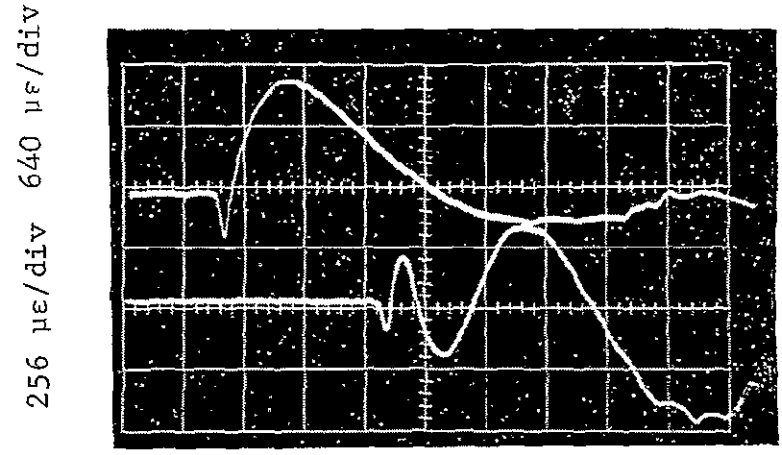

(c) 20 μsec/div

Fig. 33 STRAIN GAGE SIGNALS IN TRANSVERSELY IMPACTED $[0_2/\pm 45]_{2s}$ GRAPHITE/EPOXY SPECIMEN 9GA-1 ON 45-DEGREE AXIS

a) Gages in y-Direction
b) Gages in x-Direction
c) Gages in 45-Degree Direction

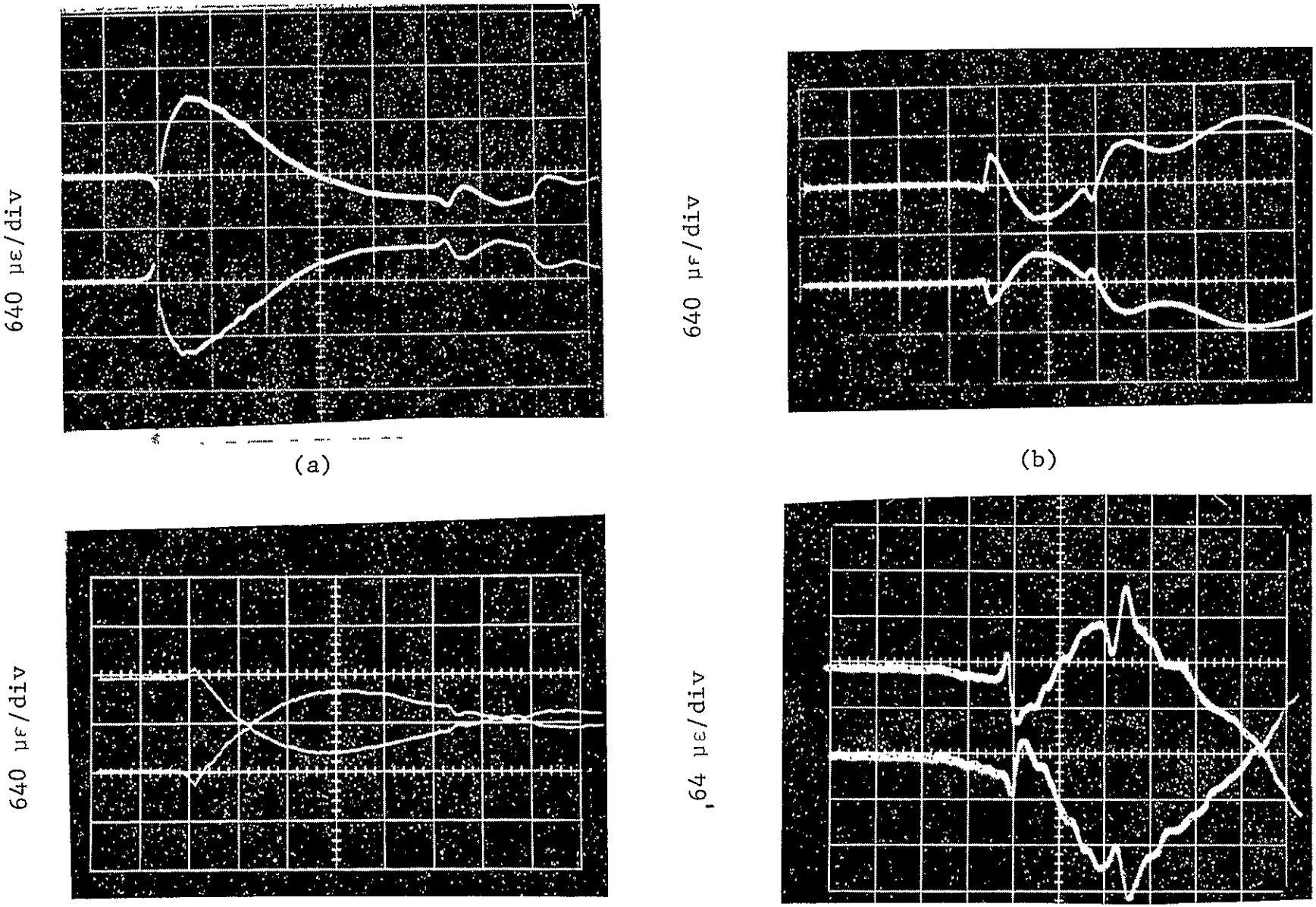

Fig. 34 STRAIN GAGE SIGNALS ON OPPOSITE FACES OF TRANSVERSELY IMPACTED $[0_2/\pm45]_{2s}$ GRAPHITE/EPOXY SPECIMEN 9GA-1 ALONG y-AXIS (Sweep: 20 μsec/div)
(a) Gages in y-direction 2.54 cm (1 in) from center
(b) Gages in y-direction 7.62 cm (3 in) from center
(c) Gages in x-direction 2.54 cm (1 in) from center
(d) Gages in x-direction 7.62 cm (3 in) from center

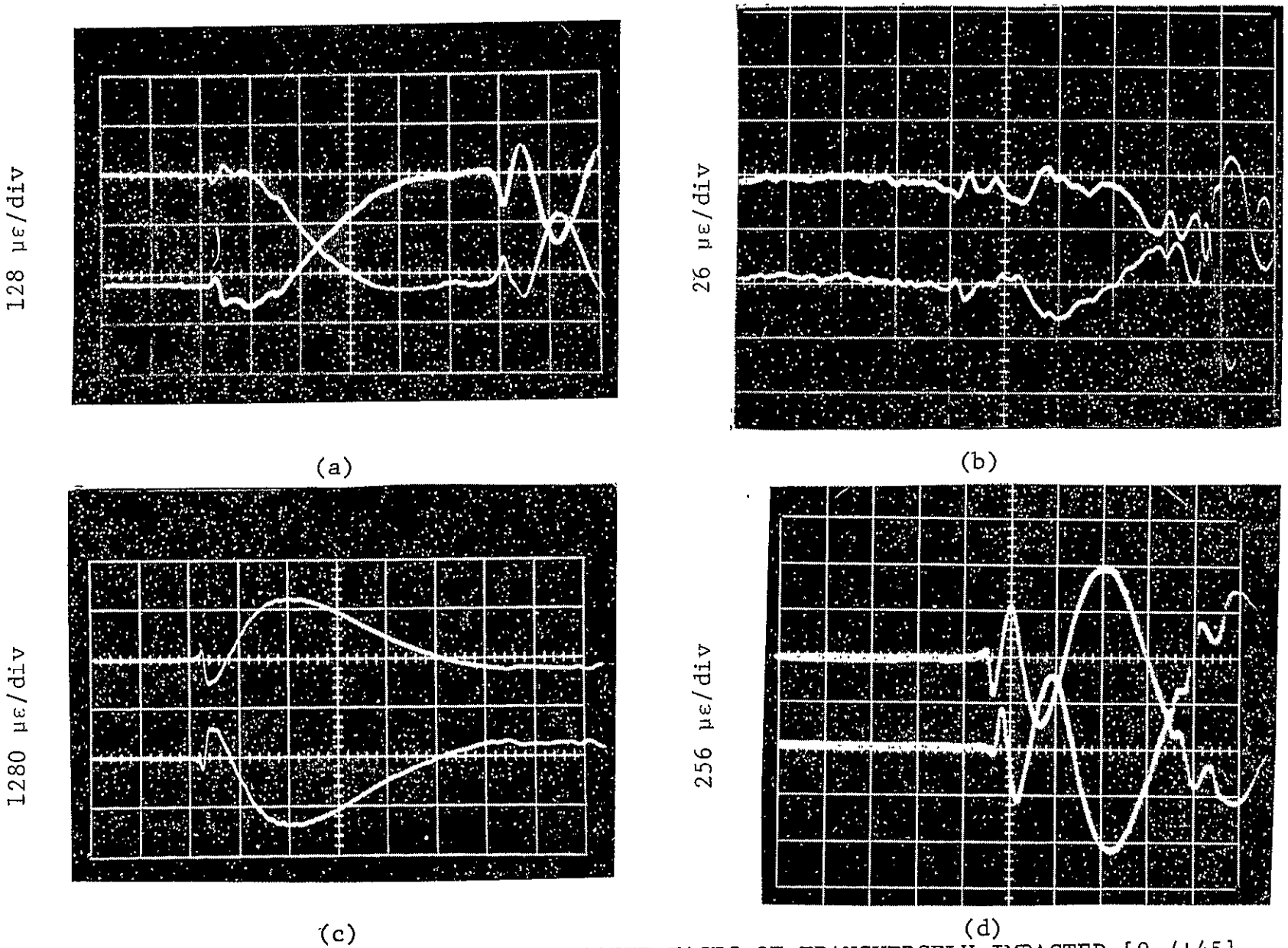

Fig. 35 STRAIN GAGE SIGNALS ON OPPOSITE FACES OF TRANSVERSELY IMPACTED $[0_2/\pm45]_{2s}$ GRAPHITE/EPOXY SPECIMEN 9GA-1 ALONG x-AXIS (Sweep: 20 μsec/div)
(a) Gages in y-direction 2.54 cm (1 in) from center
(b) Gages in y-direction 7.62 cm (3 in) from center
(c) Gages in x-direction 2.54 cm (1 in) from center
(d) Gages in x-direction 7.62 cm (3 in) from center

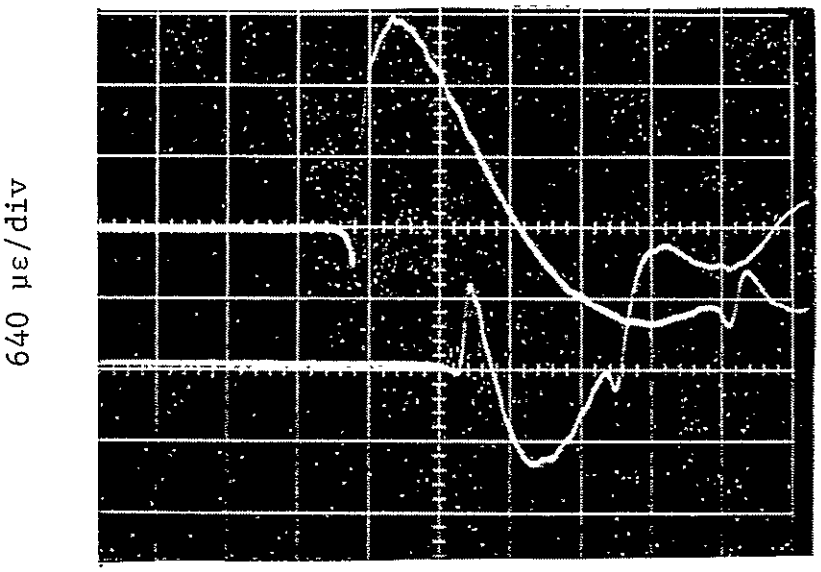

(a)

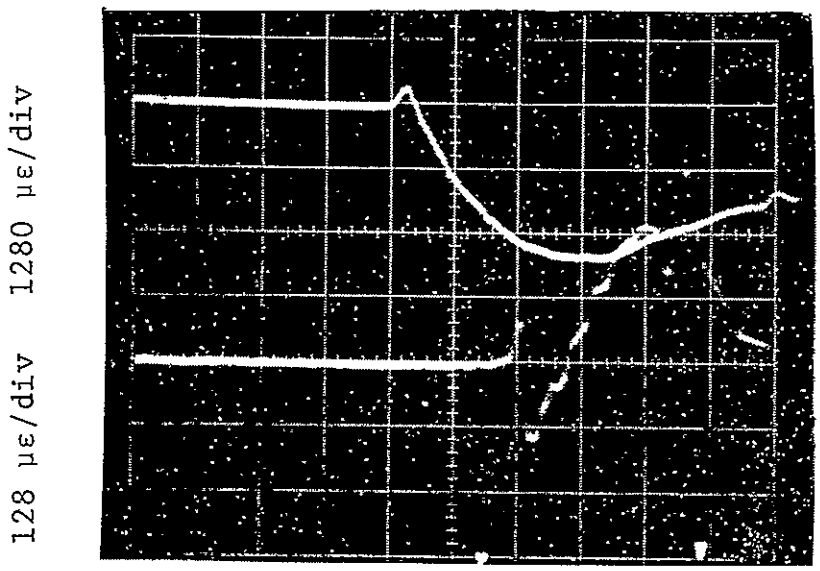

(b)

Fig. 36 DIFFERENCES OF STRAIN GAGE SIGNALS FROM OPPOSITE FACES OF TRANSVERSELY IMPACTED $[0_2/\pm 45]_{2s}$ GRAPHITE/EPOXY SPECIMEN 9GA-1 ALONG y-AXIS
(Sweep: 20 μsec/div)
(a) Gages in y-direction 5.08 cm (2 in) apart
(b) Gages in x-direction 5.08 cm (2 in) apart

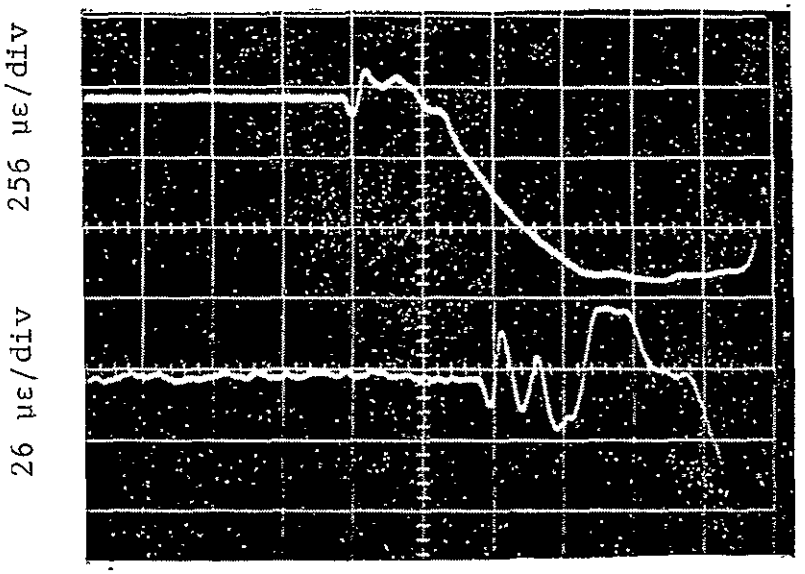

(a)

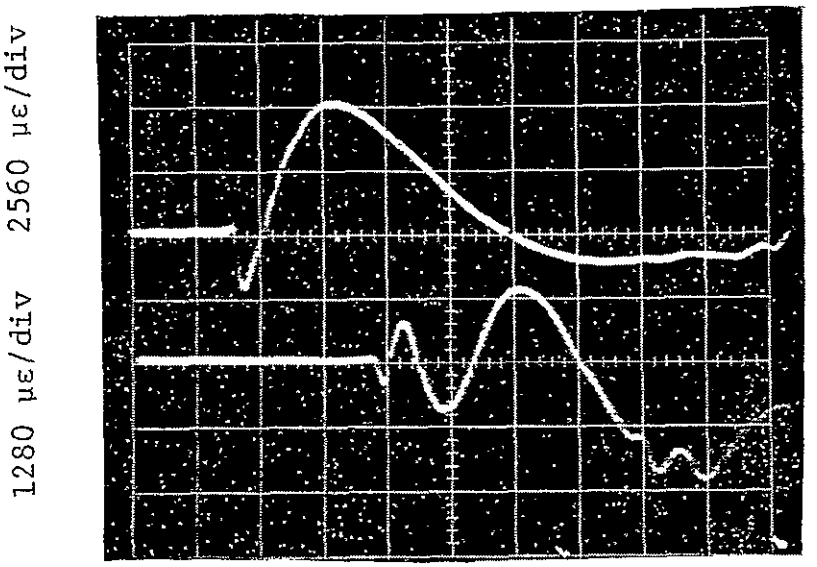

(b)

Fig. 37 DIFFERENCES OF STRAIN GAGE SIGNALS FROM OPPOSITE FACES OF TRANSVERSELY IMPACTED $[0_2/\pm 45]_{2s}$ GRAPHITE/EPOXY SPECIMEN 9GA-1 ALONG x-AXIS (Sweep: 20 μsec/div)

(a) Gages in y-direction 5.08 cm (2 in.) apart
(b) Gages in x-direction 5.08 cm (2 in.) apart

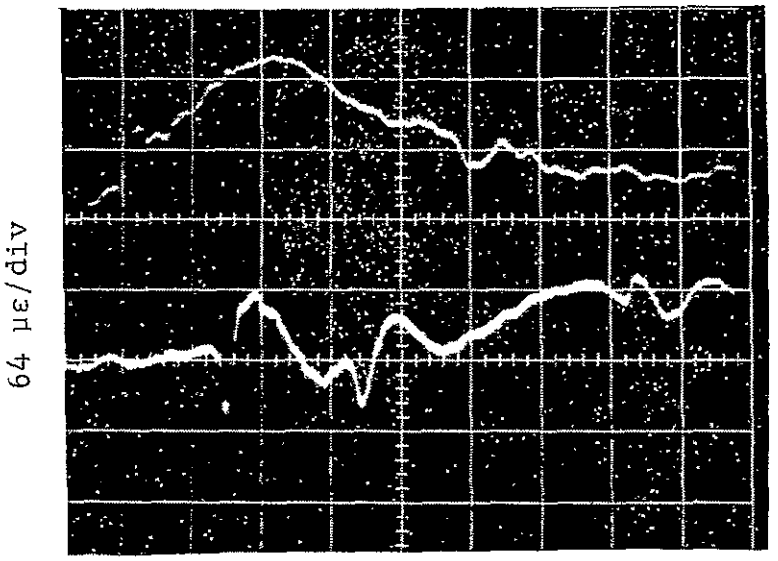

(a)

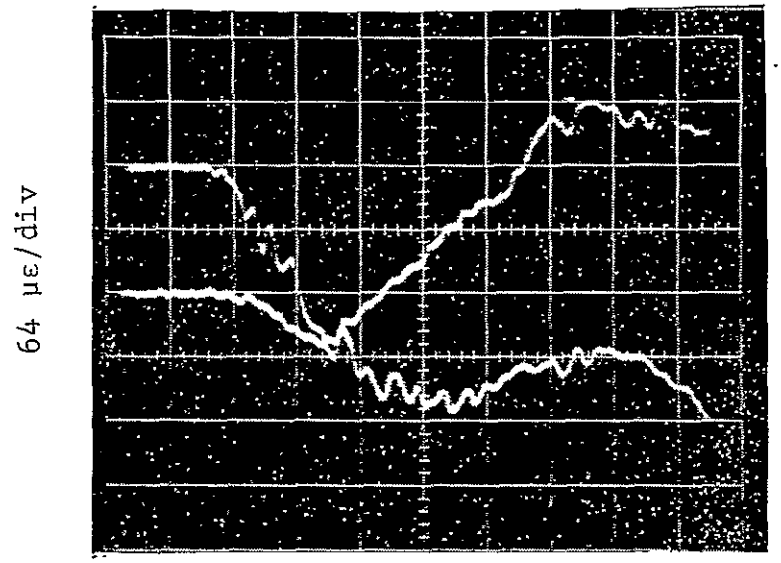

(b)

Fig. 38 SUMS OF STRAIN GAGE SIGNALS FROM OPPOSITE FACES OF TRANSVERSELY IMPACTED $[0_2/\pm 45]_{2s}$ GRAPHITE/EPOXY SPECIMEN 9GA-1 ALONG y-AXIS (Sweep: 20 μsec/div)

(a) Gages in y-direction 5.08 cm (2 in.) apart
(b) Gages in x-direction 5.08 cm (2 in.) apart

C.2

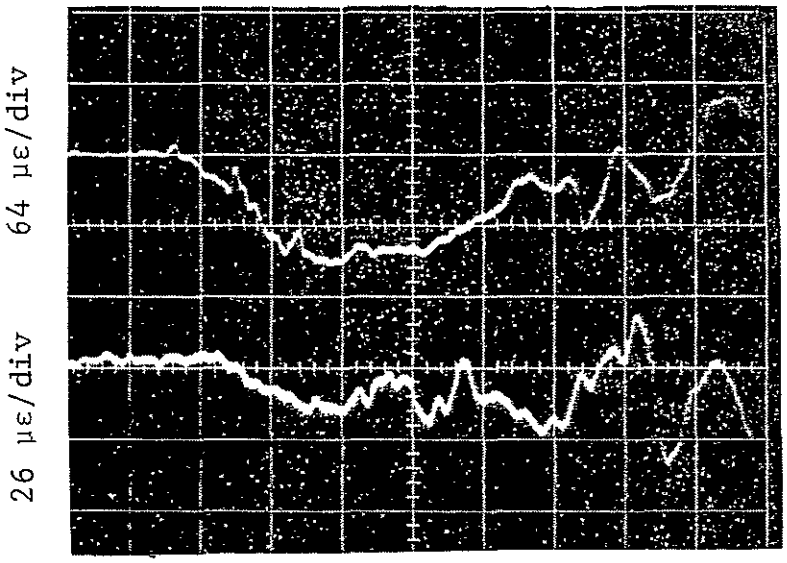

(a)

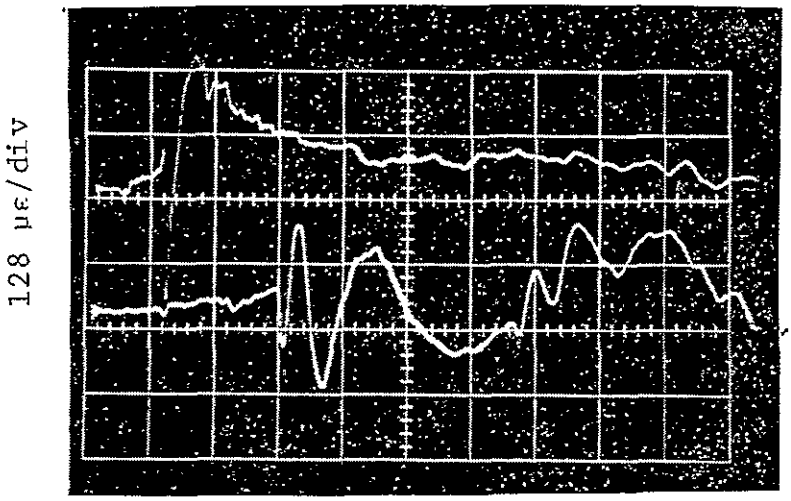

(b)

Fig. 39 SUMS OF STRAIN GAGE SIGNALS FROM OPPOSITE FACES OF TRANSVERSELY IMPACTED $[0_2/\pm45]_{2s}$ GRAPHITE/EPOXY SPECIMEN 9GA-1 ALONG x-AXIS
(Sweep: 20 μsec/div)
(a) Gages in y-direction 5.08 cm (2 in.) apart
(b) Gages in x-direction 5.08 cm (2 in.) apart

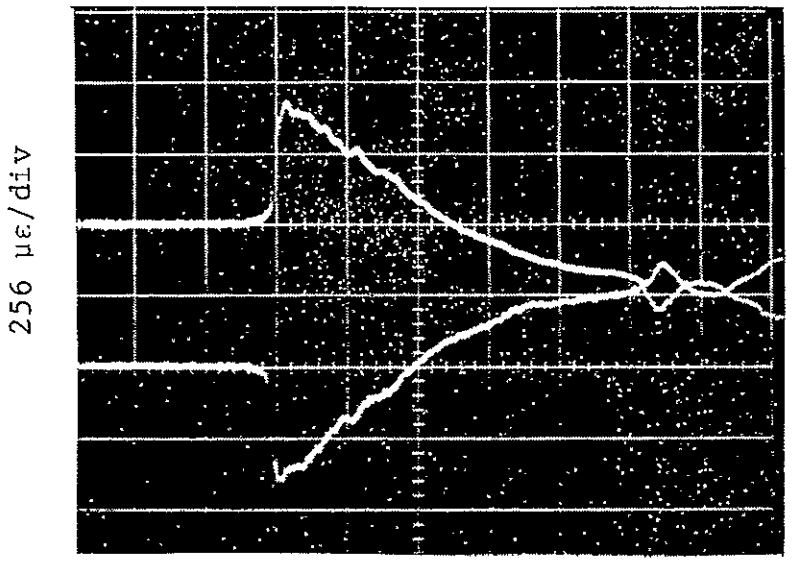

(a)

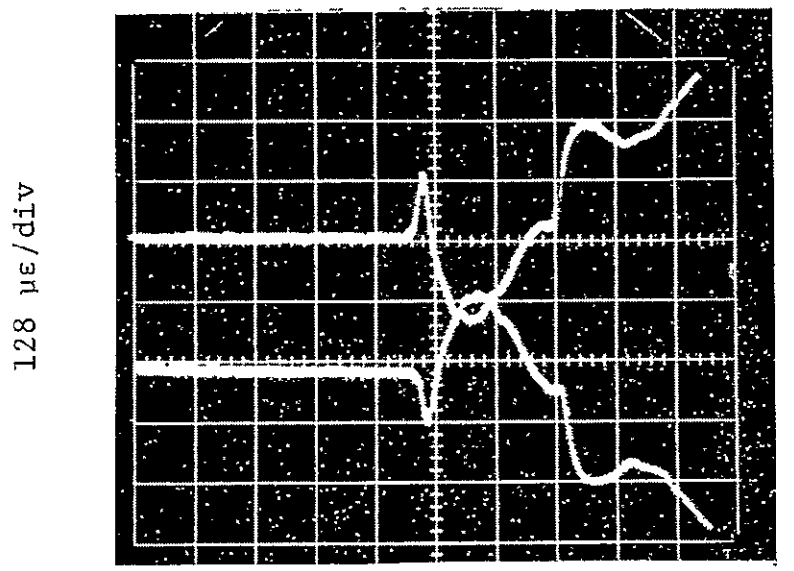

(b)

Fig. 40 OBLIQUE IMPACT. STRAIN GAGE SIGNALS ON OPPOSITE FACES OF TRANSVERSELY IMPACTED $[0_2/\pm 45]_{2s}$ GRAPHITE/EPOXY SPECIMEN 9GA-1 ALONG y-AXIS

(Sweep: 20 μsec/div)

(a) Gages in y-direction 2.54 cm (1 in.) from center
(b) Gages in y-direction 7.62 cm (3 in.) from center

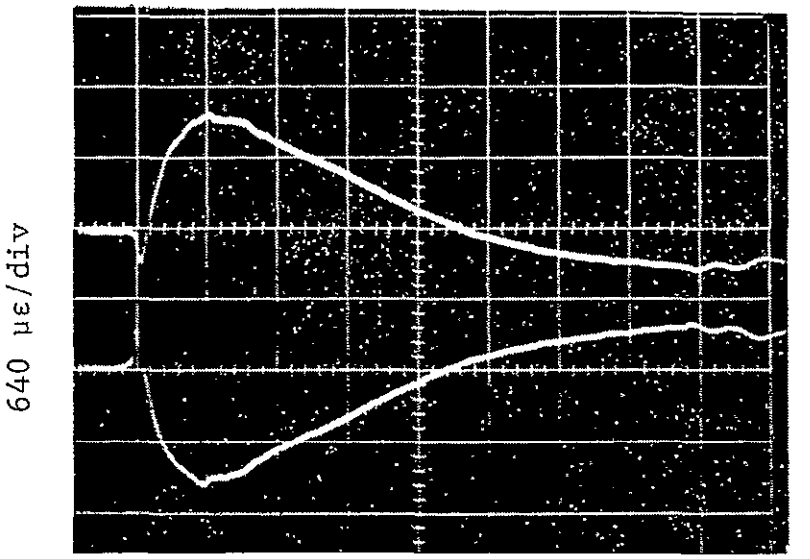

(a)

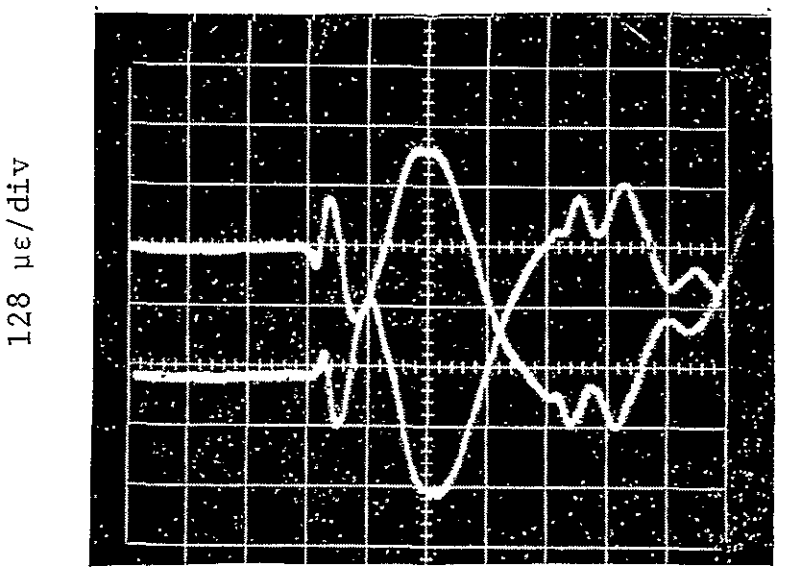

(b)

Fig. 41 OBLIQUE IMPACT. STRAIN GAGE SIGNALS ON OPPOSITE FACES OF TRANSVERSELY IMPACTED $[0_2/\pm 45]_{2s}$ GRAPHITE/EPOXY SPECIMEN 9GA-1 ALONG x-AXIS

(Sweep: 20 μsec/div)

(a) Gages in x-direction 2.54 cm (1 in.) from center
(b) Gages in x-direction 7.62 cm (3 in.) from center

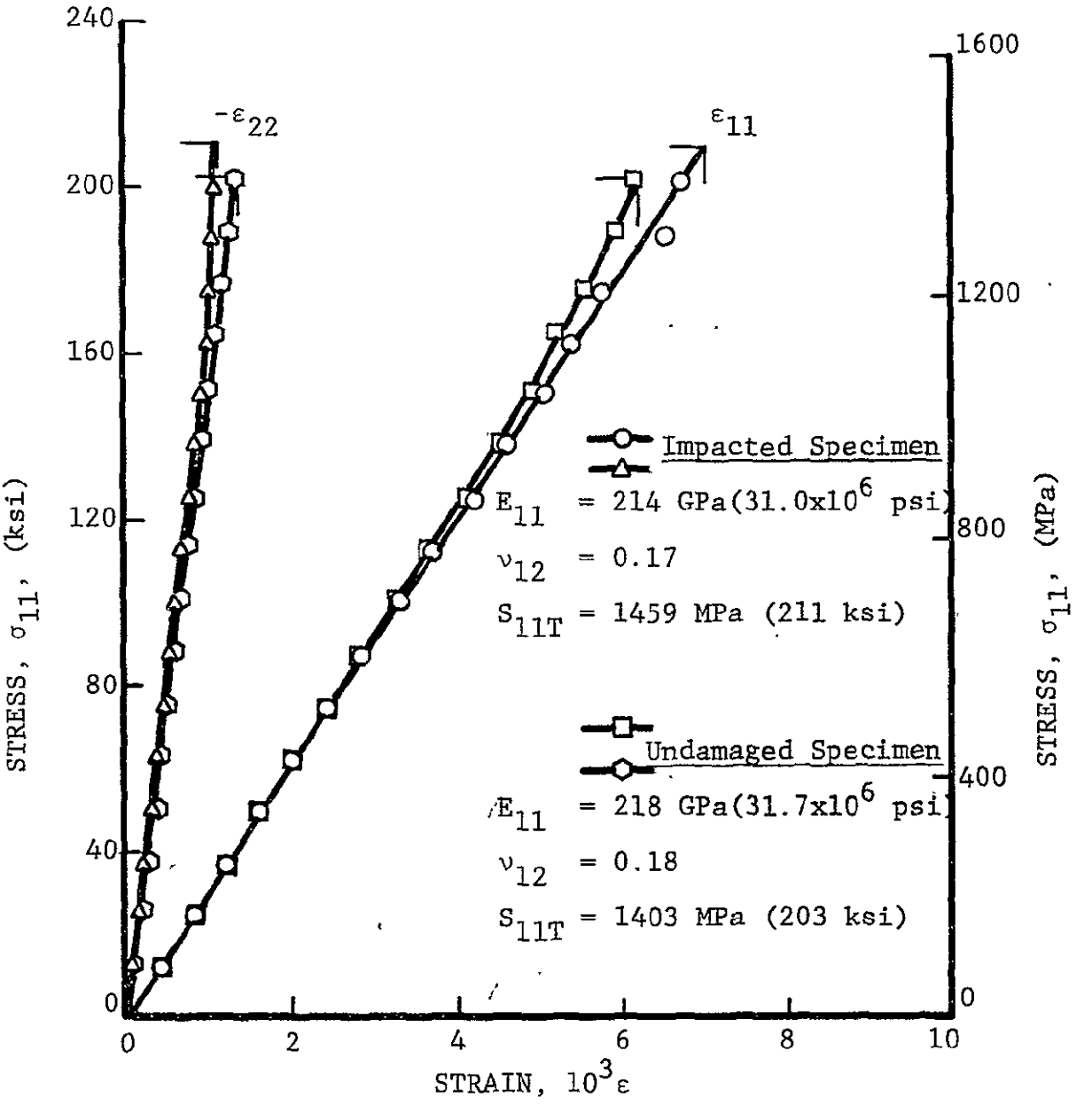

Fig. 42 STRAINS IN $[0]_{16}$ BORON/EPOXY SPECIMENS UNDER UNIAXIAL TENSION FROM UNDAMAGED AND IMPACTED LAMINATES (Impact Velocity: 210 ms^{-1}; 690 ft/sec)

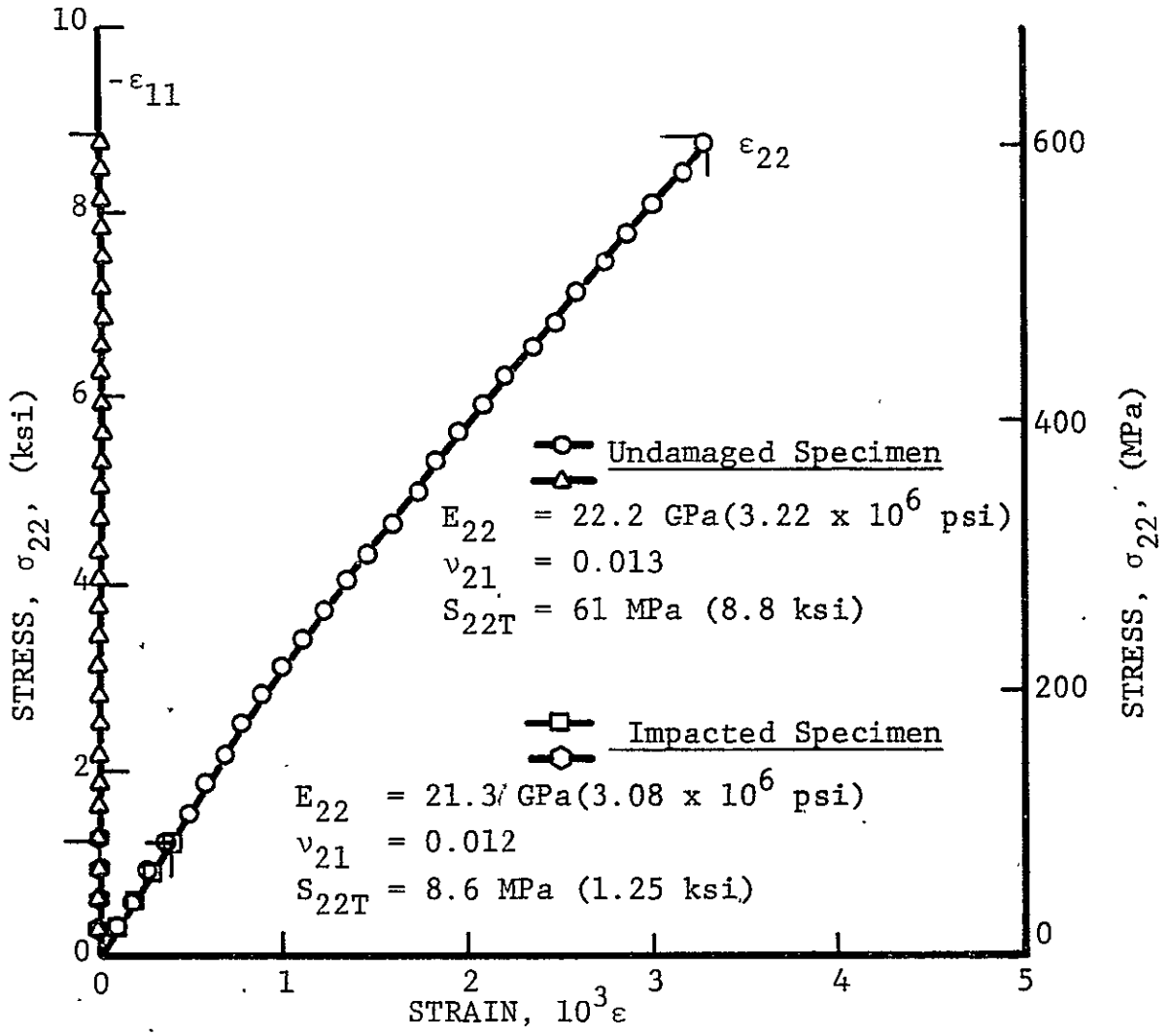

Fig. 43 STRAINS IN [90_{16}] BORON/EPOXY SPECIMENS UNDER UNIAXIAL TENSION FROM UNDAMAGED AND IMPACTED LAMINATES (Impact Velocity: 210 ms^{-1}; 690 ft/sec)

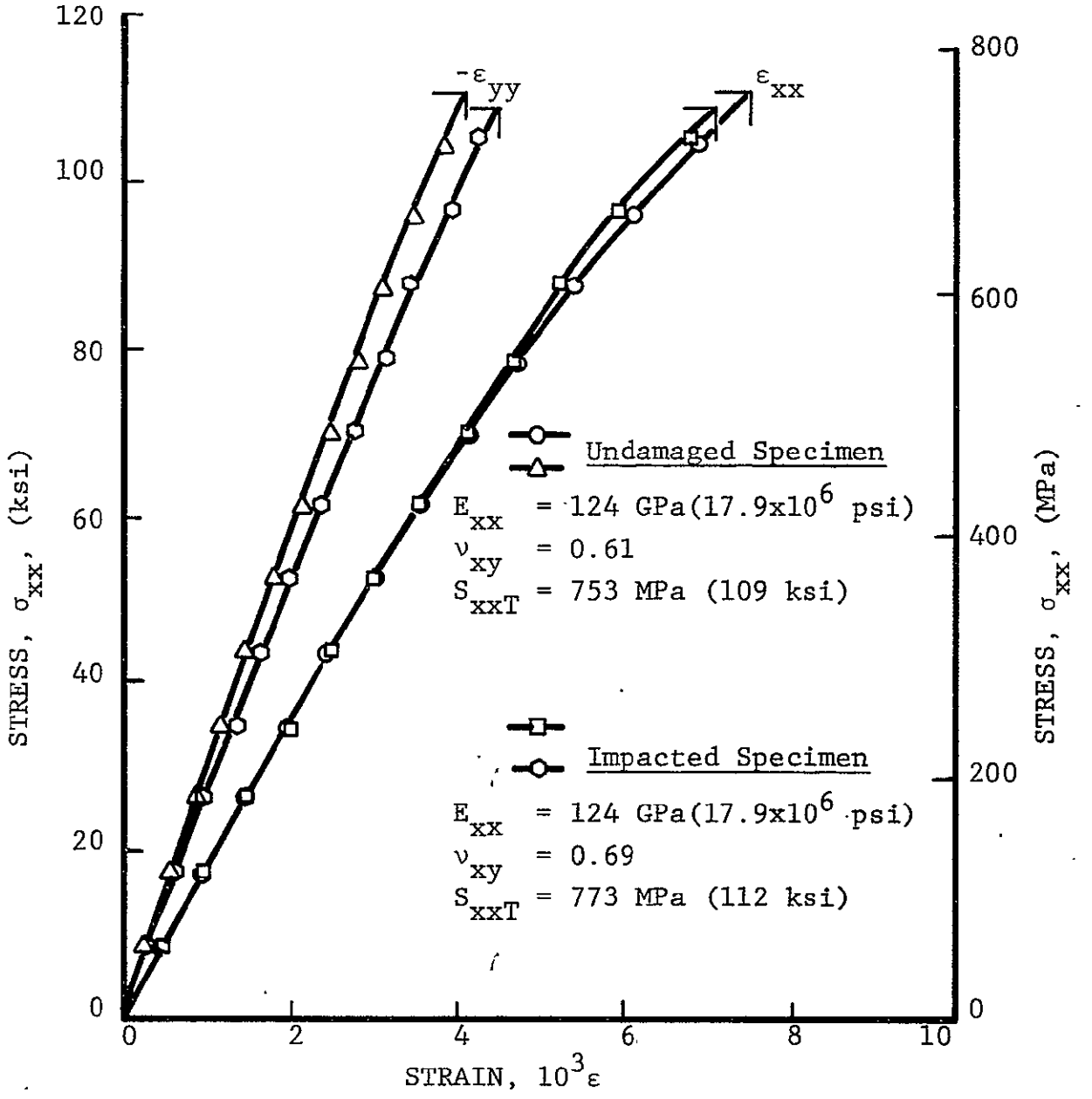

Fig. 44 STRAINS IN $[0_2/+45]_{2s}$ BORON/EPOXY SPECIMENS UNDER UNIAXIAL TENSION FROM UNDAMAGED AND IMPACTED LAMINATES (Impact Velocity: 210 ms^{-1}; 690 ft/sec)

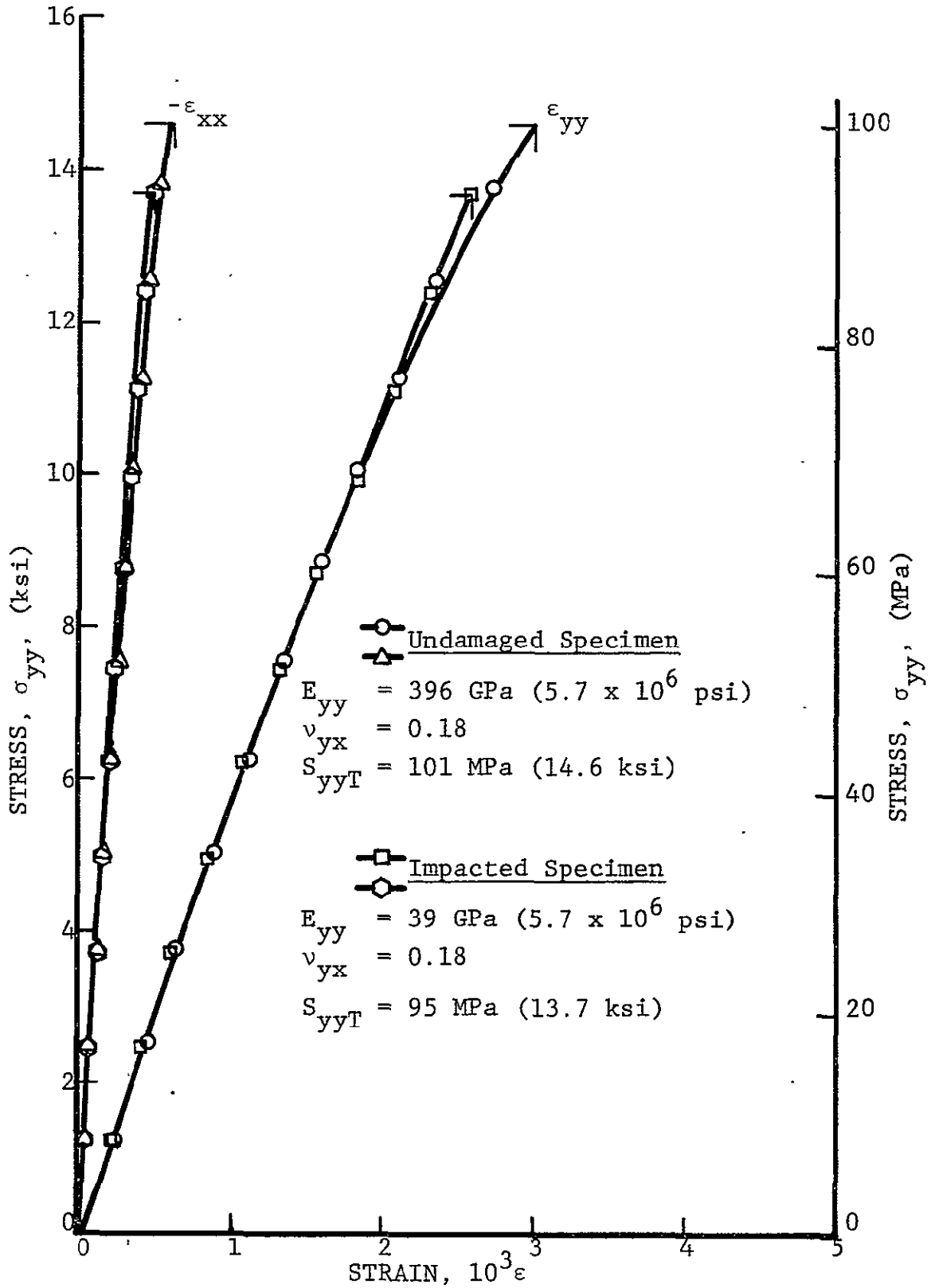

Fig. 45 STRAINS IN $[90_2/\pm45]_{2s}$ BORON/EPOXY SPECIMENS UNDER UNIAXIAL TENSION FROM UNDAMAGED AND IMPACTED LAMINATES (Impact Velocity: 210 ms^{-1}; 690 ft/sec)

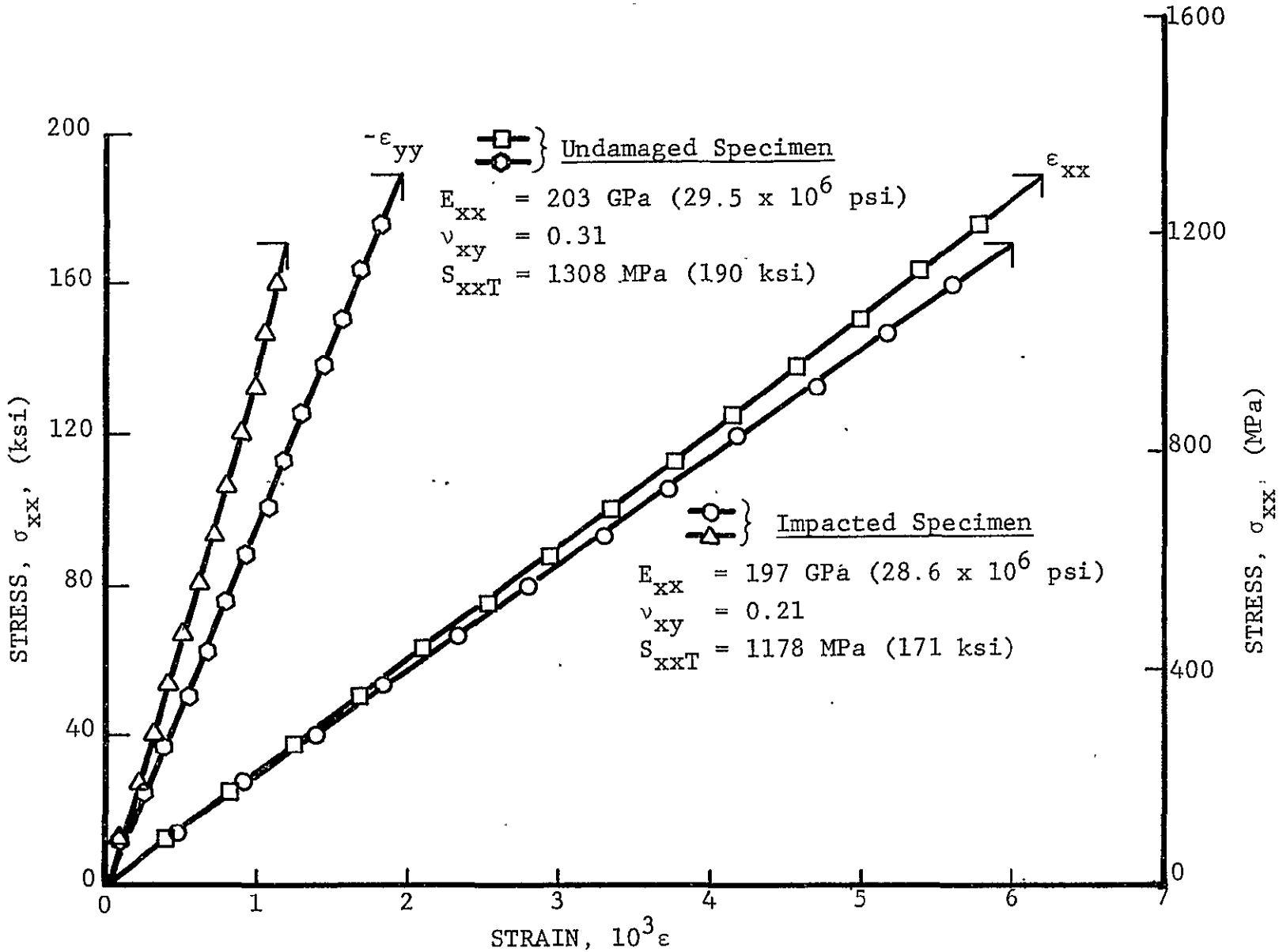

Fig. 46 STRAINS IN $[0_{16}]$ GRAPHITE/EPOXY SPECIMENS UNDER UNIAXIAL TENSION FROM UNDAMAGED AND IMPACTED LAMINATES (Impact Velocity: 192 ms^{-1}; 630 ft/sec)

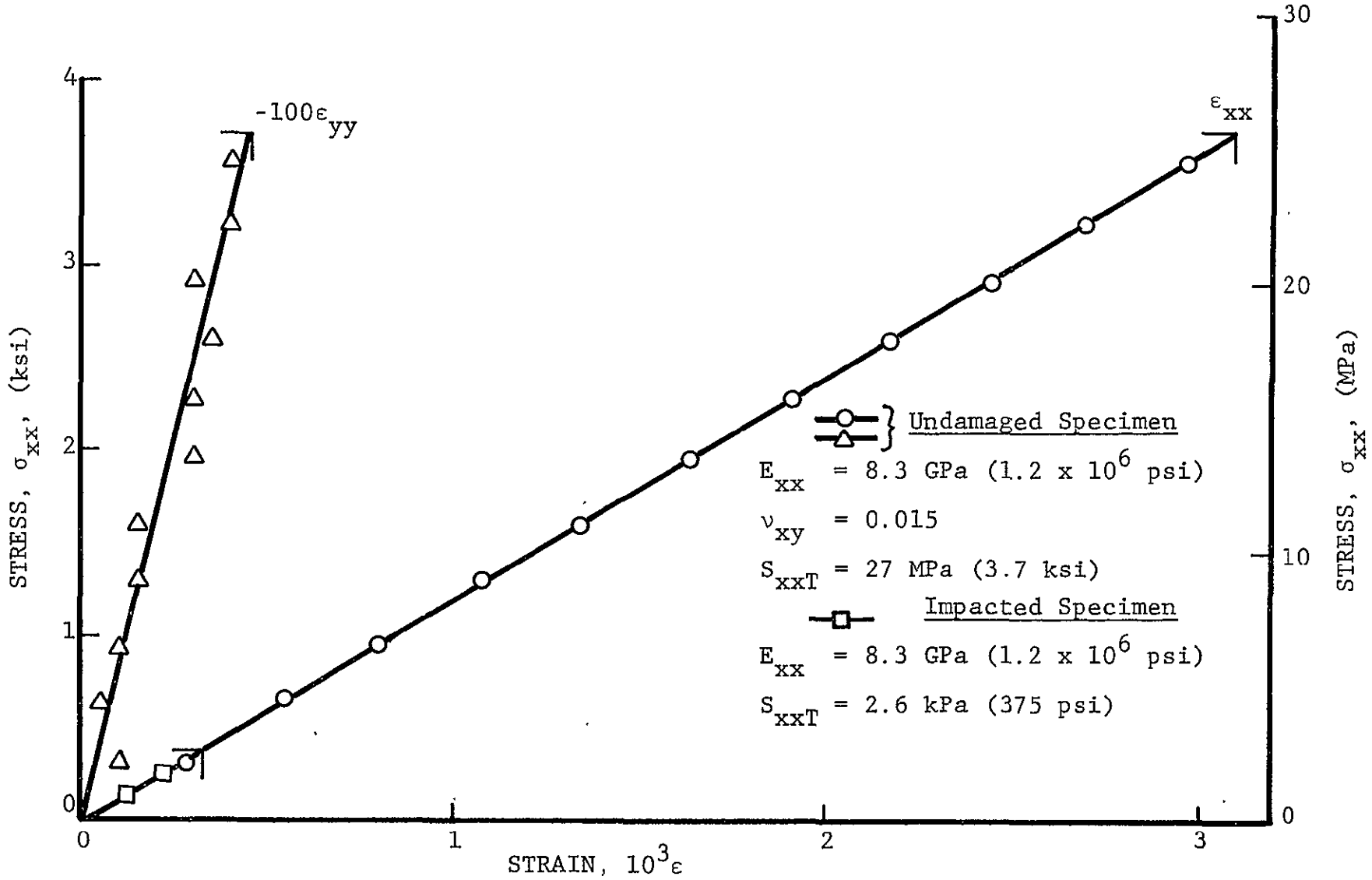

Fig. 47 STRAINS IN $[90_{16}]$ GRAPHITE/EPOXY SPECIMENS UNDER UNIAXIAL TENSION FROM UNDAMAGED AND IMPACTED LAMINATES (Impact Velocity: 192 ms^{-1}; 630 ft/sec)

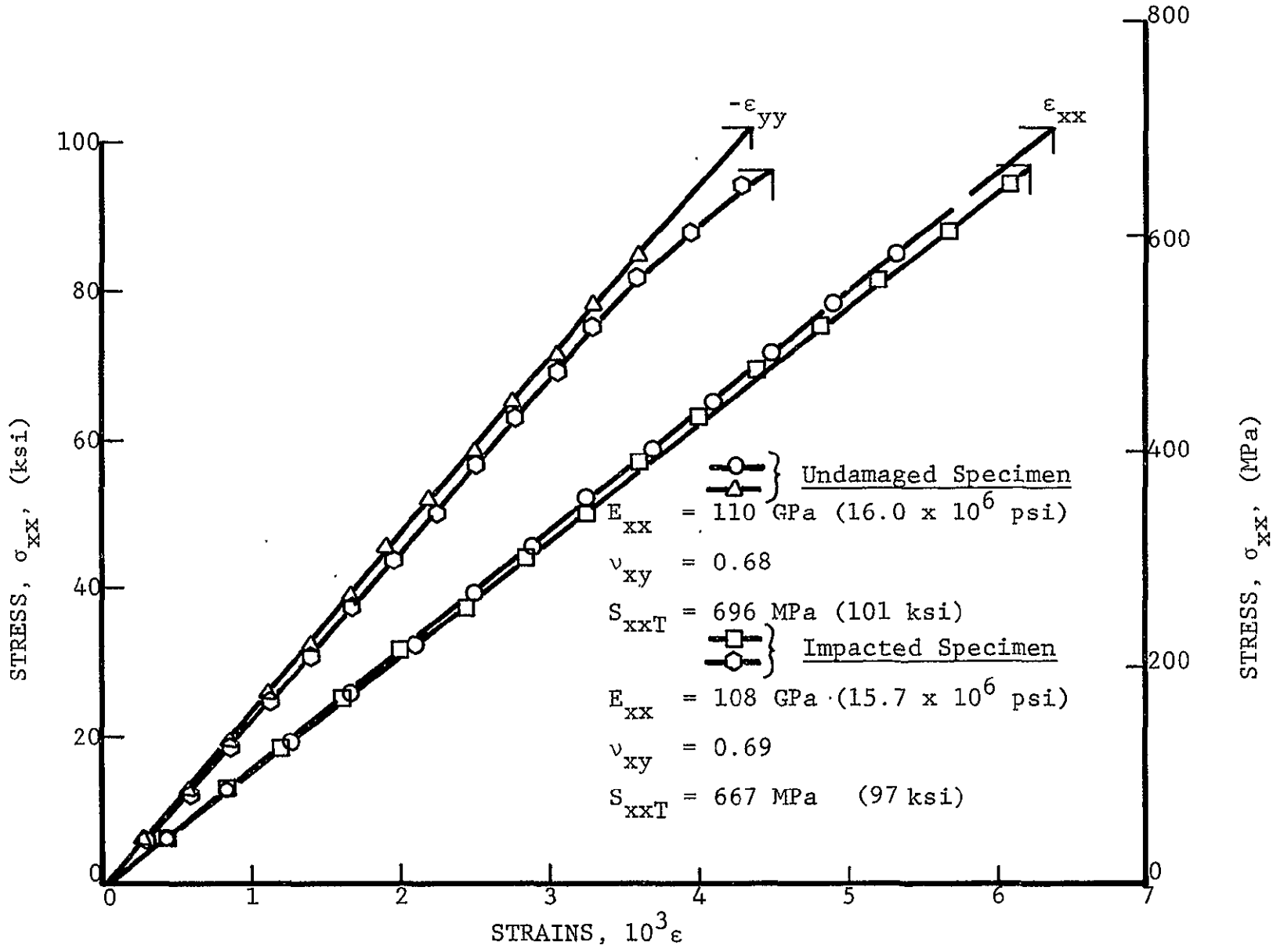

Fig. 48 STRAINS IN $[0_2/\pm45]_{2s}$ GRAPHITE/EPOXY SPECIMENS UNDER UNIAXIAL TENSION FROM UNDAMAGED AND IMPACTED LAMINATES (Impact Velocity: 192 ms^{-1}; 630 ft/sec)

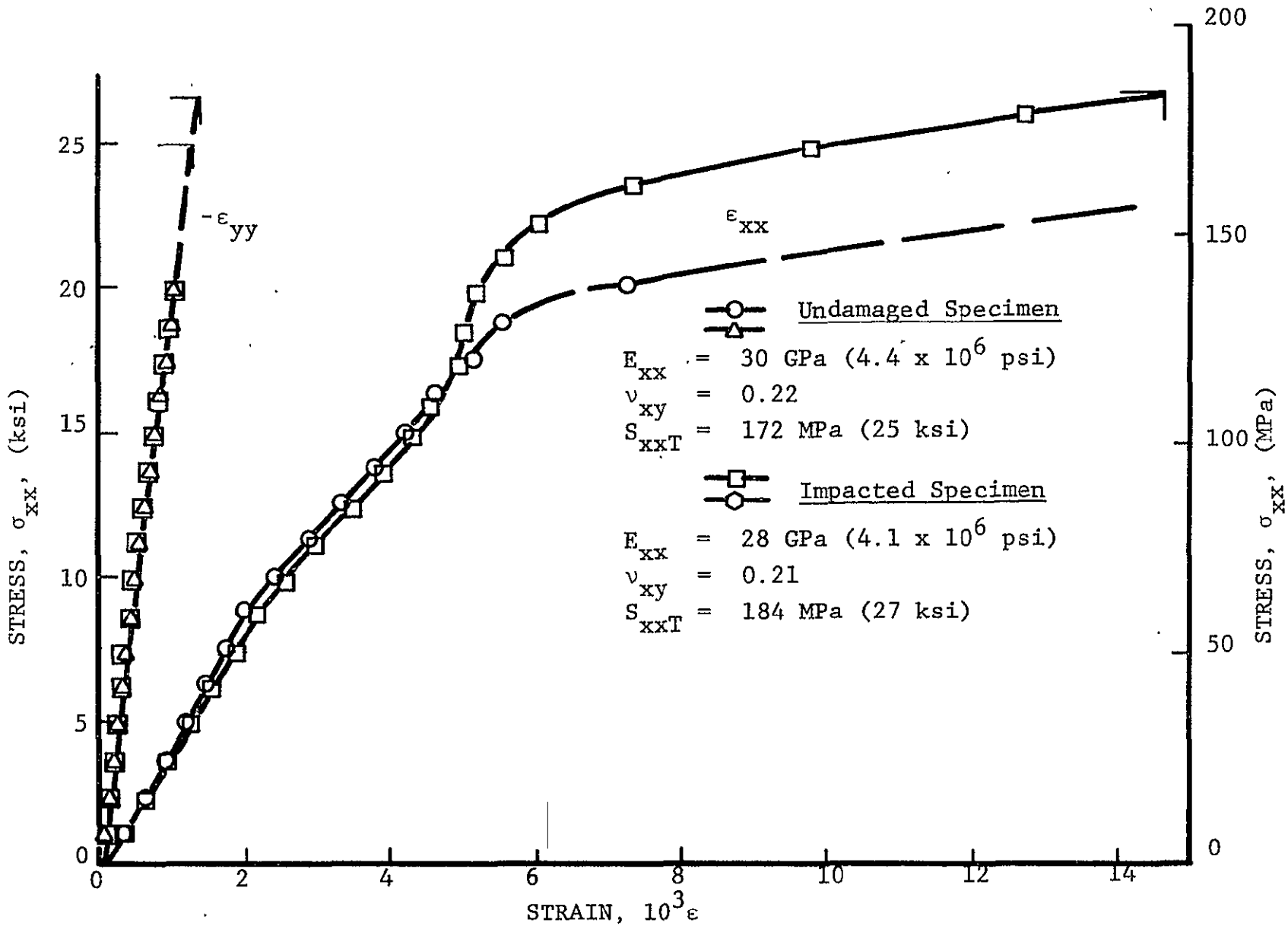

Fig. 49 STRAINS IN $[90_2/\pm45]_{2s}$ GRAPHITE/EPOXY SPECIMENS UNDER UNIAXIAL TENSION FROM UNDAMAGED AND IMPACTED LAMINATES (Impact Velocity: 192 ms^{-1}; 630 ft/sec)

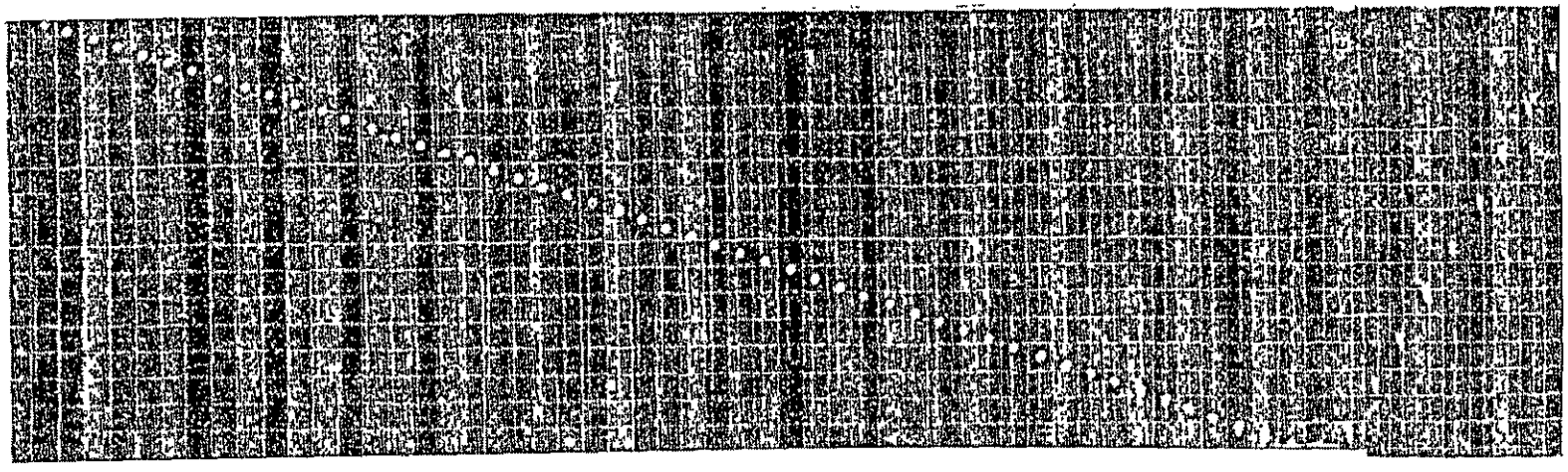

Fig. 50 SEQUENCE OF FRAMES OF PHOTOGRAPHIC (FASTAX) RECORD OF A 7.9 mm (5/16 in.) DIAMETER SILASTIC SPHERE IMPACTING A $[0_{16}]$ BORON/EPOXY PLATE AT 250 ms^{-1} (820 ft/sec) (141 μs/frame)

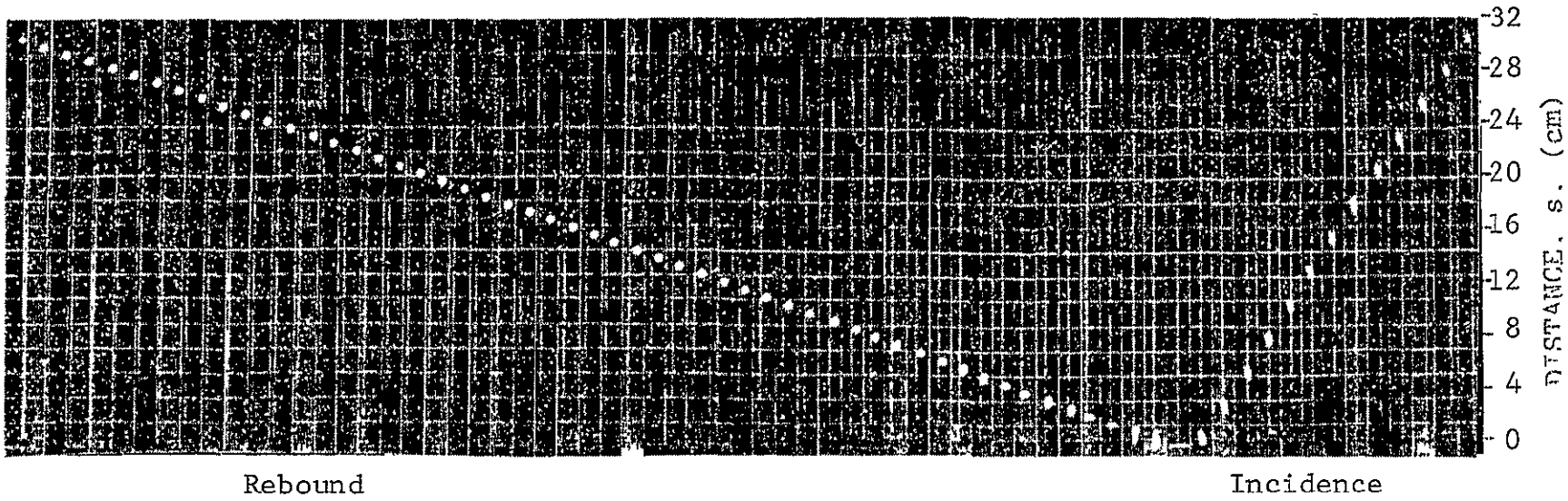

Fig. 51 SEQUENCE OF FRAMES OF PHOTOGRAPHIC (FASTAX) RECORD OF A 7.9 mm (5/16 in) DIAMETER SILASTIC SPHERE IMPACTING A $[0_{16}]$ BORON/EPOXY PLATE AT 192 ms^{-1} (630 ft/sec) (141 μs/frame)

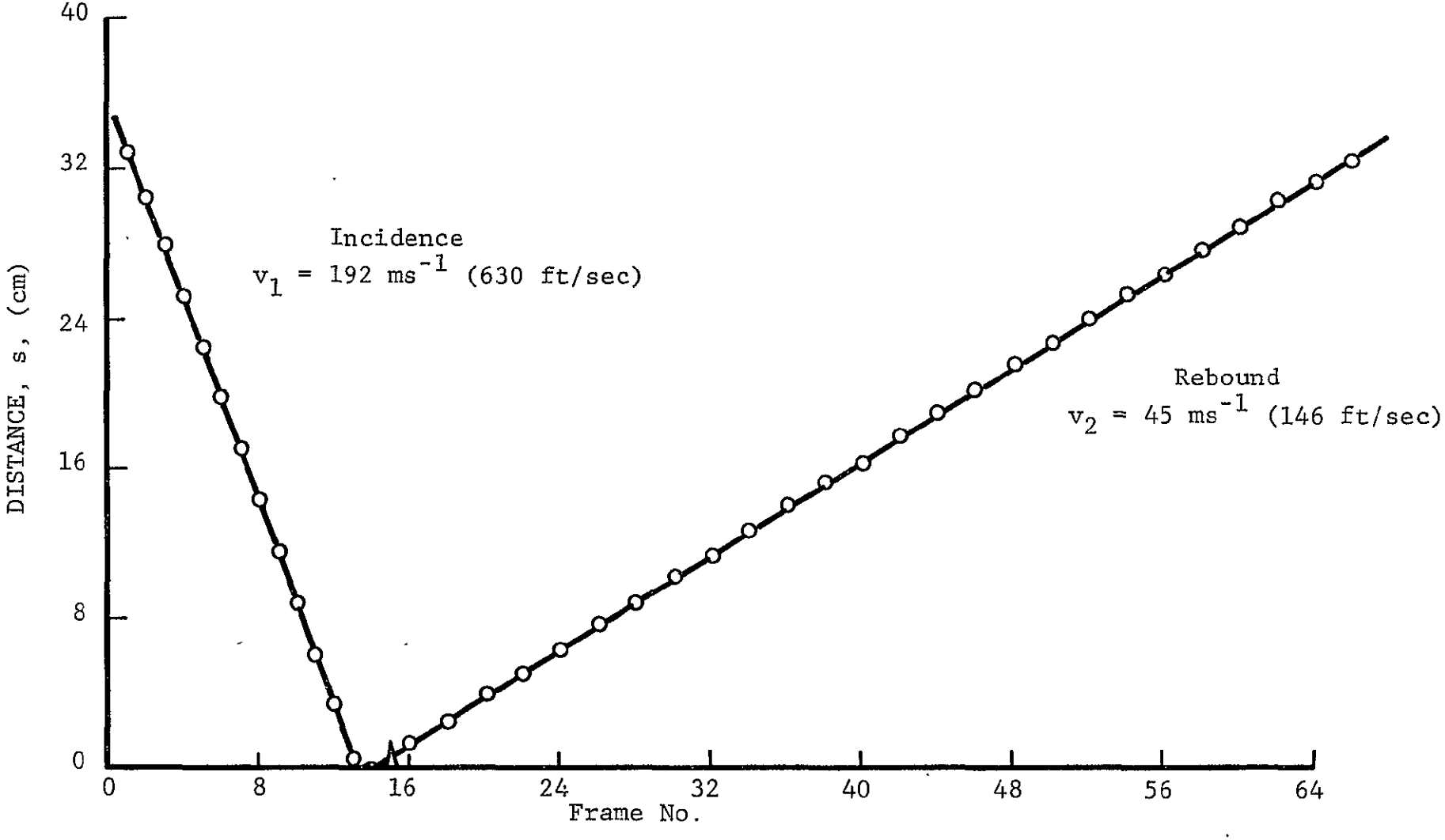

Fig. 52 PROJECTILE DISTANCE FROM IMPACTED PLATE AS A FUNCTION OF FRAME NUMBER (Barrel Pressure: 276 kPa, 40 psi; Plate: $[0_{16}]$ Boron/Epoxy; 141 μs/frame)

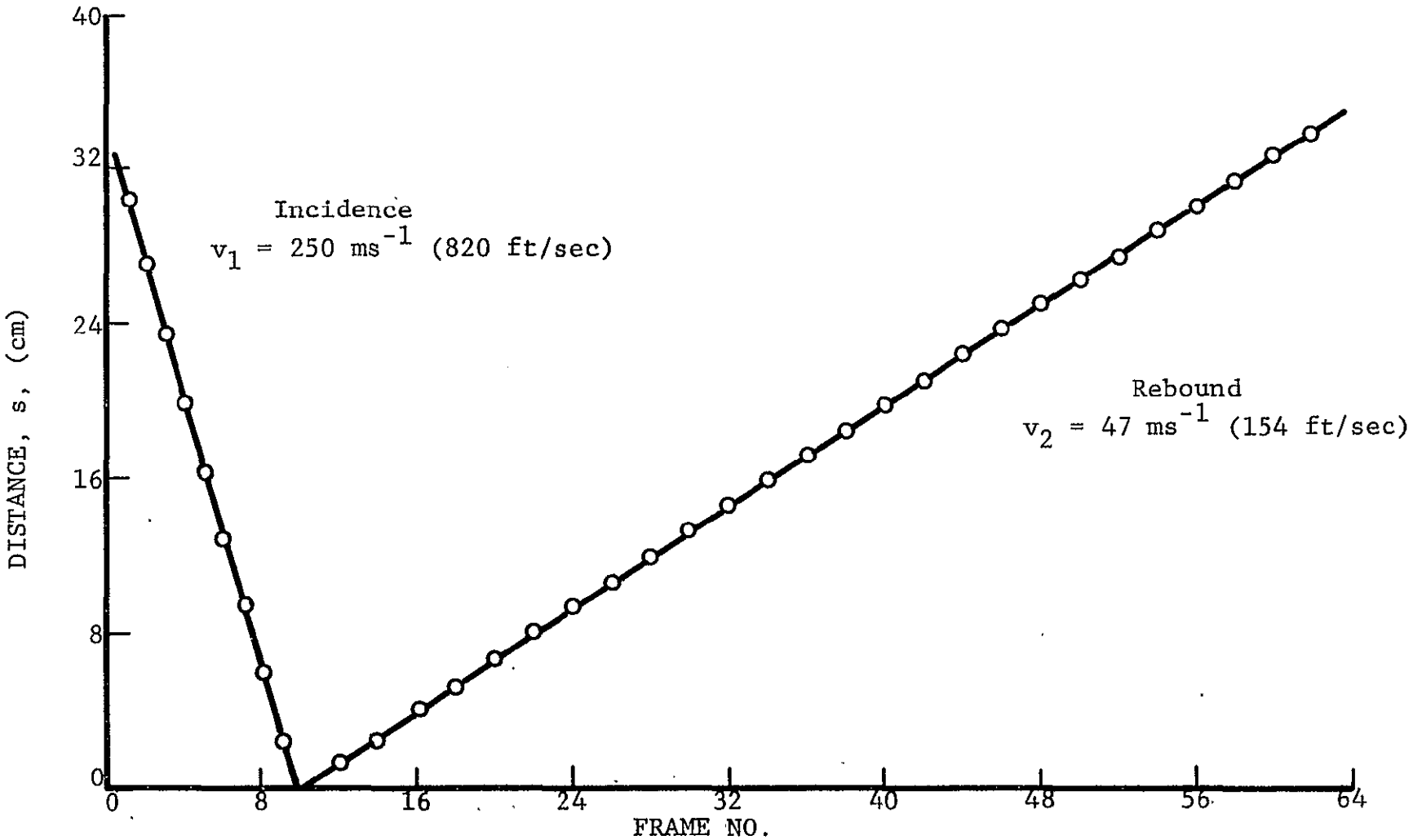

Fig. 53 PROJECTILE DISTANCE FROM IMPACTED PLATE AS A FUNCTION OF FRAME NUMBER (Barrel Pressure: 587 kPa, 85 psi; Plate: $[0_{16}]$ Boron/Epoxy; 141 μs/frame)

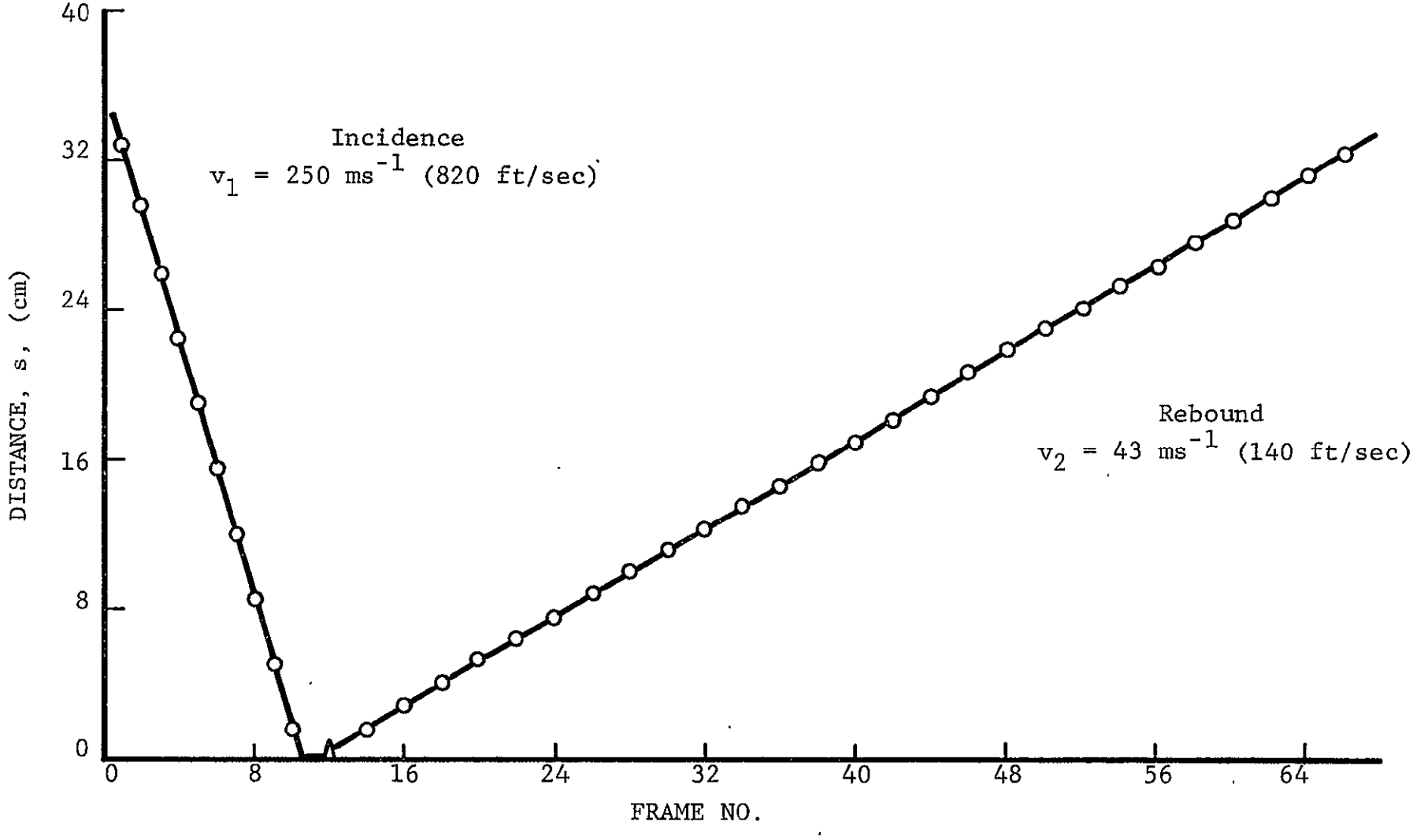

Fig. 54 PROJECTILE DISTANCE FROM IMPACTED PLATE AS A FUNCTION OF FRAME NUMBER (Barrel Pressure: 656 kPa, 95 psi; Plate: $[0_2/\pm45]_{2s}$ Boron/Epoxy; 138 μs/frame)

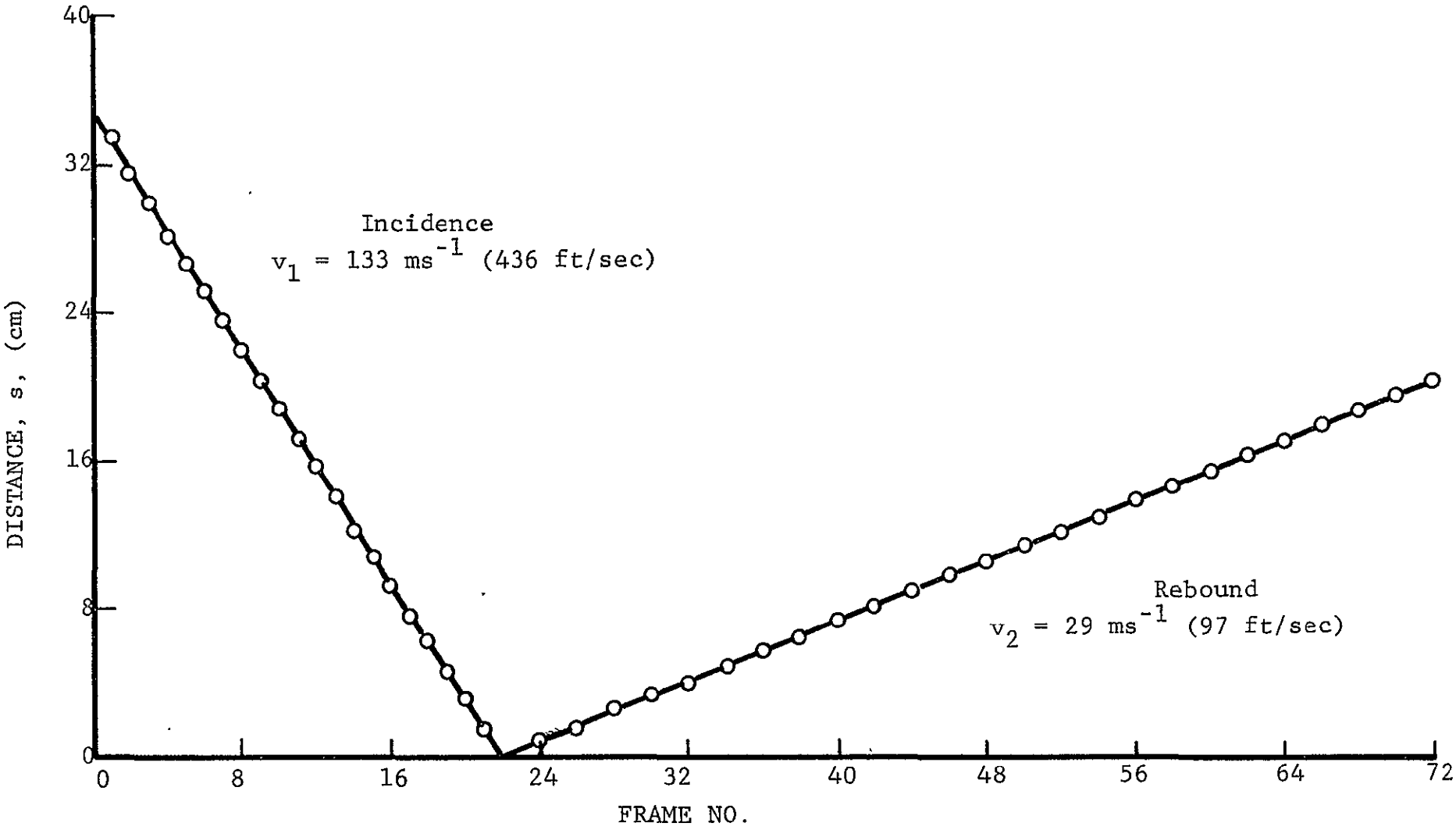

Fig. 55 PROJECTILE DISTANCE FROM IMPACTED PLATE AS A FUNCTION OF FRAME NUMBER (Barrel Pressure: 69 kPa, 10 psi; Plate: $[0_{16}]$ Graphite/Epoxy; 138 μs/frame)

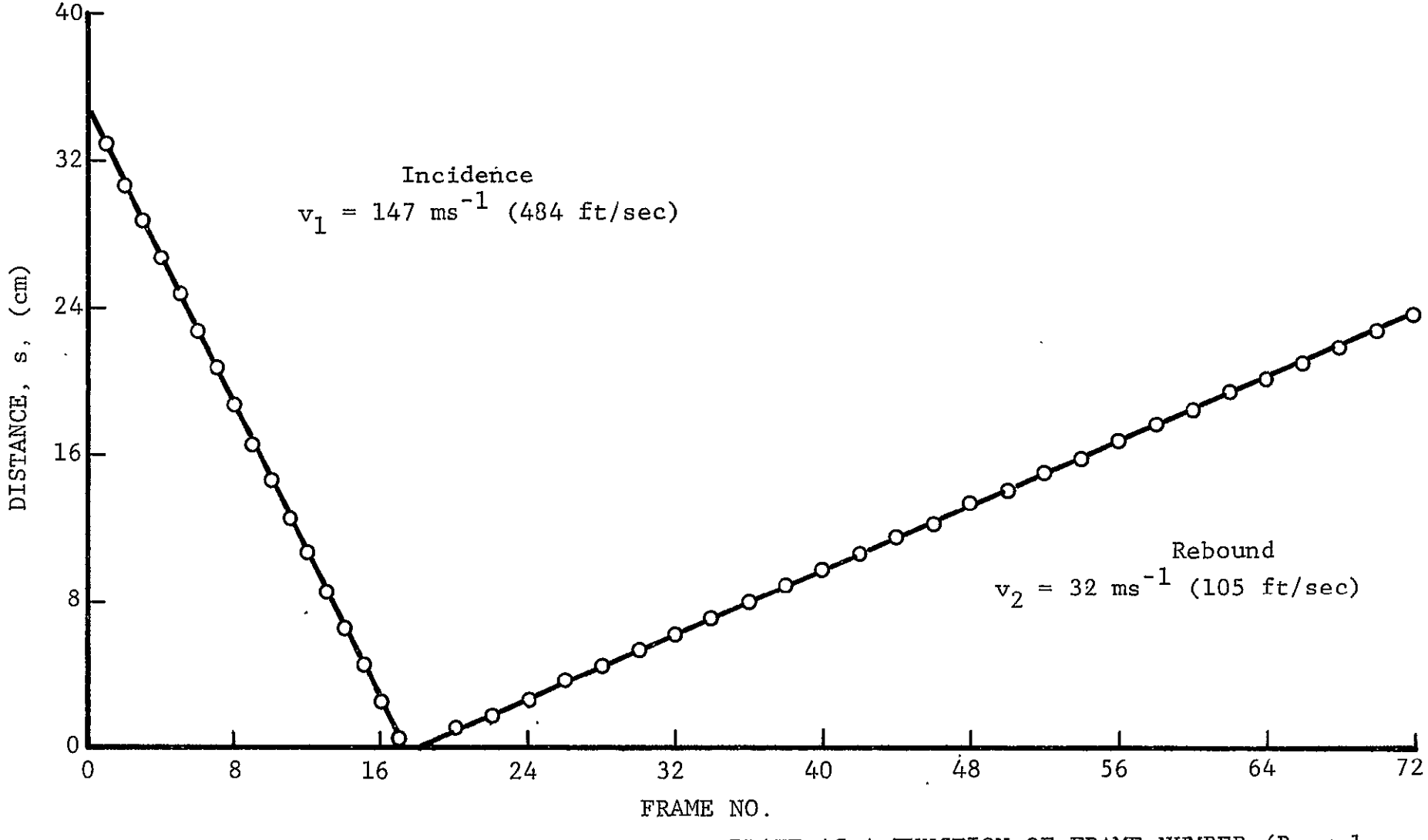

Fig. 56 PROJECTILE DISTANCE FROM IMPACTED PLATE AS A FUNCTION OF FRAME NUMBER (Barrel Pressure: 138 kPa, 20 psi; Plate: $[0_{16}]$ Graphite/Epoxy; 137 μs/frame)

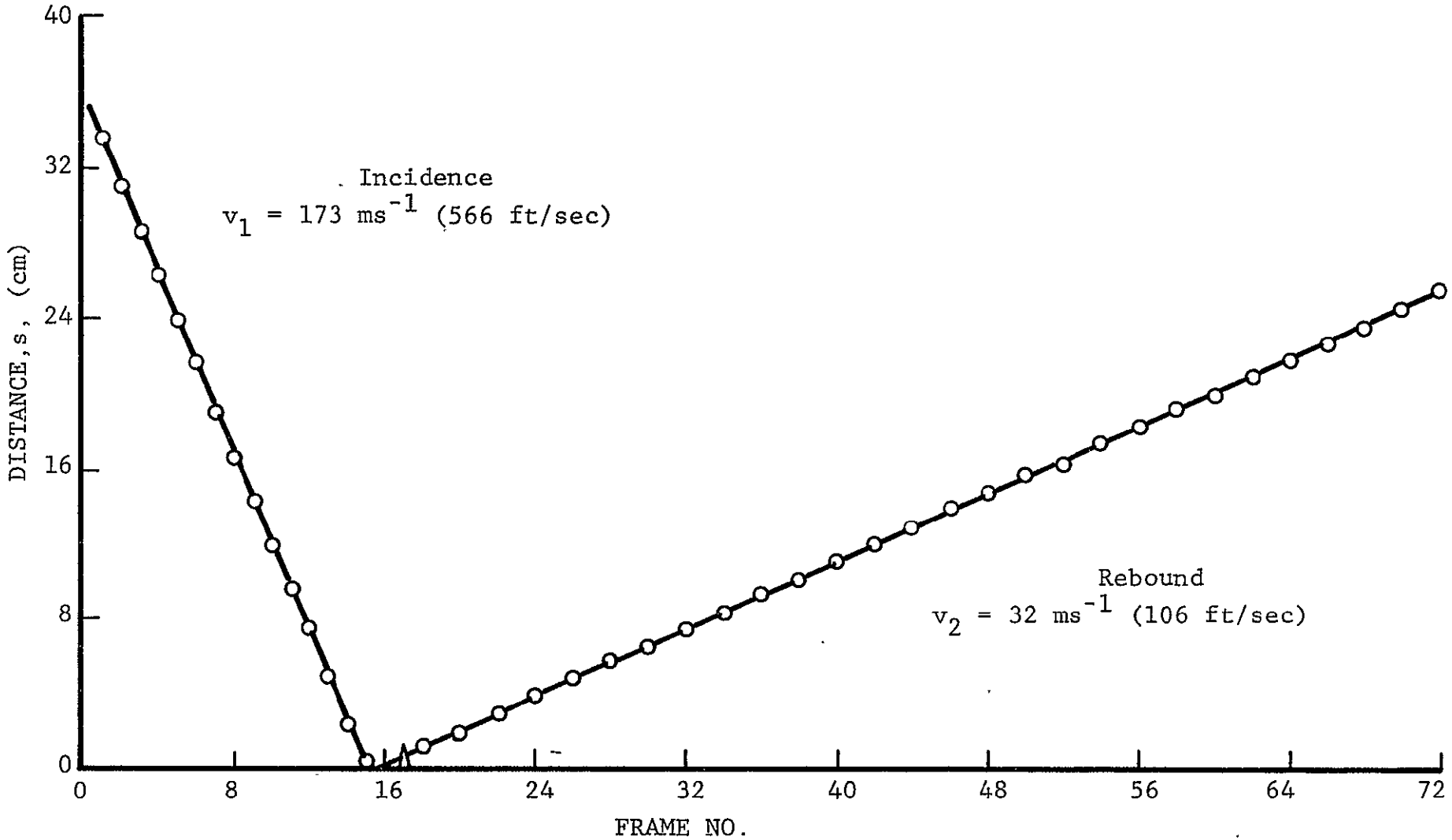

Fig. 57 PROJECTILE DISTANCE FROM IMPACTED PLATE AS A FUNCTION OF FRAME NUMBER (Barrel Pressure: 207 kPa, 30 psi; Plate: $[0_{16}]$ Graphite/Epoxy; 138 μs/frame)

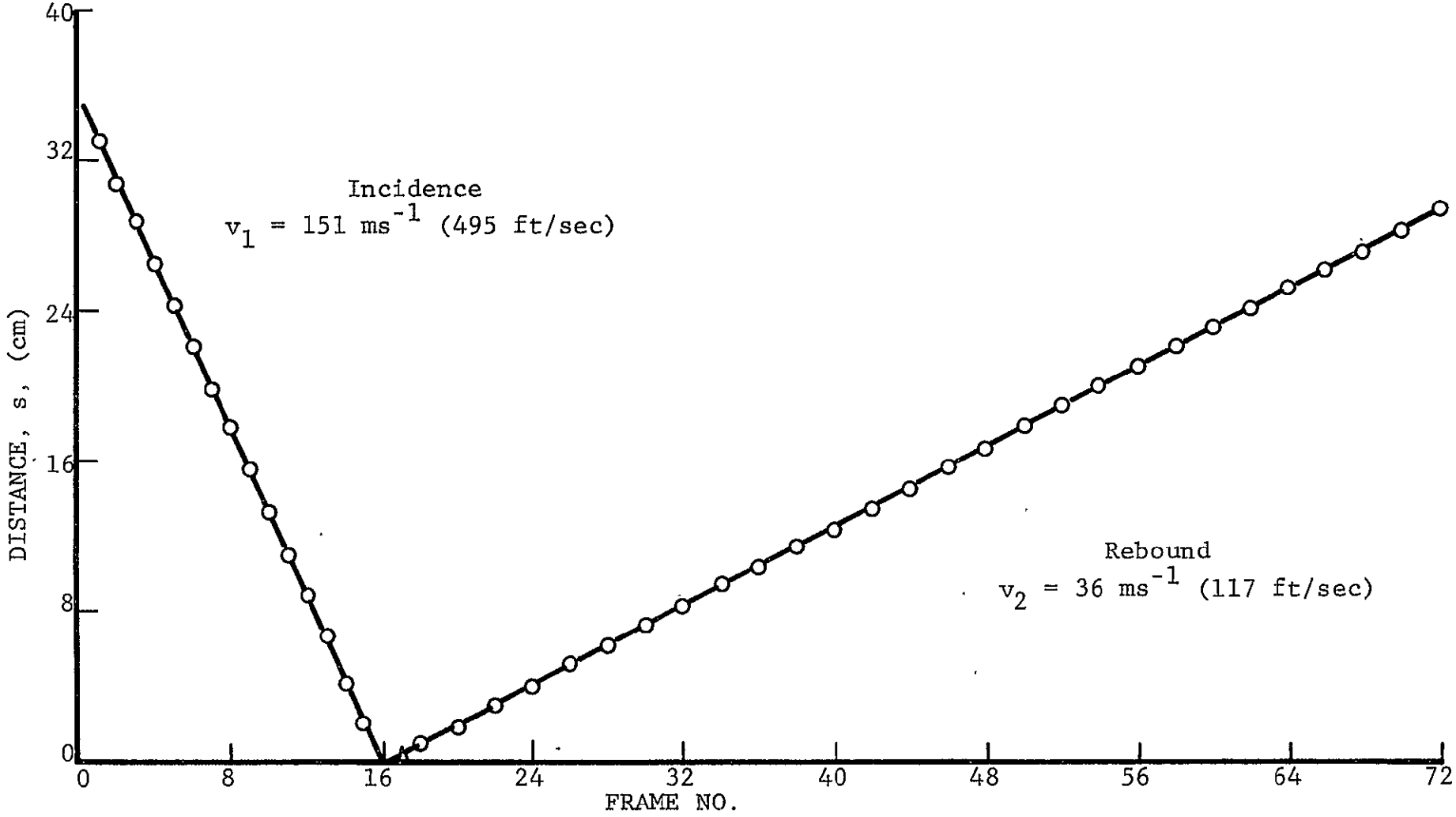

Fig. 58 PROJECTILE DISTANCE FROM IMPACTED PLATE AS A FUNCTION OF FRAME NUMBER (Barrel Pressure: 138 kPa, 20 psi; Plate: $[0_2/\pm 45]_{2s}$ Graphite/Epoxy; 146 μs/frame)

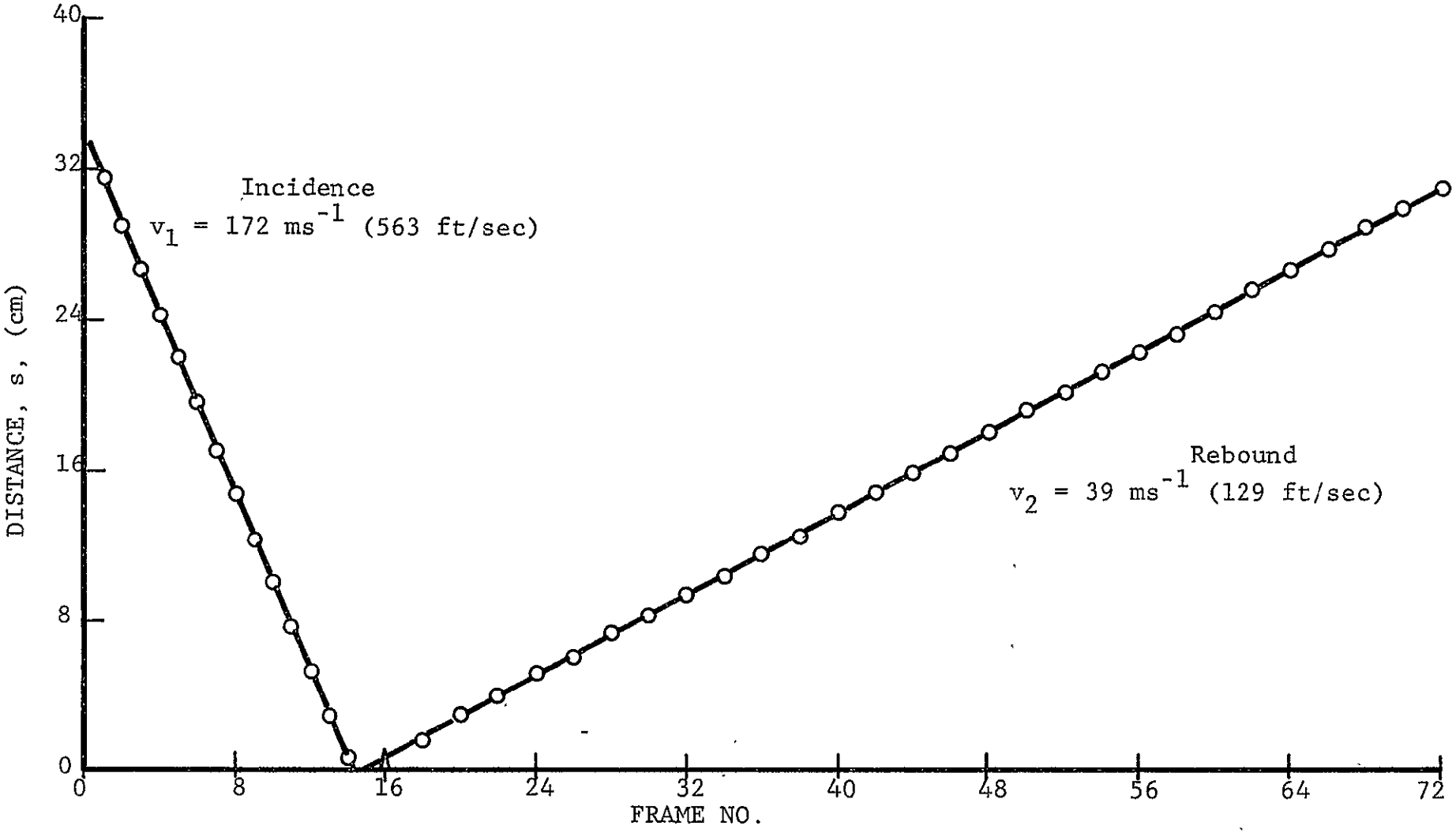

Fig. 59 PROJECTILE DISTANCE FROM IMPACTED PLATE AS A FUNCTION OF FRAME NUMBER (Barrel Pressure: 207 kPa, 30 psi; Plate: $[0_2/\pm 45]_{2s}$ Graphite/Epoxy; 137 μs/frame)

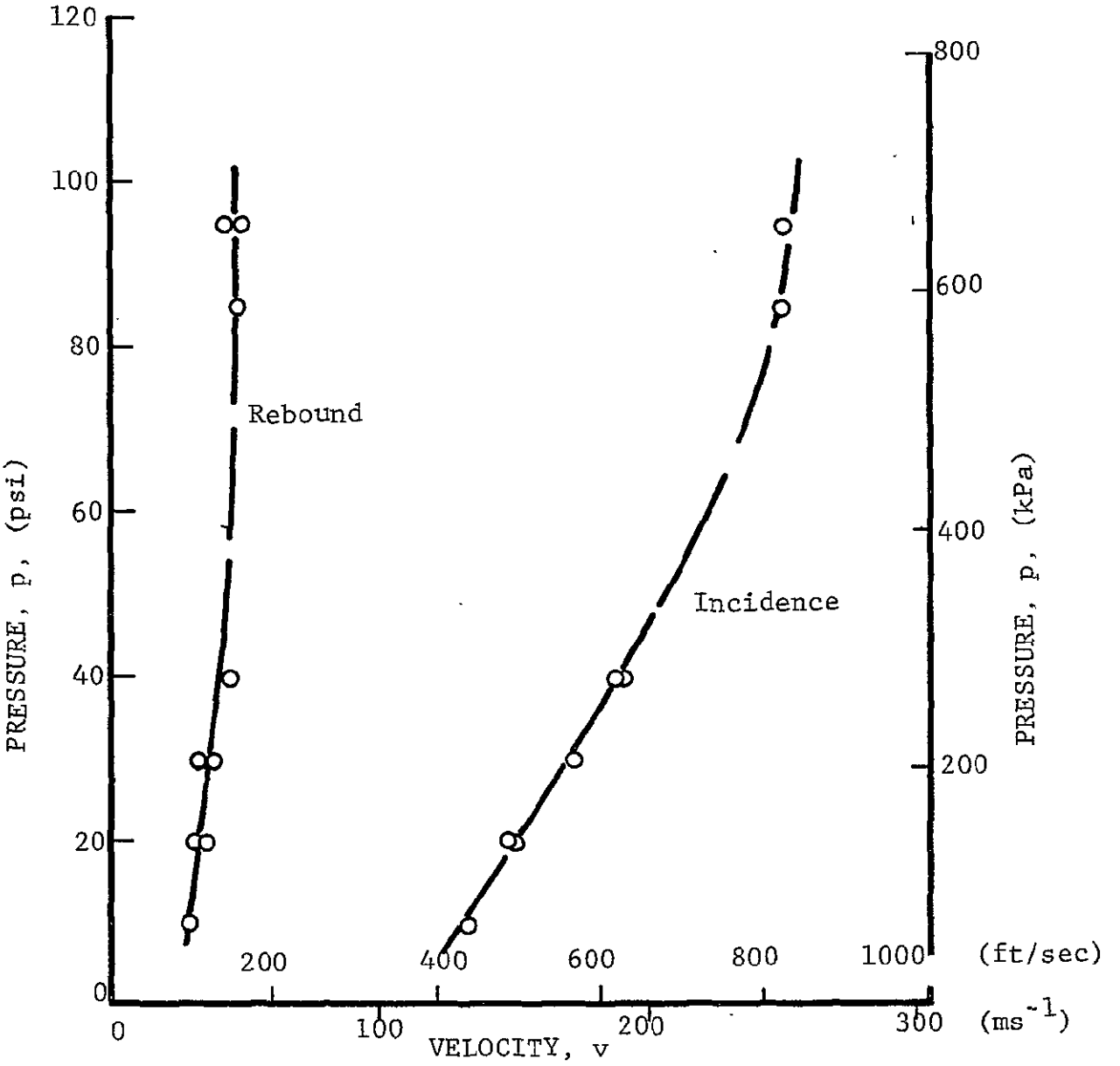

Fig. 60 INCIDENT AND REBOUND VELOCITY OF 7.9 mm (5/16 in) DIAMETER SILASTIC SPHERES AS A FUNCTION OF CHAMBER PRESSURE

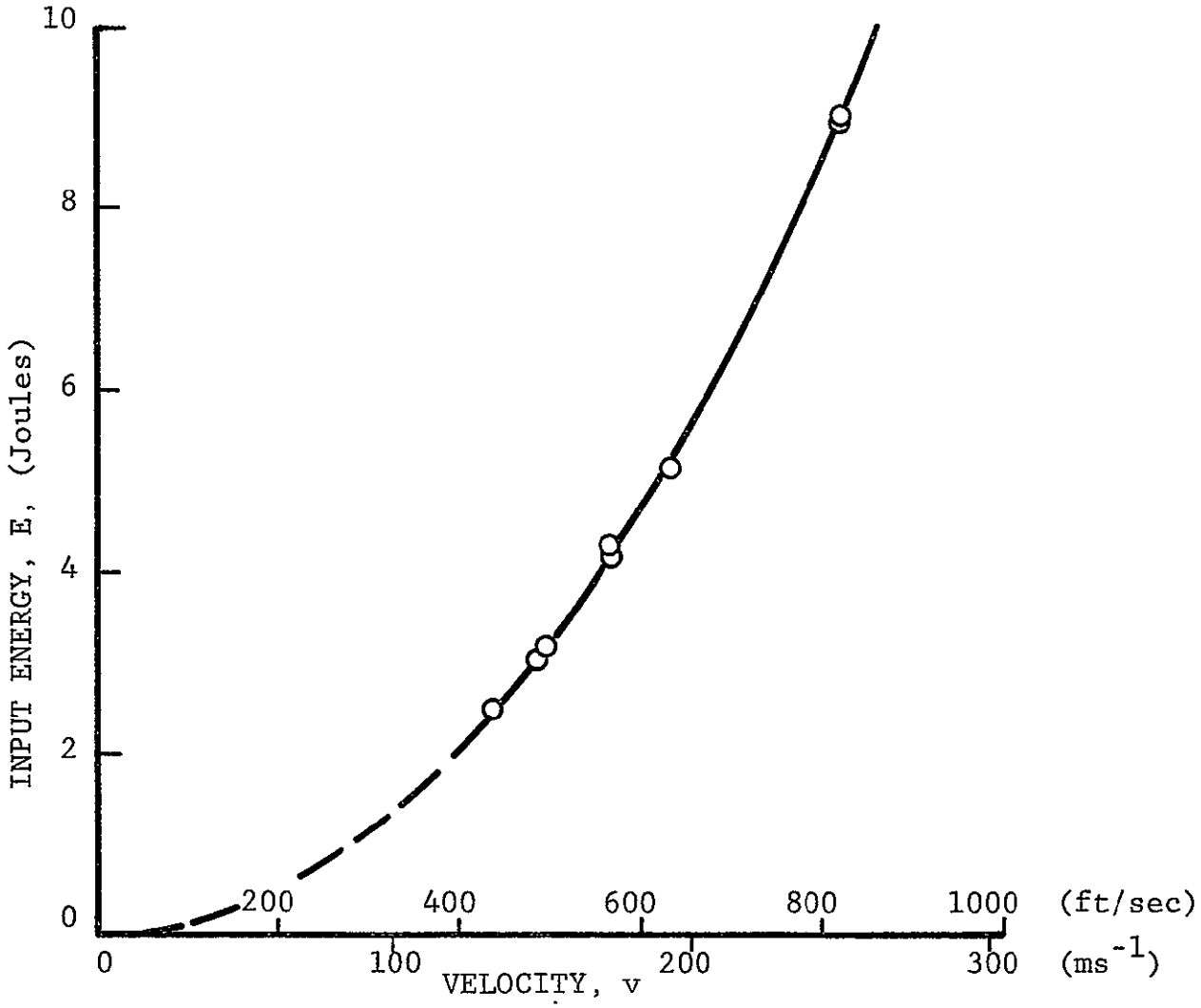

Fig. 61 ENERGY IMPARTED BY 7.9 mm (5/16 in) DIAMETER SILASTIC SPHERES ON GRAPHITE/EPOXY AND BORON/EPOXY LAMINATES AS A FUNCTION OF IMPACTING VELOCITY

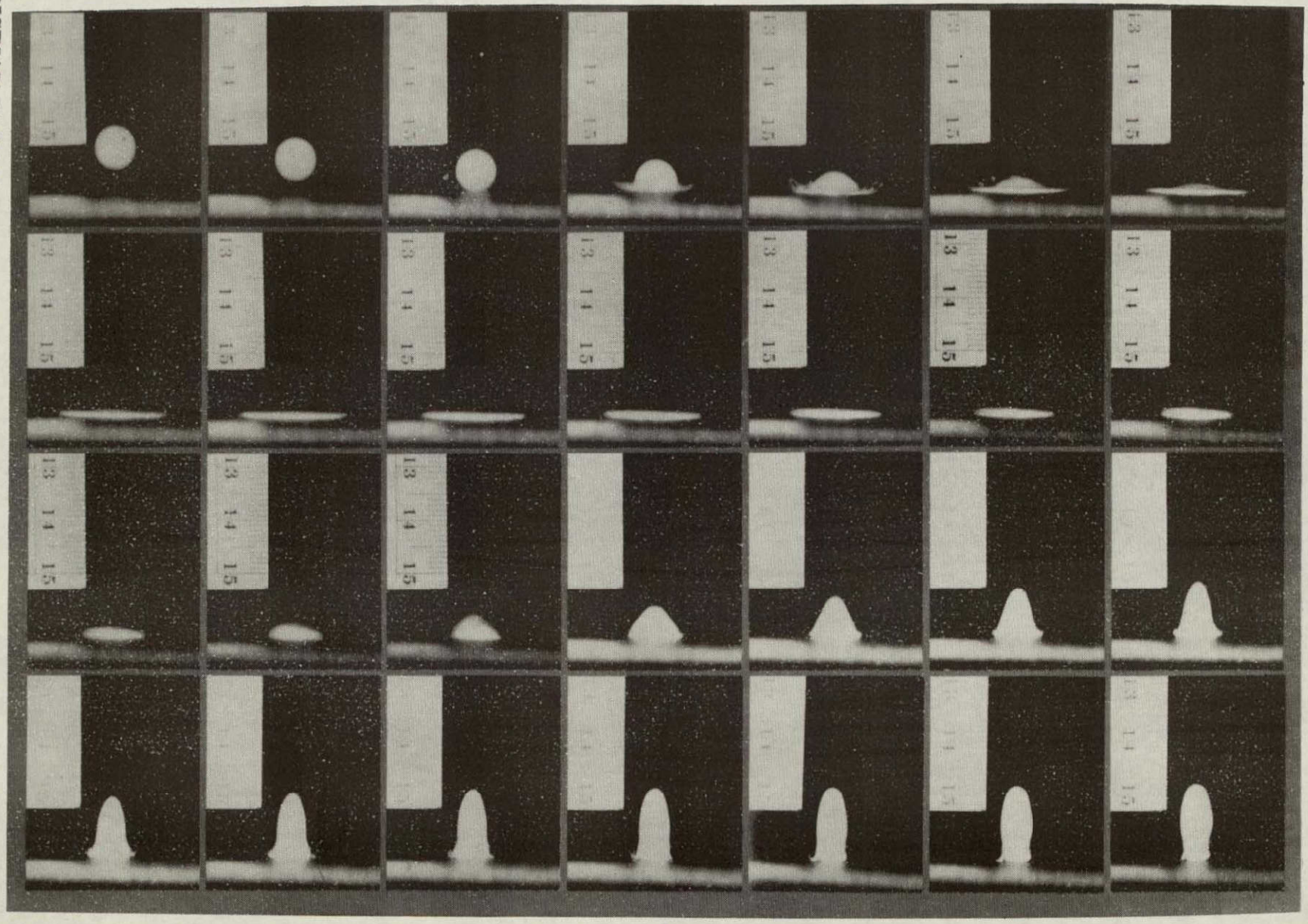

Fig. 62 IMPACT OF 7.9 mm (5/16 in.) DIAMETER SILASTIC SPHERE ON $[0_2/\pm45]_{2s}$ BORON/EPOXY PLATE AT 180 ms^{-1} (590 ft/sec). (Camera Speed: 85,700 frames/second).

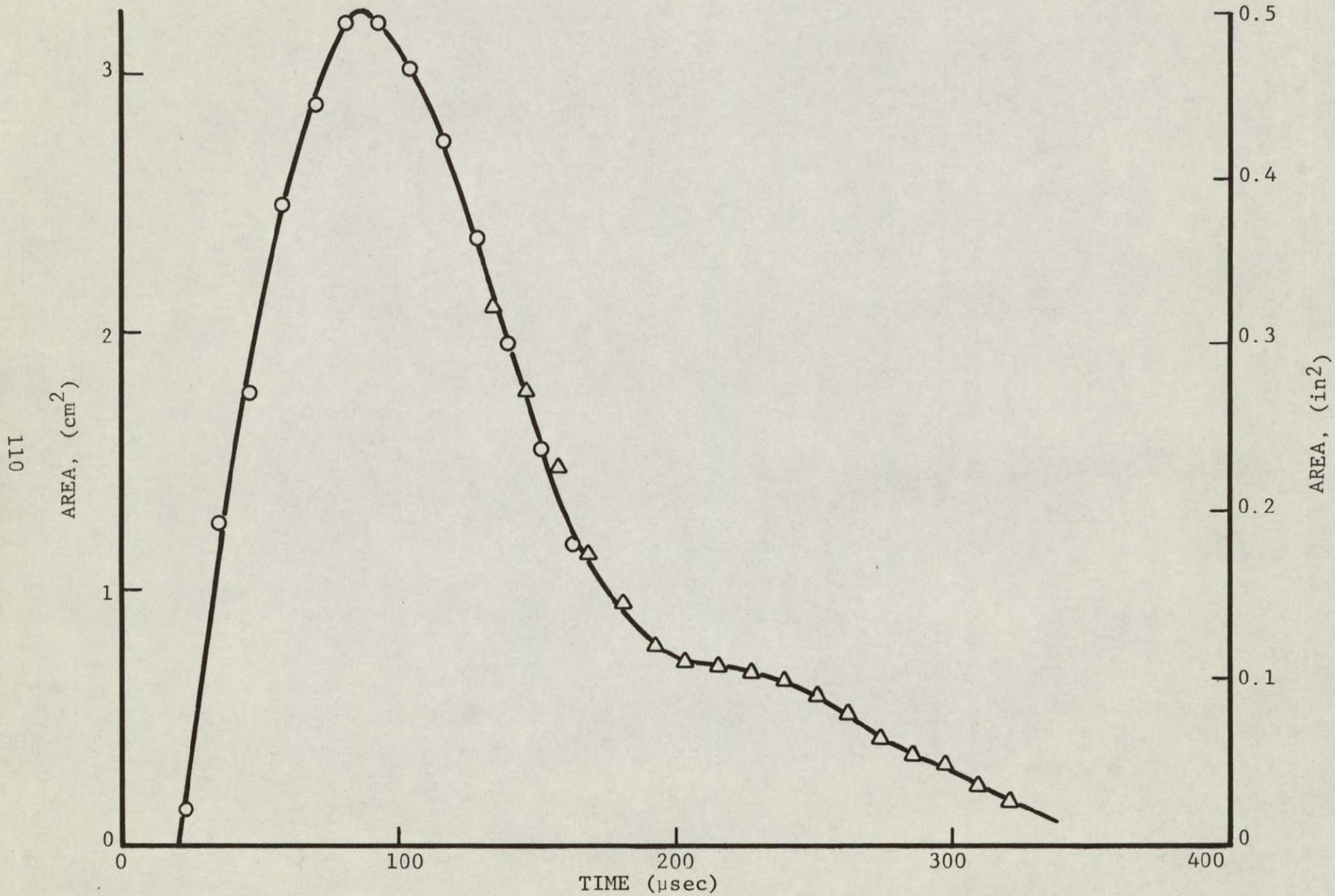

Fig. 63 CONTACT AREA OF PROJECTILE WITH TARGET PLATE AS A FUNCTION OF TIME (7.9 mm diam. Silastic Sphere Impacting at 180 ms^{-1})

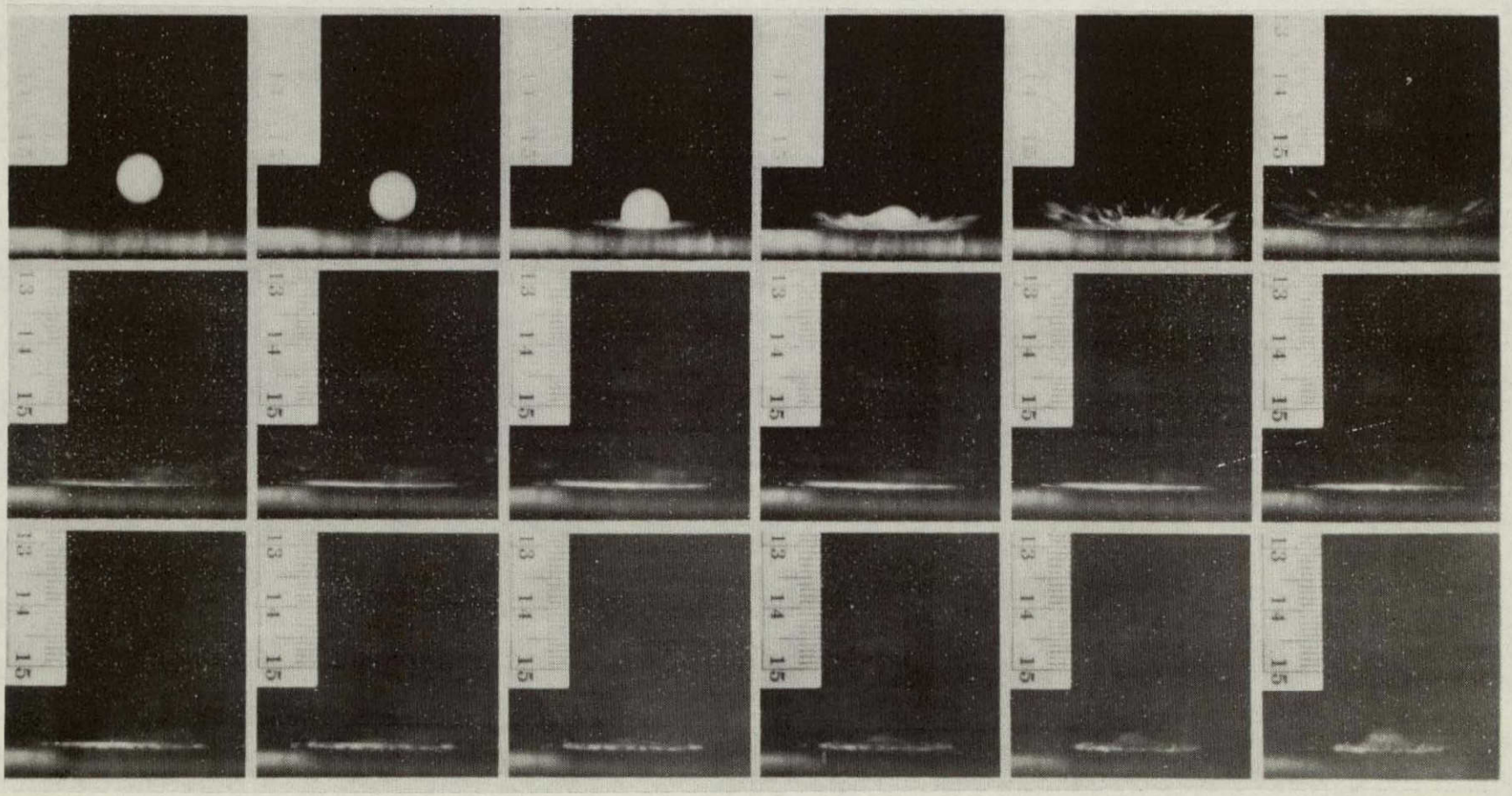

Fig. 64 IMPACT OF 7.9 mm (5/16 in) DIAMETER SILASTIC SPHERE ON $[0_2/\pm45]_{2s}$ BORON/EPOXY PLATE AT 242 ms^{-1} (794 ft/sec). (Camera Speed: 85,700 frames/second)

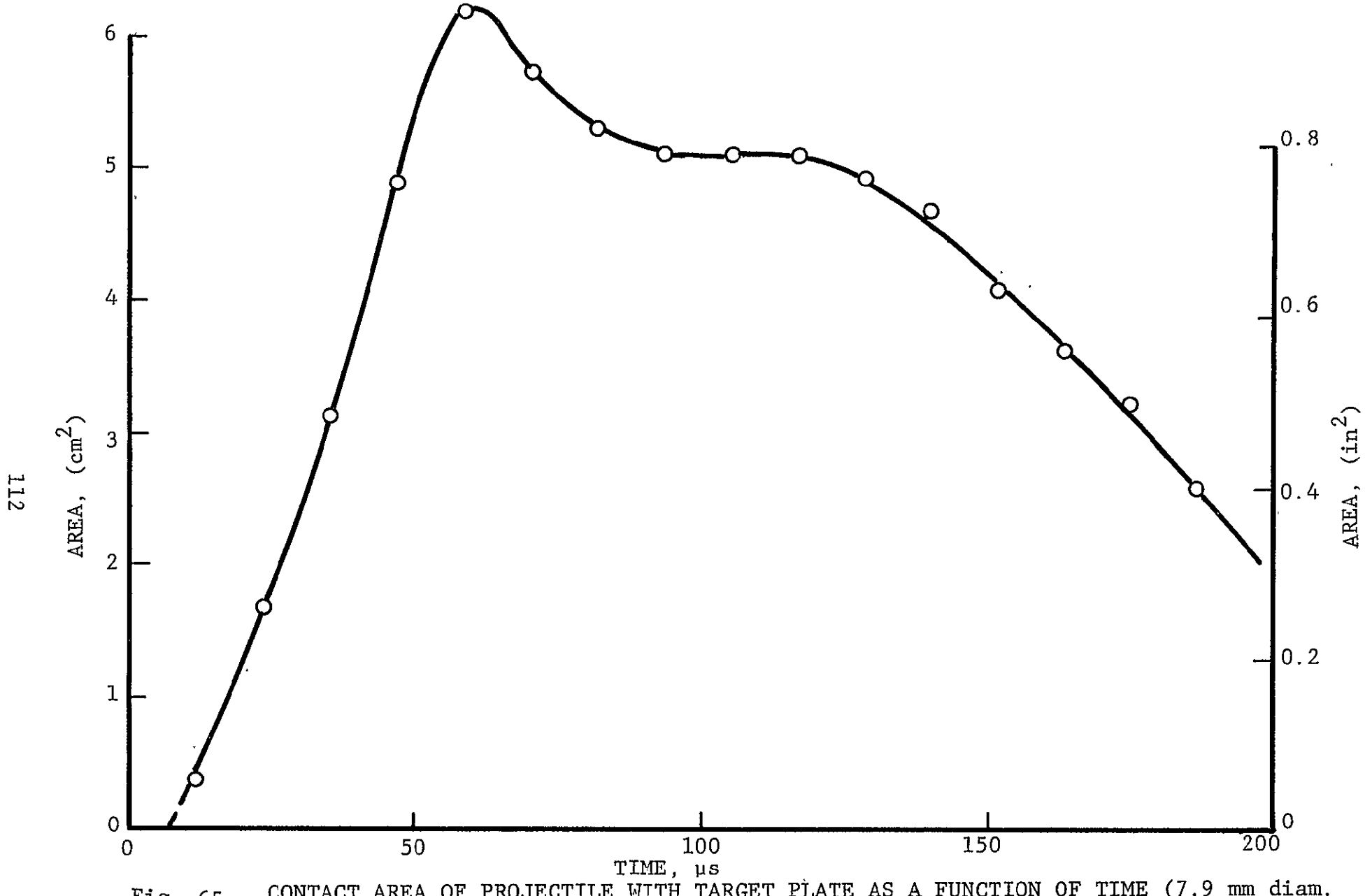

Fig. 65 CONTACT AREA OF PROJECTILE WITH TARGET PLATE AS A FUNCTION OF TIME (7.9 mm diam. Silastic Sphere Impacting at 242 ms^{-1} 794 ft/sec)

REFERENCES

1. Moon, F.C., "A Critical Survey of Wave Propagation and Impact in Composite Materials," Report for NASA-Lewis Research Center, NASA CR-121226, May 1973.

2. Musgrave, M.J.P., "On the Propagation of Elastic Waves in Aeolotropic Media," Proc. Roy. Soc. London, A, Vol. 226, 1954, p. 339.

3. Synge, J.L., "Elastic Waves in Anisotropic Media," J. Math. and Physics, Vol. 35, 1957, p. 323.

4. Buchwald, V.T., "Elastic Waves in Anisotropic Media," Proc. Roy Soc. London, A, Vol. 253, 1959, p. 563.

5. Moon, F.C., "Theoretical Analysis of Impact in Composite Plates," Report for NASA-Lewis Research Center, NASA CR-121110.

6. Moon, F.C., "Stress Wave Calculations in Composite Plates Using the Fast Fourier Transform," Computers and Structures, Vol. 3, 1973, pp. 1195-1204.

7. Dally, J.W., Link, J.A. and Prabhakaran, R., "A Photoelastic Study of Stress Waves in Fiber Reinforced Composites," Proc. 12th Midwestern Mech. Conf., 1971, pp. 937-949.

8. Tauchert, T.R. and Moon, F.C., "Propagation of Stress Waves in Fiber-Reinforced Composite Rods," AIAA Journal, Vol. 9, No. 8, 1971, pp. 1492-1498.

9. Tauchert, T.R. and Guzelsu, A.N., "An Experimental Study of Dispersion of Stress Waves in a Fiber-Reinforced Composite," J. Appl. Mech., Vol. 39, 1972, pp. 98-102.

10. Arseneaux, P.J., "An Experimental Investigation of Stress Waves in Rods of a Fiber-Reinforced Composite," Brown University Tech. Report No. 21, for U.S. Army Research Office, Contract No. DA-31-124-ARO(D)-358.

11. Rowlands, R.E., Daniel, I.M. and Prabhakaran, R., "Wave Motion in Anisotropic Media by Dynamic Photomechanics," Exp. Mech., Vol. 14, No. 11, Nov. 1974, pp. 433-439.

DISTRIBUTION LIST

Advanced Research Projects Agency
Washington, D.C. 20525
Attn: Library

Advanced Technology Center, Inc.
LTV Aerospace Corporation
P.O. Box 6144
Dallas, Texas 75222
Attn: D.H. Petersen

Air Force Flight Dynamics Laboratory
Wright-Patterson Air Force Base, Ohio 45433
Attn: G.P. Sendeckyj (FBC)
R.S. Sandhu

Air Force Materials Laboratory
Wright-Patterson Air Force Base, Ohio 45433
Attn: J.D. Ray (LTN)
H.S. Schwartz (LN)
T.J. Reinhart (MBC)
G.P. Peterson (LC)
E.J. Morrisey (LAE)
A. Hopkins (LLN)
S.W. Tsai (MBM)
N.J. Pagano
J.M. Whitney (MBM)
J.C. Halpin

Air Force Office of Scientific Research
Washington, D.C. 20333
Attn: J.F. Masi (SREP)

Air Force Office of Scientific Research
1400 Wilson Blvd.
Arlington, VA 22209
Attn: SIGL
W.J. Walker

Air Force Rocket Propulsion Laboratory
Edwards, CA 93523
Attn: Library

Army Mobility Research & Development Laboratory
Langley Research Center, Mail Stop 188A
Hampton, VA 22065
Attn: R.L. Foye

Bell Helicopter Co.
P.O. Box 482
Ft. Worth, Texas 76101
Attn: H. Zinberg

The Boeing Company
P.O. Box 3999
Seattle, Washington 98124
Attn: J.T. Hoggatt, MS 88-33

The Boeing Company
Vertol Division
Morton, PA 19070
Attn: W.D. Harris
R.A. Pinckney

Battelle Memorial Institute
Columbus Laboratories
505 King Avenue
Columbus, Ohio 43201
Attn: E.F. Rybicki
B. Noton

Brunswick Corporation
Defense Products Division
P.O. Box 4594
43000 Industrial Avenue
Lincoln, Nebraska
Attn: R. Morse

Chemical Propulsion Information Agency
Applied Physics Laboratory
8621 Georgia Avenue
Silver Spring, MD 20910
Attn: Library

Commander
Natick Laboratories
U.S. Army
Natick, MA 01762
Attn: Library

Commander
Naval Air Systems Command
U.S. Navy Department
Washington, D.C. 20360
Attn: M. Stander, AIR-42032D
C. Bersch

Commander
Naval Ordnance Systems Command
U.S. Navy Department
Washington, D.C. 20360
Attn: B. Drimmer, ORD-033
J. Kinna, ORD-033A

Cornell University
Dept. Theoretical & Applied Mech.
Thurston Hall
Ithaca, New York 14853
Attn: F.C. Moon

Defense Metals Information Center
Battelle Memorial Institute
Columbus Laboratories
505 King Avenue
Columbus, Ohio 43201

Department of the Army
U.S. Army Material Command
Washington, D.C. 20315
Attn: AMCRD-RD

Department of the Army
U.S. Army Aviation Materials Laboratory
Ft. Eustis, Va. 23604
Attn: I.E. Figge, Sr.
R. Berrisford

Department of the Army
U.S. Army Aviation Systems Command
P.O. Box 209
St. Louis, Mo. 63166
Attn: R. Vollmer, AMSAV-A-UE

Department of the Army
Plastics Technical Evaluation Center
Picatinny Arsenal
Dover, New Jersey 07801
Attn: H.E. Pebly, Jr.

Department of the Army
Watervliet Arsenal
Watervliet, New York 12189
Attn: F.W. Schmiedershoff

Department of the Army
Watertown Arsenal
Watertown, Ma. 02172
Attn: A. Thomas
D.W. Oplinger
E.M. Lenoe

Department of the Army
Redstone Arsenal
Huntsville, Alabama 35809
Attn: R.J. Thompson, AMSMI-RSS

Department of the Navy
Naval Ordnance Laboratory
White Oak
Silver Spring, Maryland 20910
Attn: R. Simon

Department of the Navy
U.S. Naval Ship R&D Laboratory
Annapolis, Maryland 21402
Attn: C. Hersner, Code 2724

Department of the Navy
Air Vehicle Technology Dept.
Naval Air Development Center
Structures Division
Warminster, PA 18974
Attn: E.J. McQuillen

Director
Deep Submergence Systems Project
6900 Wisconsin Avenue
Washington, D.C. 20015
Attn: H. Bernstein, DSSP-221

Director
Naval Research Laboratory
Washington, D.C. 20390
Attn: Code 8430
I. Wolock, Code 8433

E.I. DuPont DeNemours and Co.
DuPont Experimental Station
Wilmington, Delaware 19898
Attn: C.H. Zweben

Fiber Science, Inc.
245 East 157th Street
Gardena, California 90248
Attn: L.J. Ashton

General Dynamics
P.O. Box 748
Ft. Worth, Texas 76100
Attn: J.E. Ashley
M.E. Waddoups

General Dynamics/Convair
P.O. Box 1128
San Diego, California 92112
Attn: J.L. Christian

General Electric Co.
Evendale, Ohio 45215
Attn: C. Stotler
R. Ravenhall
C.A. Steinhagen

Goldsworthy Engineering, Inc.
Lomiter Blvd.
Torrance, California 90505
Attn: B.H. Jones

General Motors Corp.
Detroit Diesel-Allison Division
Indianapolis, Indiana
Attn: M. Herman

Grumman Aerospace Corporation
Bethpage, Long Island, N.Y. 11714
Attn: S. Dastin
J.B. Whiteside

Hamilton Standard Division
United Aircraft Corporation
Windsor Locks, Connecticut 06096
Attn: W.A. Percival

Hercules, Inc.
Allegheny Ballistics Laboratory
P.O. Box 210
Cumberland, Maryland 21052
Attn: A.A. Vicario

Illinois Institute of Technology
10 West 32nd Street
Chicago, Illinois 60616
Attn: L.J. Broutman

Jet Propulsion Laboratory
4800 Oak Grove Drive
Pasadena, California 91103
Attn: A.C. Knoell
W. Jensen

Lawrence Livermore Laboratory
P.O. Box 808, L-421
Livermore, California 94550
Attn: T.T. Chiao
E.M. Wu

Lockheed-Georgia Co.
Advanced Composites Information Center
Dept. 72-14, Zone 402
Marietta, Georgia 30060

Lockheed Missiles and Space Co.
P.O. Box 504
Sunnyvale, California 94087
Attn: R.W. Fenn

McDonnell Douglas Aircraft Corporation
P.O. Box 516
Lambert Field, MS 63166
Attn: J.C. Watson

McDonnell Douglas Aircraft Corporation
3855 Lakewood Blvd.
Long Beach, California 90810
Attn: L. B. Greszczuk

Massachusetts Institute of Technology
Cambridge, MA 02139
Attn: F.J. McGarry
J.F. Mandell

Material Sciences Corporation
1777 Walton Road
Blue Bell, Pa. 19422
Attn: B.W. Rosen

NASA-Ames Research Center
Moffett Field, California 94035
Attn: Library
D.P. Williams

NASA-Flight Research Center
P.O. Box 273
Edwards, California 93523
Attn: Library

NASA-George C. Marshall Space Flight Center
Huntsville, Alabama 35812
Attn: D.D. Thompson, S&E, ASTN-PPA
C.E. Cataldo, S&E-ASTN-MX
Library

NASA-Goddard Space Flight Center
Greenbelt, MD 20771
Attn: Library

NASA-Langley Research Center
Hampton, VA 23665
Attn: E.E. Mathauser, MS 188a
R.A. Pride, MS 188a
J.G. Davis, MS 188a
L. Roderic, MS 188e
J.R. Davidson, MS 188e
M.C. Card
Library

NASA-Lewis Research Center
21000 Brookpark Road
Cleveland, Ohio 44135
Attn: Contracting Officer, MS 500-313
Tech. Report Control, MS 5-5
Technical Utilization, MS 3-19
AFSC Liaison, MS 501-3
Rel. and Quality Assur., MS 500-211
R.A. Signorelli, MS 106-1
M.P. Hanson, MS 501-7
R.H. Kemp, MS 49-3
R.F. Lark, MS 49-3
J.C. Freche, MS 49-1
R.H. Johns, MS 49-3
N.T. Saunders, MS 105-1
C.C. Chamis, MS 49-3 (16 copies)
T.T. Serafini, MS 49-1
Library, MS 60-3 (2 copies)
Director, ASRDI, MS 6-2 (2 copies)

DISTRIBUTION LIST (Cont'd)

NASA-Lyndon B. Johnson Space Center
Houston, Texas 77001
Attn: R.E. Johnson, SMD-ES5
S. Glorioso, SMD-ES52
Library

NASA Headquarters
Washington, D.C. 20546
Attn: G.C. Deutsch

NASA Scientific and Tech. Information Facility
P.O. Box 33
College Park, MD 20740
Attn: Acquisitions Branch (10 copies)

National Aeronautics and Space Administration
Office of Advanced Research and Technology
Washington, D.C. 20546
Attn: L.A. Harris, Code RWS

National Aeronautics and Space Administration
Office of Technology Utilization
Washington, D.C. 20546

National Bureau of Standards
Eng. Mech. Section
Washington, D.C. 20234
Attn: R. Mitchell

National Technology Information Service
Springfield, VA 22151 (6 copies)

National Science Foundation
Engineering Division
1800 G Street, N.W.
Washington, D.C. 20540
Attn: Library

Northrop Space Laboratories
3401 West Broadway
Hawthorne, CA 90250
Attn: D. Stanbarger

Pratt & Whitney Aircraft
East Hartford, CT
Attn: A.J. Dennis

Rockwell International
Los Angeles Division
International Airport
Los Angeles, CA 90009
Attn: L.M. Lackman

Sikorsky Aircraft Division
United Aircraft Corporation
Stratford, CT 06602
Attn: Library

Space and Missile Systems Organization
Air Force Unit Post Office
Los Angeles, CA 90045
Attn: Technical Data Center

Structural Composites Industries, Inc.
6344 N. Irwindale Avenue
Azusa, CA 91702
Attn: E.E. Morris

TRW, Incorporated
23555 Euclid Avenue
Cleveland, Ohio 44117
Attn: W.E. Winters

Union Carbide Corporation
P.O. Box 6116
Cleveland, Ohio 44101
Attn: J.C. Bowman

United Technologies Research Center
East Hartford, CT 06108
Attn: R.C. Novak

University of Dayton Research Institute
Dayton, Ohio 45409
Attn: W.S. Blain

University of Delaware
Dept. of Mechanical and Aerospace Engineering
107 Evans Hall
Newark, DE 19711
Attn: R.B. Pipes

University of Oklahoma
School of Aerospace Mechanical and Nuclear Engineering
Norman, Oklahoma 73069
Attn: C.W. Bert

DISTRIBUTION LIST (Cont'd)

University of Wisconsin
Dept. of Engineering Mechanics
Madison, Wisconsin 53706
Attn: R.E. Rowlands

University of Wyoming
Dept. of Mechanical Engineering
Larmie, WY 82070
Attn: D.F. Adams

V.P.I. and S.U.
Dept. of Eng. Mech.
Blacksburg, VA 24061
Attn: R.H. Heller
H.F. Brinson